University of Padova

Department of Information Engineering

Master Thesis in Bioengineering

Computational model of an astrocyte as spatial potassium buffer at the neurovascular unit

Supervisor
Morten Gram Pedersen
University of Padova

Co-supervisor
Kerstin Lenk
Graz University of Technology

Master Candidate
Matteo Baldan

Academic Year
2021-2022

A mio papà

Abstract

Astrocytes are sponge-like cells present in brains and spinal cord that provide homeostasis and regulation of the central nervous system. Astrocytes are highly heterogeneous in morphological appearance, demonstrating remarkable adaptive plasticity capabilities to their surroundings, the same ones that define the functional maintenance of the nervous system through aging. They perform many supporting and active functions, including biochemical control of endothelial cells, provision of nutrients to the nervous tissue, maintenance of ion balance and regulation of the cerebral blood flow. Recent years have witnessed an increasing interest in neuron–glia communication due to the realization of their participation in cognitive functions and information processing, as well as being involved in many brain disorders and neurodegenerative diseases. Astrocytes act in neurovascular coupling by reacting to neural activity and by mediating potassium concentration in the perivascular space around smooth muscle cells. High neural activity demands a larger supply of nutrients and oxygen, which is answered by a propagation of calcium through the astrocyte, that ultimately triggers potassium exchanges between endfeets and perivascular space. This results in a control of the local smooth muscle cell's activity, bringing to regulation of dilation and constriction of nearby blood vessels and therefore regulation of the cerebral blood flow.

The aim of the thesis project is to develop a reproducible computational model of an astrocyte's endfoot cooperating with the neurovascular unit at the blood-brain barrier. This work presents a multi-compartmental state space model describing the astrocyte as a single cell that interacts with different domains, such as the perisynaptic and perivascular spaces. The model consists of a set of coupled ordinary differential equations that represent the dynamics of all states. It implements several biological phenomenon and merges together characteristics of past studies by focusing on how the calcium signaling would trigger the activation of specific potassium transporters, such as inward rectifying channel ($Kir_{4.1}$) and big conductance (BK) channels. Additionally, the model allows to define a geometrical organization of how many astrocyte's processes and how they are qualitatively distributed in space are present in a simulation. This, in order to investigate on spatial-temporal patterns during external glutamate stimulations, which simulate high neural activity.

The results showed that there is actually, buffering of potassium during external glutamate stimuli, led by calcium dynamics that propagate the information from

synaptic areas to the blood-brain barrier. All analysis are made implementing a computational model using *Python* and *MATLAB* as coding languages.

Sommario

Gli astrociti sono cellule presenti nel cervello e nel midollo spinale con una forma caratteristica radiale, la quale richiama una stella. Queste cellule contribuiscono all'omeostasi e alla regolazione del sistema nervoso centrale, inoltre, dimostrano notevoli capacità di adattamento all'ambiente che le circonda. Quest'ultima caratteristica permette di attribuire alla loro presenza la capacità di mantenimento funzionale del sistema nervoso durante l'invecchiamento. Gli astrociti svolgono molte funzioni attive e di supporto, incluse il controllo biochimico delle cellule endoteliali, la fornitura di nutrienti al tessuto nervoso, il mantenimento dell'equilibrio ionico e la regolazione del flusso sanguigno cerebrale. Negli ultimi anni, si è assistito ad un crescente interesse per le comunicazioni neurone-glia, considerando la loro partecipazione alle funzioni cognitive e al loro coinvolgimento in molti disturbi cerebrali e malattie neurodegenerative. Gli astrociti agiscono sulla cosiddetta unità neurovascolare reagendo alla attività neurale locale, e mediando la concentrazione di potassio nello spazio perivascolare in prossimità delle cellule muscolari liscie. Alta attività neurale richiede un maggiore afflusso di nutrienti e ossigeno, il quale trova risposta in una propagazione di calcio attraverso gli astrociti vicini, che portano ad attivare scambi di potassio tra il cosiddetto endfoot e lo spazio perivascolare. Questo fenomeno si rappresenta in un controllo dell'attività di cellule muscolari liscie, le quali hanno il compito di regolare la dilatazione e costrizione dei vasi sanguigni vicini.
L'obiettivo è di sviluppare un modello computazione riproducibile di un astrocita in grado di cooperare con l'unità neurovasculare al livello della barriera ematoencefalica. Questo lavoro presenta un modello multi-compartimentale di stato in grado di descrivere l'astrocita come una cellula singola, in grado di interagire con ambienti perisinaptici e perivascolari. Il modello consiste in un insieme di equazioni differenziali, dipendenti tra loro, in grado di rappresentare la dinamica di ogni variabile di stato. Implementa svariati fenomeni biologici e integra caratteristiche di studi passati, concentrandosi sul fenomeno di attivazione di specifiche proteine di trasporto di potassio, una volta raggiunte da una propagazione di calcio. Tra le proteine studiate, un maggiore interesse è riposto sui canali $Kir_{4.1}$ e BK. In aggiunta, il modello permetterà di definire una organizzazione geometrica dell'astrocita, conferendo la possibilità di studiare pattern spaio temporali delle varie variabili di stato durante una stimolazione esterna di glutamato, la quale rappresenta un'alta attività nervosa locale.

I risultati mostrano come, durante una stimolazione esterna di glutamato, sia

presente un rilascio di potassio nell'ambiente perivascolare, controllato dalla dinamica del calcio proveniente da regioni distanti dell'astrocita. Tutte le analisi sono state implementate usando linguaggi di programmazione come *Python* e *MATLAB*.

Contents

Listing of figures

Listing of tables

Listing of acronyms

NVU ..... Neurovascular unit

CBF ..... Cerebral blood flow

BBB ..... Blood-brain barrier

CNS ..... Central nervous system

GFAP ..... Glial fibrillary acidic protein

NG2 ..... Nerve antigen 2 glial cells

NTF ..... Neurotrophic factor

LIF ..... Leukemia inhibitor factor

CT-1 ..... Cardiotrophin-1

FACS ..... Fluorescence-activated cell sorting

PAP ..... Perisynaptic process

SMC ..... Smooth muscle cell

IP_3 ..... Inositol triphosphate

ATP ..... Adenosine triphosphate

ADP ..... Adenosine diphosphate

$Kir_{4.1}$ ..... Potassium inward rectifying channel 4.1

BK ..... Big conductance channel

EET ..... Epoxyeicosatrienoic acids

NKCC ..... Sodium-potassium-chloride co-transporters

ER ..... Endoplasmic reticulum

IS ..... Intracellular space

ES ..... Extracellular space

PV ..... Perivascular space

IP_3R ..... Inositol triphosphate receptor channel

SERCA ..... Sarco endoplasmatic reticulum calcium ATPase

mGluR ..... Metabotropic gluatamate receptor

GPCR ..... G-protein-coupled receptor

PLC ..... phosphoinositide-specific phospholipase C

CICR ..... Calcium induced calcium release

$IP_{3\text{-}3K}$ ..... IP_3-kinase

IP-5P ..... Inositol polyphosphate 5-phosphatase

GluT ..... Glutamate transporter

EAAT ..... Excitatory aminoacid transporters

NKA ..... Sodium-potassium-ATPase active transporters

NCX ..... Sodium-calcium exchangers

TRPV4 ..... Transient receptor potential ion-channel 4

AQP4 ..... Aquaporin-4 channels

SVR ..... Surface to volume ratio

$ratio_{er}$ ..... Ratio between IS's and ER's volume

GABA ..... Gamma-aminobutyric acid

D-serine ..... Right-enantiomer of Serine

ODE ..... Ordinary differential equation

MRI ..... Magnetic resonance imaging

BOLD ..... Blood-oxygen-level dependent

fMRI ..... Functional magnetic resonance imaging

1

Introduction

The conventional view of the brain has long been a large network of neurons supported by other cerebral cells and anatomical structures. However, it has been and it is still changing, accepting a more engaging role of other components of the brain, such as, for example, the glial cells. Which are now considered to act within the so-called neurovascular unit (NVU) along with the neurons. The term NVU is coined to describe the relationship between brain cells and blood vessels.

The NVU incorporates the cellular and extracellular components, involved in regulating the cerebral blood flow (CBF) and the blood-brain barrier (BBB) functions. Among the cells that participate in it there is the astrocyte, a type of glial cells capable of fullfilling various regulatory functions in the central nervous system (CNS). Across their different functions, they are considered to mediate the neurovascular coupling, also called as functional hyperemia. This phenomenon occurs when synaptic activity induces dilation in nearby microvasculature and allows increase in blood flow. Astrocyte supports it by regulating potassium ions (K^+) and transporting them from high concentration regions, to low concentration regions, which, regarding functional hyperemia, would be describing perisynaptic and perivascular areas. Therefore, astrocytes act as potassium spa-

tial buffers.

The scientific community started a few decades ago to learn the value of this specific glial cell type inside the CNS, and proceeded in investigating furthermore their nature. It has been found that astrocytes display a morphological heterogeneity comparable to that of neurons, therefore a detailed mapping of which forms and functions they have and do across the brain is of paramount importance. However, this task is far from being trivial because of no universal marker being discovered yet [1]. A large part of the experimental studies tried to investigate their characteristics through animal trials, particularly over mice. Therefore, many efforts were put in mathematical models, trying to synthesize their behavior and overcome the experimental difficulties of requiring animal trials in the first place. Their validation would provide reproducible tools to the scientific community in order to develop knowledge of the biological phenomena that occur in the human brain and investigate specific pathological and healthy state conditions.

The current situation shows much effort on the part of the scientific community, given the presence of a wide variety of models. Unfortunately, a recent study has shown that a high percentage of these are not reliable. [3].

Among the various models proposed by the scientific community, one way to classify them is to divide them in three families, the single astrocytes, the astrocytes networks and the neuron-astrocyte networks models [3]. Most of them focuses on calcium, where calcium concentration is considered to be the first messenger of astrocytes and its dynamics provide an insight on the behaving of the cell and the actions it is performing.

The aim of this research would be to investigate the dynamics of potassium in the perivascular space and to investigate how the activity of potassium transporters at the endfoot level is triggered by an external glutamate stimulation at the perisynaptic level. Furthermore, understand which potassium transporter has a bigger impact on the potassium exchanges between the astrocyte and the perivascular space. The idea is to start from a computational model that implements the studies of Oschmann et al. [4]; Goordleeva et al. [5], and implement an endfoot compartment that interacts with the perivascular space domain. The design of the endfoot compartment will be starting from the studies of Witthoft

et al. [6].

The focus will be on the definition of the expression of the $Kir_{4.1}$ and BK channels, described in section [2.2.1], and on how the propagation of the information of high local neural activity would be impacting on their activity. Furthermore, describing an approximation of the smooth muscle cells (SMC), in direct contact with the perivascular space and therefore hyperpolarized or depolarized by the potassium exchanges between the endfoot and the latter. Where the former information, would be related to the propagation of calcium through the astrocyte during an external glutamate stimulation. In fact, not only it will be interested to understand why the calcium is related to the potassium buffering, but more than that, how the astrocytes are able to sense spatial information and act in the environment they belong.

This study assumes to majorly rely on results from previous literature in the topic, and on medical studies, presenting the physiology of the investigated cells. The common thread trusted by this thesis will be put on the renowned Verkhratsky and Nedergaard anthology, *Physiology of Astroglia* [1]. The assumptions to this work will be that no stochastic behavior is going to be attributed to either the astrocyte model or the external glutamate stimulation, and that every space in the astrocyte is going to be modeled as a unique compartment.

2

Physiology of astrocytes

2.1 Definition and Origin

Astroglia are a class of neural cells belonging to the ectoderm, the second germ layer appearing when an embryonic clump of cells goes through gastrulation. Gastrulation refers to the process during which the embryo reorganizes itself into the three germ layers: endoderm, ectoderm, and mesoderm. The ectoderm, in particular, is known to be divided in two parts: the ectoderm itself and the neuroectoderm, precursor of the central nervous system (CNS) [7]. The neuroectoderm is going to be the focus of the origin of astroglia just as much as for neurons, both interacting with each other and being part of the same system.

The concept of neuroglia was introduced by Rudolph Virchow in 1826-1827 as the environment described as a connective substance present in the brain and spinal cord, in which elements of the nervous system are embedded. In other words, representing a collective term for cells of neuroepithelial (astrocytes, oligodendrocytes progenitor cells, oligodendrocytes, ependymal cells), of neural crest (peripheral glia) and of myeloid (microglia) origin [2]. The very first account of glial cells were defined as radial-like cells from Heinrich Müller and Bergmann [8], respectively giving their name to specific types of glial cells in 1851 and 1857,

both located in the retina. Not long after their first definition, the concept of parenchymal glia started to establish itself as the group of cells, not just with the task of creating the CNS's connective structural components, but also to provide active functionalities. Camillo Golgi was the first one able to demonstrate that glia represented a distinct cellular population from nerve cells, and also believed that neurons and glial cells might have had a strong effect on each other possible transformations [1].

Thanks to its well known silver-chromate staining technique it was found that glial cells were characterized with high morphological heterogeneity, hypothesized to be related with functionalities and showing presence of fine processes extended in all directions. Extensions were directed towards perisynaptic or perivascular spaces, the latter by plastering blood vessels. Not every type of glial cell was represented by this particular morphology, and in 1895, Michael von Lenhossék introduced the term astrocyte, which prophetically proposed to define a subtype of parenchymal glial cells. Astroglia are also known as astrocytes and are part of glial cells, which together with oligodendrocytes are the most diffused in the CNS. The term astrocytes, for protoplasmic parenchymal neuroglia, was proposed and influenced by Santiago Ramòn y Cajal. Cajal is recognized as the discoverer of the origin of the astrocytes from radial glia, due to its pioneristic astroglia-specific gold and mercury chloride-sublimate staining. Which labeled specifically the glial fibrillary acidic protein (GFAP) as in figure [2.1].

2.2 Astrocytes

Astrocytes are the most abundant cell in the human brain and report to have a star-shaped arborization of their stem process as main structural characteristic. However, some astrocytes typologies present a much more complex shape consisting of thousands of very fine elaborated protrusions that make them look more like sponges. Their abundancy is restricted to the brain and spinal cord and are highly heterogeneous in form and function, where the form varies in respect to both the region of belonging and the population of cells they need to interact with. Their high heterogeneity demonstrates remarkable adaptive plasticity capabilities, the same ones that define the functional CNS's maintenance through

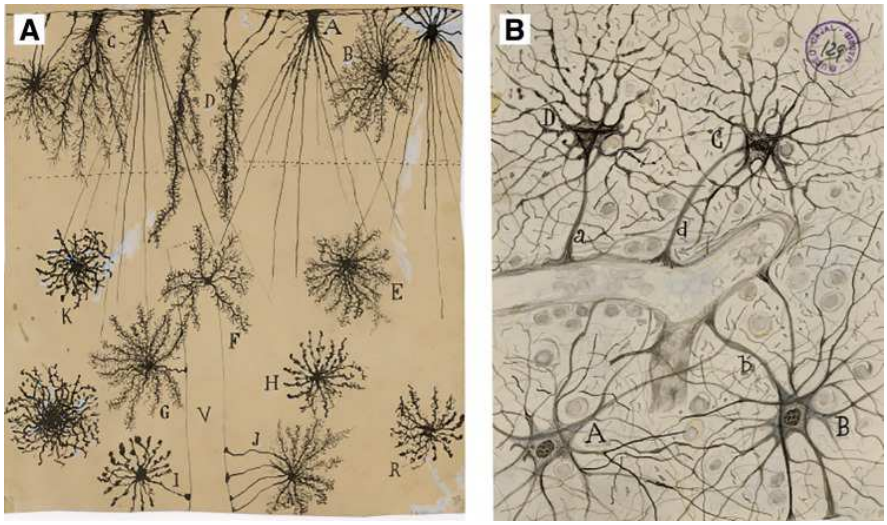

Figure 2.1: Images of astroglia part of the collection of the Cajal Legacy at the Cajal Institute of the Spanish Research Counsil (CSIC). A: Glia cells stained with Golgi's technique among different layers of the human cortex (A-R), with identification of perivascular glia (I-J). B: Perivascular astrocytes. Taken from [1].

development and aging of the brain.

Astrocytes are classified in various typologies, where the main ones are the fibrous and protoplasmic types. The first, being prevalent in the white matter of the CNS, while the second in the gray matter. The thesis in exam is going to provide analysis over a simplified protoplasmic type. The investigation of this peculiar neural cell has increased greatly in the past few decades because of innovation in technology and narrowing of the technical gap to acquire reliable evidence. Also, altough astrocytes were thought to not be related to neuronal electrical transmission due to their incapability of generating action potentials, now they are more and more considered to be acting an important role in the regulation of the neurosynaptic transmission by controlling levels of neurotransmitter concentrations in surrounding synapses [9].

Astrocytes, just like neurons, originate from the neuroepithelium radial glia, which is the universal neural progenitor [10]. However, their development is fundamentally different since they do not come from dedicated progenitor cells after asymmetric division of radial glia. Rather, they develop from transformations of radial glia or from nerve antigen 2 (NG2) glial cells. The latter comprising a cycling population of glial cells, that appear in the early phases of development of the brain and preserved in adult CNS [11].

The first stage of CNS development is solely neuronogenic and consists of asymmetric division of radial glial, producing either immature neurons or intermediate progenitors. The factor that leads to this stage is simultaneously inducing neurogenesis and suppressing the gliogenic route. This inhibition is allowing a massive wave of neuronogenesis, populating early neuronal layers and a first connectome, the widely intertwined network of neural cells also known as syncytium.

Subsequently, the gliogenic route onset is triggered due to the control of a set of transcription factors. The most notable are cytokines from the IL-6 family, including neurotrophic factor (NTF), leukemia inhibitor factor (LIF), and cardiotrophin-1 (CT-1). All activate the gliogenesis cascade through the signal-transducing co-receptors LIFRβ and gp130 (transmembrane protein, progenitor of all cytokines) [1, 12]. CT-1, instead, is expressed from newborn neurons and appears to be an agonist of LIFRβ and gp130, which is why it is argued as the timing mechanism that coordinates neuronogenesis and gliogenesis. The embryonic astrogliogenesis, however, is responsible for only a small fraction of the astrocytes populating the adult CNS. The main part of postnatal astrogenesis, which accounts for 50% of all astrocytes, is associated with the symmetric division of already differentiated types of astrocytes and occurs throughout the CNS.

The morphological and therefore functional heterogeneity of astrocytes appears to be widespread across all CNS. However, local populations tend to acquire regional specificity and peculiar relationships with neurons that would share the same place of birth. Furthermore, a positive correlation is identified between maturation of both astrocytes and neurons if the two share similar molecular factors by definition of the neighborhood. Identification of astrocytes is far from a trivial task, especially because there is no universal marker that may label all cell of astroglial lineage. Existing techniques include classical histological staining and immunocytochemistry, while in less cases, it is possible to use genetically controlled expression of astroglia-specific fluorescent markers and fluorescent techniques (*e.g.*, intraglial injection or incubation with fluorescent probes). Genetic profiling of astrocytes allows the targeting of specific transcription signatures of expressed proteins, which is done in the most common cases using fluorescence-activated cell sorting (FACS), a specialized type of flow cytometry that uses fluorescent markers to target and isolate cell groups.

One key characteristic regarding this study on Astrocytes is the investigation of their processes. As their shape suggests, they leave the body of the cell with a radial geometry and branch out to reach either synapses or blood vessels. In the first case, they are defined as perisynaptic processes (PAPs), while in the second as endfeets. To be more precise, the endfoot corresponds to the furthest section of a process that starts from the body of the cell and ends with the plastering of a blood vessel. Perisynaptic processes are part of tripartite synapses and allow the respective astrocyte to control the neuron-glia signaling mechanisms. Where for tripartite synapses we refer to the composition of presynaptic neuron, postsynaptic neuron and their intimate association with a surrounding glia. Both classes of processes, as well as the whole cell, are ble to express both the endoplasmic reticulum and Golgi apparatus satellite structures, which provide local capability of expressing proteins, particularly transmembrane proteins.

2.2.1 Astrocytes as potassium spatial buffers

Astrocytes control homeostasis of the CNS at all levels of organizations, starting from molecular to whole organ, as depicted in figure [2.3]. They are able to do that by transporting major ions, by catabolizing neurotransmitters and by releasing neurotransmitters precursors and scavengers of reactive oxygen species as well.

Ion concentrations fluctuate a lot in the nervous tissue, and our body responds to them by maintaining their local distribution, in other words is capable of achieving the so-called Ionostasis. This phenomenon happens in our body regarding of the perturbances given from major systemic processes and is of paramount importance for nervous functions, because it defines overall excitability and major signaling processes. Astrocytes contribute to ionostasis through numerous ion transporters, not allowing ions such as potassium (K^+), chlorine (Cl^-), calcium (Ca^{2+}) and sodium (Na^+) to leave physiological ranges. Their interactions with the environment that surrounds them are undeniable and are related to the value of equilibrium potentials of each ion, reported in figure [2.2]. The very same results that were discovered and validated in many experiments.

The most canonical function of the astroglia is the control of the K^+ concentration inside the interstitial fluid. Local concentrations of K^+ increase significantly

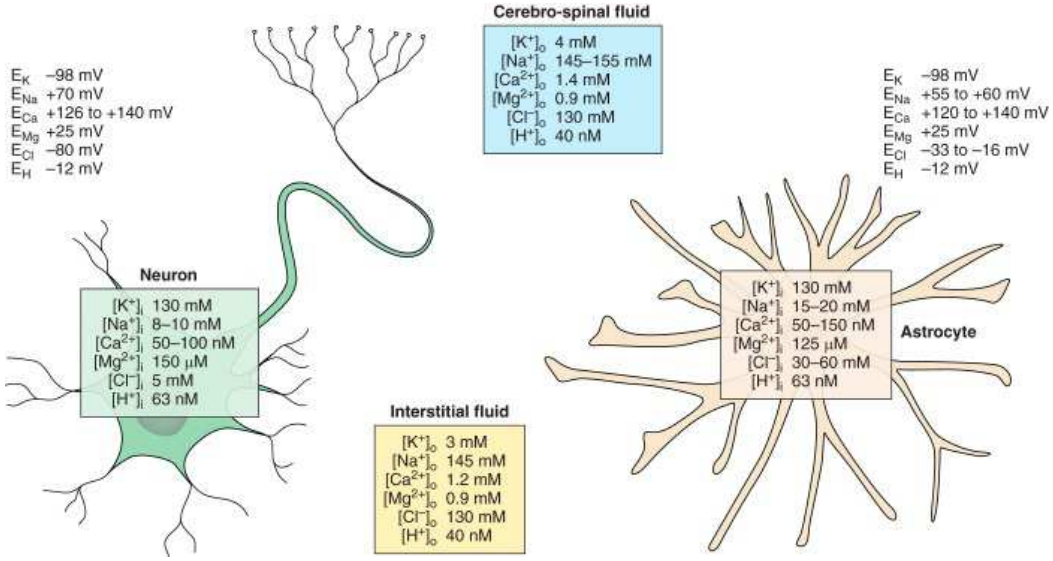

Figure 2.2: Ion distribution and corresponding values of equilibrium potentials between cerebrospinal fluid, interstitial space, and cytoplasm of both astrocytes and neurons. Taken from [1].

during neuronal activation, and elevated distribution of it could affect markedly other mechanisms such as, acid-base homeostasis, energy metabolism, and volume regulation of nearby cells. Possible pathological outcomes of high sustained concentration of K^+ are: neural dysfunction, hematoma, and brain metabolic distress [13]. Therefore, maintaining its level is critical for synaptic transmission and the proper functioning of the neuron-glia signaling network.

Astrocytes control K^+ concentration by up-taking and releasing them, respectively, from high- and low-concentration regions. The transportation is mediated through several overlapping mechanisms, which can be generally classified into: diffusion through passive K^+ channels, active transport of Na^+/K^+-ATPase channels and by simple diffusion in space[1]. The aforementioned potassium shuttle turns out to be possible because of the so called, syncytium, a connectome made up of various astrocytes and neural cells connected through gap junctions. The gap junctions are the definition of specialized proteins, which connects directly the cytoplasms of two different adjacent cells, which in the case of astrocytes, would provide for an ultrastructural cytoplasmic continuity and contribute to the functional role of the syncytium. The following transmission through the gap junctions comprises the first messenger molecules, such as Ca^{2+} ions, and the

second messengers, such as inositol triphosphate (IP_3).

Potassium signaling

Astrocytes have been classified as spatial K^+ buffers, especially when operating at the perisynaptic processes level, where they take excess potassium and release it at the endfoot. In both particular regions, a key actor in the process is the inward rectifying channel ($K_{ir}4.1$) [14], specifically important because of being efficient in narrow spaces, such as synaptic clefts and perivascular spaces. In vitro experiments have shown that $K_{ir}4.1$ are indeed responsible for the resting membrane potential of astrocytes and therefore responsible for K^+ permeability [15]. It is to known that apart from contributing to the resting membrane potential, the role of $K_{ir}4.1$ channels needs still to be investigated due to the differences in their expression across different brain regions, and therefore regional variability in K^+ buffering contribution. Another key actor in the release of up-taken K^+ is the so called, Big Conductance (BK) channel, a voltage and Ca^{2+} activated K^+ channel, involved in the regulation of neurotransmitter release and neuronal excitability. The relative outflow of K^+ with respect to the $K_{ir}4.1$ channel is much higher and can be derived from the ion current created by the exchange of ions between the intracellular and extracellular space. As the name suggest, these channels have a relatively high single channel conductivity, reflecting the produced ion current when activated. Compared to $K_{ir}4.1$ channels, BK channels are targeted to endfeet processes [16].

$K_{ir}4.1$ is one subtype of K_{ir} family, product of KCNJ10 gene. It is detected in many types of astroglia, including protoplasmic and fibrous astrocytes, and in many different regions of the brain, including the hippocampus, neocortex, optic nerve, cerebellum, spinal cord, and retina. However, its expression is not exclusively of astroglia and glial cells, in fact it is also found in neurons, smooth muscle cells and others.

$K_{ir}4.1$ channels are known to be major contributors to the resting membrane potential of astroglial cells and as the name suggest, they show a greater inflow of ions, rather than an outflow from the cell. However, the direction of the flow highly depends on which mode they are activated into, which is toggled by both

the membrane potential and the ratio between the external and internal K^+ concentration. Therefore, Kir channels behaviour depends more on an electrochemical gradient of K^+, where evidence demonstrated a large inward K^+ conductance at hyperpolarized potentials or potentials negative to the potassium equilibrium potential (E_K). Meanwhile, at depolarized potentials, smaller outward K^+ currents are observed, mediated by a voltage-dependent block of outward currents by positively charged polyamines and Mg^{2+} [17].

The big conductance Ca^{2+}-activated channels are K^+ transporters expressed in a wide variety of cells, including glia and neurons. In astrocytes, they are identified in the perivascular endfeets and are involved in various tasks, such as potassium buffering, regulation of neurotransmitter release, and neuronal excitability. Their gating mechanisms is both dependent on voltage and on ligands binding. The necessary ligands are Ca^{2+} and Mg^{2+}, even if epoxyeicosatrienoic acids (EET) might also act on BK activation. The latter is still unclear if it acting directly on the activation mechanism of endfeet's BK channels or indirectly leading to calcium influx and therefore, membrane depolarization, both of which activate BK channels ([18];[16]. As the name suggest, big conductance K^+ channels have a much larger single channel conductance then other potassium channels with a unitary conductance in the range of 100-300 pS [18].

The other two K^+ transporters in astrocytes are represented by $Na-K$ pumps (NKA) and sodium-potassium chloride cotransporters (NKCC), where the first actively consumes ATP to produce an inward movement of K^+ from the synaptic cleft and an outward flow of sodium from the astrocyte. NKA are activated under conditions of high extracellular potassium concentration and high intracellular sodium concentration; therefore, they have counter-gradient activity. The pumps exchange three Na^+ ions for two K^+ ions each cycle. Instead the NKCC produce an inward flux of both K^+ and Na^+ that increases when the concentration of both ions decreases in the intracellular space. They are known to be electrically neutral since they move togheter two positive charges, brought by the Na^+ and K^+, and two negative charges, brought by the two parts of Cl^-. The combination of NKA and $NKCC$ provides competing exchanges between the intracellular and extracellular space, particularly in the synaptic cleft area, where neural activity also has influence on potassium dynamics [6]. However, the NKCC transporters

are not implemented in the model.

Calcium signaling

Intracellular calcium is identified to be the main messenger variable for astrocytes, and is mainly stored inside the endoplasmic reticulum (ER). Ca^{2+} are exchanged and moved by the astrocyte within various biological pathways, the exchanges could be between intracellular and extracellular spaces, or between ER and intracellular space. Calcium exchanges between the ER and the intracellular space is mediated by three different ionic currents: the first one, related to the controlled release of calcium ions by the IP_3 and calcium dependent IP_3 receptor channels (IP_3R). Then, the second one by uptake of calcium back into the ER through the Sarco Endoplasmatic Reticulum Calcium ATPase (SERCA) pump. Which are active transporters of calcium ions in exchange of energy consumption. And finally, calcium leaks (Ca^{2+}_{leak}) that could describe all the other exchanges of material that are not negligible together but are not related to a specific channel protein.

Among the aforementioned ionic currents, the first two are considered key actors in the calcium-induced Ca^{2+} release (CICR) exchange phenomenon, which acts between the ER and intracellular space during external stimulation and describe the release of Ca^{2+} from internal storages when induced by intracellular calcium itself. IP_3R and SERCA pumps activity appears to a produce a negligible net change and intracellular Ca^{2+} levels are set by the contributions of the passive leak and of low regime SERCA pumps.

Astrocytes show changes in intracellular Ca^{2+} when they are able to sense local external neural activity. This occur through two different metabolic pathways, respectively the mGluR-dependent pathway and the GluT-dependent pathway. Both depend on glutamate, which is a neurotransmitter that is released in synpatic clefts during high neural activity. In case the synaptic activity is large enough, glutamate starts to be sensed by the astrocyte's perysinaptic processes and triggers propagation of Ca^{2+} across the body of the cell.

The mGluR-dependent pathway, as the name suggests, involves metabotropic glutamate receptors (mGluRs), proteins that belong to a G protein-coupled fam-

ily (GPCR) and participate in the modulation of synaptic transmission and neuronal excitability throughout the CNS. The GPCR represents the most abundant receptor gene family in the human genome, able to be activated when bound to specific ligand, causing transduction of intracellular signals. The activation consists of a shift in the shape of the G-protein due to the binding of the ligand, which in this case is represented by glutamate. When glutamate binds to *mGluRs*, they stimulate the phosphoinositide-specific phospholipase C β (PLC_β) and phosphoinositide-specific phospholipase C γ (PLC_γ) to increase the production of intracellular IP_3. An increase or decrease in IP_3 concentration mediates the activity of IP_3 R channels. In fact, this creates an indirect relationship between fluctuations in external glutamate stimulus and intracellular calcium concentrations. At first, only a few of local IP_3R channels would react to the increment of IP_3. However, a lasting stimulation increases their probability of opening and produces an increment in Ca^{2+} intracellular concentration as well. Thus it induces further Ca^{2+} releases from ER and provide to sustain the self-amplifying release mechanisms defined as CICR [19].

When high intracellular calcium concentrations are reached, IP_3R inactivation takes place, terminating the CICR. While, in parallel, SERCA pumps activate and re-balance the calcium concentration by pumping it back into the ER. The basal values of the calcium intracellular concentration recover consequently and there is no further inhibition of IP_3R channels. This allows a still high enough intracellular IP_3 concentration to reopen IP_3R and start again a new cycle, leading to oscillations. The reduction in IP_3 concentration is mediated by the IP_3-kinase (IP_3-3K), an enzyme that facilitates phosphorylation of IP_3 to IP_4 ([20]) and by inositol polyphosphate 5-phosphatase (IP-5P), which is another enzyme capable of dephosphorylation of IP_3 into IP_2.

The other major metabolic pathway, which provides a source of calcium ions, is mainly attributed to the indirect activation of calcium entry after an increase of glutamate transporters (GluT) activity. These transporters are none other than excitatory amino acid transporters (EAATs), particularly EAAT1 and EAAT2, predominant in glial cells. Evidence showed that GluT, for each glutamate molecule, transport three different Na^+ ions into the cell and one K^+ ion outside. However, the stoichiometry and identity of the coupled ions, identified

in the EAATs activity, was hotly debated by the scientific community in the past decade, as reported by Tzingounis, A. and Wadiche, J. [21]. Belonging to the GluT-dependent pathway, Na^+-K^+-ATPase active transporters (NKA) and Na^+/Ca^{2+} exchangers (NCX) are also associated with it. The first ones being active transporters able to pump sodium and potassium ions against their respective gradient by consumption of ATP and the second ones being able to exchange between the cellular membrane sodium and calcium ions.

During external gluatamate stimulations, GluT channels generates an inwardly directed Na^+ gradient and an outwardly directed K^+ gradient and involve Na^+-K^+-ATPase active transporters. The latter respond by moving Na^+ and K^+ through the cellular membrane against their gradients and by re-balancing them to basal values. However, the GluT dependent pathway provide for a source of Ca^{2+}, which actual inflow occurs through the transmembrane Na^+/Ca^{2+} exchangers. These channels are highly concentrated around the GluT transporters and during rapid rise of sodium local concentrations are found to be working in reverse mode, transporting Na^+ ions outside of the cell and Ca^{2+} inside. The NCX are bidirectional ion transporters, able to work in forward mode by producing an efflux of calcium ions, and in reverse mode by producing an influx of calcium ions [22].

Along with the previously described calcium sources, one should take into account that astrocytes also creates connections through gap junctions between each others, allowing communication and exchange of various different compounds, including different ions and IP_3. Inside the same astrocyte, instead, once calcium events are triggered in PAPs, Ca^{2+} and IP_3 can diffuse through the cell and propagate the information coming from the external stimulation. Therefore, the first Ca^{2+} events are usually small and fast and follows minimal synaptic activity, while propagation in not stimulated sections of the cell and the triggering of CICR phenomenon contribute to slower events. The result is described by a propagation wave of calcium oscillations with high dependence on the duration of the stimulation. The longer the stimulation, the more intense the oscillations and the longer the possible travel time, together with a slight decrease in the oscillations amplitude during propagation.

One other possible calcium transporter channel found in astrocyte, is the so-

called transient receptor potential cation (TRPV4) channel. It is one of the six belonging to a subfamily of ion channels (TRPV) that is highly calcium selective, and that can be activated by various osmotic, mechanical and chemical stimuli. This particular channel has been shown to regulate the Ca^{2+} influx into the astrocytes. The gating mechanisms is still debated in the scientific community, given its wide complexity and wide variety of the aforementioned factors that could activate it and therefore may have a key role in Ca^{2+} exchanges [23].

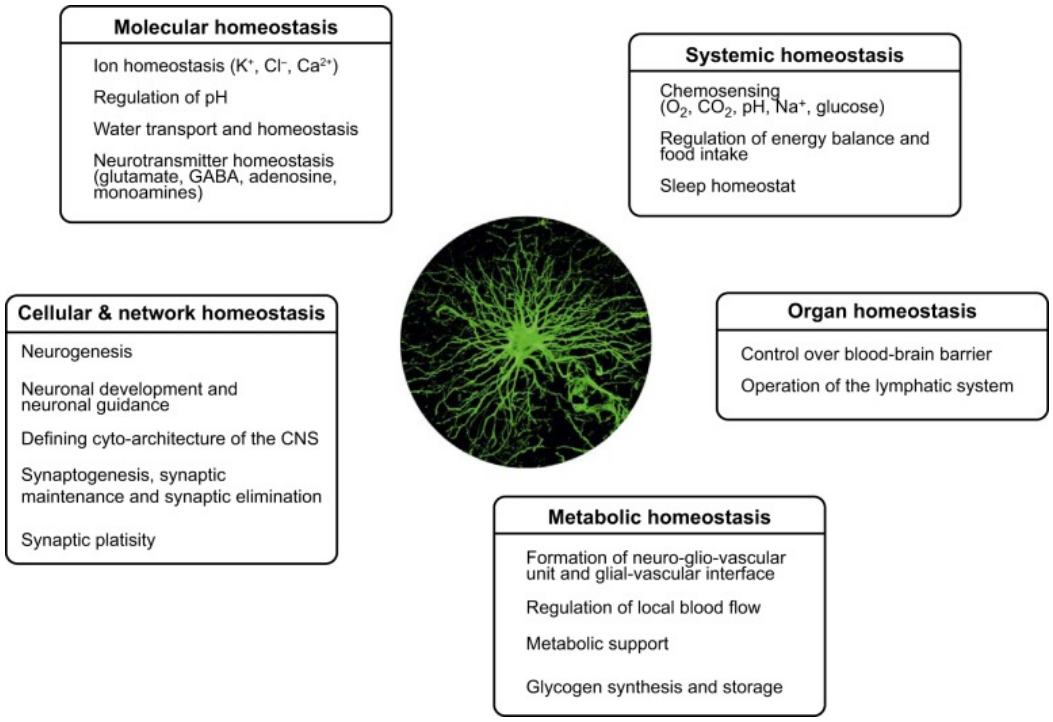

Figure 2.3: Homeostatic functions of astroglia. Taken from [1].

2.2.2 Neurovascular Coupling

This section will focus on the neurovascular coupling between brain and blood vessels, and how it is sustained and supported from astrocytes. We will introduce the definition of the blood-brain barrier (BBB), a structural component formed by tight junctions among endothelial cells, pericytes, and astrocytic endfeets. It restricts the entry of neurotoxins and pathogens from the bloodstream into the brain parenchyma [24]. BBB malfunctioning is known to cause the following:

- Neuronal damage
- Synaptic dysfunction
- Loss of neuronal connectivity in many neurodegenerative diseases

The overall scheme of how is designed the NVU is reported in figure [2.4] and shows how the anatomical structure is composed by neurons, astrocytes, endothelial cells of BBB, myocytes, pericytes and extracellular matrix components.

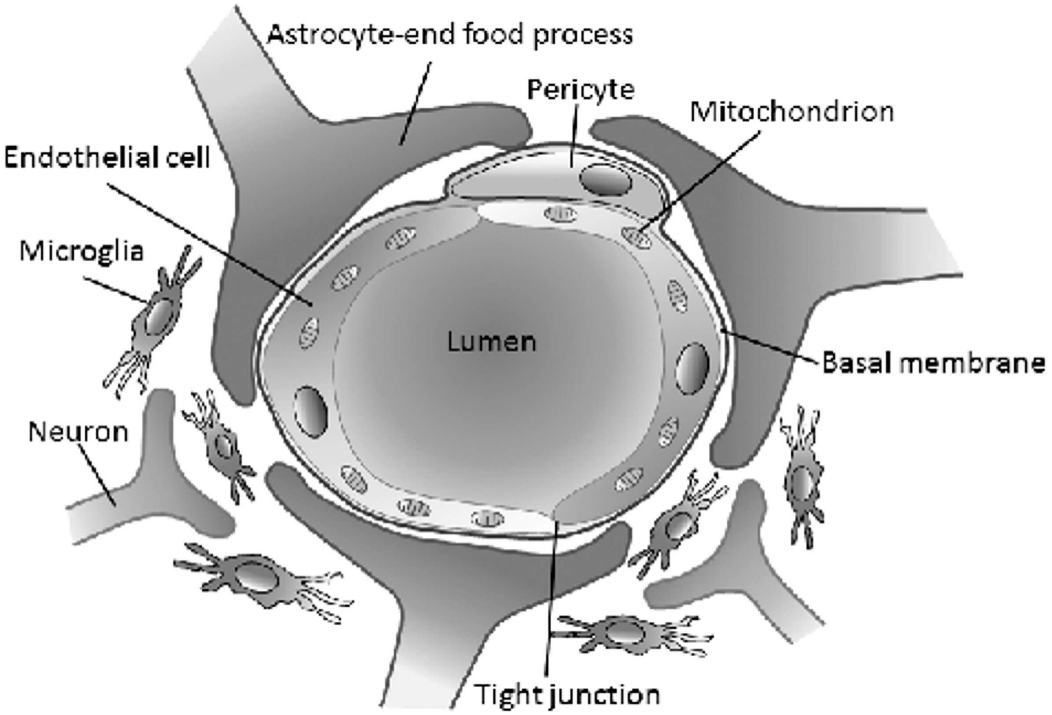

Figure 2.4: Neurovascular Unit scheme. Taken from [2].

The blood vessels are surrounded by the so called, smooth muscle cells (SMC), designated cells able to dilate and constrict the radius of brain arteries. This process is mediated by the membrane potential of the muscle cells themselves, respectively vasodilating or vasoconstricting when there is hyper-polarization or depolarization [25]. A major signal that has the potential to be at the center of this regulation process is K^+ concentration. Hyperpolarization of the cellular membrane means that the membrane potential becomes more negative at a particular spot of the membrane, while depolarization means that the membrane

potential becomes less negative, and therefore more positive. The membrane potential is evaluated looking at the differences in ions concentration between the intracellular and extracellular space, using Nernst formulations.

Recalling what was previously discussed, astrocytes are able to act in the neurovascular unit by providing information to SMCs, to react to high local neural activity. High neural activity would create calcium events propagating through astrocytes and reaching the endfeets, which would trigger the release of potassium ions into the perivascular space. An increase in potassium concentration would mean an increase in positive charges, the very same which would make the membrane potential of the SMC more negative, increasing the gap between the intracellular space and the extracellular space, which locally would be represented by the perivascular space.

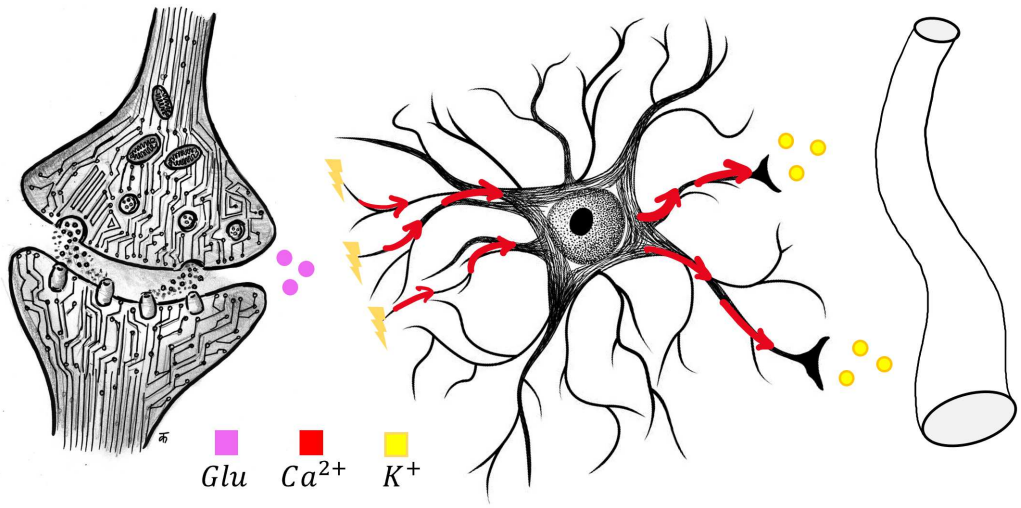

Figure 2.5: Visualization of astrocyte's signaling from synaptic activity to regulation of smooth muscle cells conditions. From left to right: synapse, astrocyte, smooth muscle cell.

Along with the release of potassium from the endfeets, other transporters expressed on the SMC's membrane would be moving potassium ions as well. Among others, $Kir_{4.1}$ channels would act as a consequence of changes in membrane potential and the perivascular concentration of potassium ions. Therefore, the consequent hyperpolarization of the SMC would cause dilation of the nearby blood vessels, making the astrocytes actually able to regulate Cerebral Blood Flow

(CBF) by being potassium spatial buffers. The smooth muscle cells membrane potential acts as a key actor in the arteriole tone because it may open or close the calcium voltage dependent channels in the SMC. This behavior may lead to changes in their intracellular calcium concentration, thus mediating the SMC's myogenic contractile behavior. Hyperpolarization results in the closure of the calcium channel, which would lead to decreased intracellular Ca^{2+} concentration, and finally dilation, vice versa; depolarization results in constriction.

The purpose of regulating the dilation of nearby blood vessels would be to provide an adequate supply of nutrients and oxygen in response to neural activity, which is a fundamental physiological process that could be exploited diagnostically. Relating changes in CBF to the level of neural activity would give the basis to various imaging techniques such as functional magnetic resonance imaging (fMRI), which uses both perfusion and blood-oxygenation level dependent (BOLD) contrast to map brain functionalities. However, in the fundamentals of these ideas, there are astrocytes that increase endfoot's Ca^{2+} concentration, consequently activating Ca^{2+}-sensitive potassium (BK) channels. A characteristic feature of the CNS is the existence of these nearby perivascular spaces, which can also be defined as unique [1]. The latters being created by the astrocytic endfeet's, which encase 99% of the entire cerebral vasculature. From the very same perivascular spaces, a series of recent studies, also identified the presence of an organized pathway for interstitial fast fluid solute clearance, it's name was designated to be "glymphatic system". The glymphatic system is now considered a part of the NVU with a high dependence on the astroglial AQP4 water channels. Proteins colocalized with the $Kir_{4.1}$ channels that move water molecules and fluid through cellular membranes.

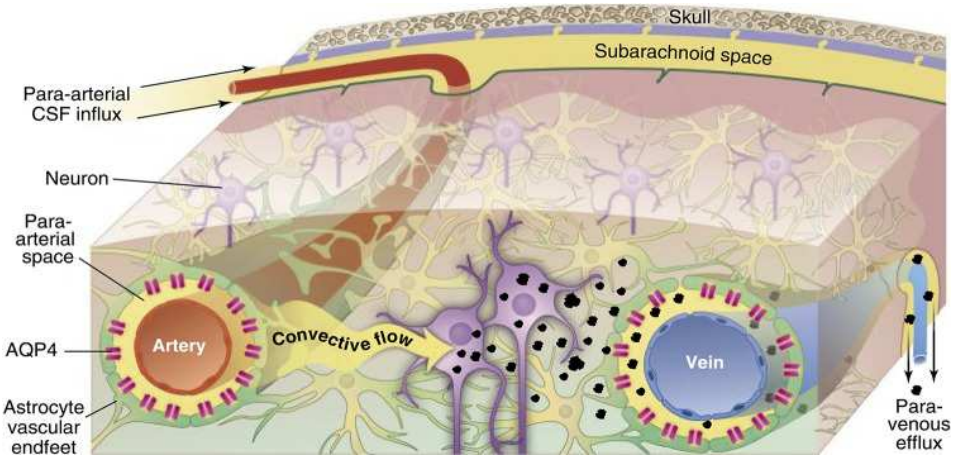

Figure 2.6: Schematic outline of the glymphatic system, with labels identifying how astrocytes and neurons take part into the NVU. The broad distributed syncytium of astrocytes and neurons supports the glymphatic system and allows the generation of convective flows of nutrients and waste products, respectively for and from the neural activity. Taken from [1].

3

Background of Astrocyte Modeling

The computational neuroscience field until the last few years has concentrated heavily on modeling neuronal functions, overseeing other possible brain cells, such as glial cells and focusing only on neurons and their behavior. Despite the short history of astrocytic modeling, the scientific community provided hundreds of models, developed to study different aspects of these kind of cells. Ranging between calcium dynamics, neural activity regulation, tripartite synapses, potassium buffering, and also vascular events. However, one recurrent problem among different studies in this pioneering field is the reproducibility and replicability of the vast majority of their respective models [3].

The evolution of astrocyte research followed three different waves, classified over which evidence they were looking for. The first one revealed positive correlation between neurotransmitter glutamate release and astrocytic calcium $[Ca^{2+}]$ concentration, yielding to waves propagation of it through cell cultures in vitro. The second wave investigated the selectivity power between astrocytes and other neuronal components of pharmacological tools. And finally, the last one that led to the search for correlation between $[Ca^{2+}]$ transients in astrocytic processes near the vascular capillaries and neural activity.

Astrocytes are still lacking reliable ways to be part of experiments in *vivo*,

therefore, the technical tools in the literature are still under development. Despite the challenges, the interest in their role increased drastically in past few decades, and many models and simulators were already trying to answer why some contradictory results between *in vivo* and *in vitro* settings could be found. All published models could be classified in three families: describing single astrocytes, astrocyte networks, and neuron-astrocyte synapses, or neuron-astrocyte networks.

The different families were developed independently and sequentially focusing on different aspects of the research branching out from parent trends, as in figure [3.1].

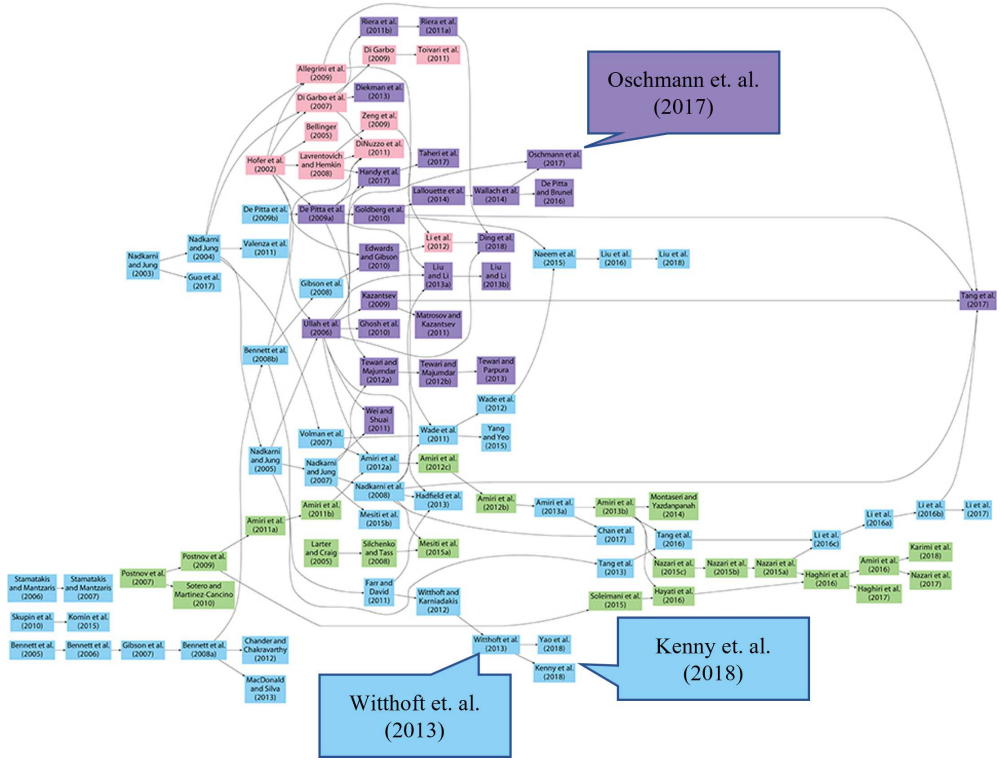

Figure 3.1: Scheme of the various lineage of models developed from early 2000's to this date. From top to bottom the Oschmann's, the Witthoft's and the Kenny's. Goordleeva et al. study was not included since being published after the Manninen review [3]. Witthoft and Kenny develop from the same lineage, while Oschmann appears to be the last of its, developing its topic to the very last state of the art.

The goal of this work is to investigate the role of astrocytes in buffering potassium when high neural activity is locally happening. The state of the art in modeling this behavior could be discerned among a few of the different models

that can be seen in figure [3.1]. First, the Oschmann et al. single cell model (2017, [4]), then the Gordleeva et al. (2019, [5]) multicompartmental take on it, and finally the branch of models developing from Farr and David (2011, [26] including Witthoft et al. (2013, [6]) and Kenny et al. (2018, [27]). All the previously mentioned are going to be the starting point of this thesis's model, discussed in chapter [4].

3.1 Model by Oschmann et al.

Oschmann and colleagues's model focus on investigating $[Ca^{2+}]$ messenger signaling in response to stimulation coming from neighboring hypothetical synapses. It models astrocytes as single cells using a state space model of 10 different states, ranging from ion concentrations to membrane differential potential and secondary messenger variables. The model makes use of a compartmental approach including three different compartments: the extracellular space, the intracellular space and the internal endoplasmic reticulum, as it can be seen in figure [3.2]. All state variables are reported in table [3.1].

The idea is that astrocytes integrate and process information coming from neighbour synapses, especially during neural high activity period, which are being released in the synaptic clefts is form of larger amounts of neurotransmitters. Astrocytes, being part of tripartite synapses uptake the excess neurotransmitter, and integrate that information to signal their control action in response to it. Calcium signaling is attributed by the scientific community to be the first messenger of astrocyte communications and is mediated by two major metabolic pathways, both activated in the presence of glutamate stimulation. The first one, related to metabotropic glutamate receptors, while the second one to Na^+/Ca^{2+} exchangers on the cellular membrane. Both are indirectly related to glutamate elevation, as previously discussed in section [2.2.1]. The overall effect of the two metabolic pathways, over the change of intracellular calcium concentration, is described in the following dynamic equation.

$$\frac{d[Ca^{2+}]_i}{dt} = \frac{A}{F \cdot Vol} \cdot I_{NCX} + \frac{A \cdot \sqrt{ratio_{ER}}}{F \cdot Vol} \cdot (I_{IP_3R} - I_{Serca} + I_{C_{ER}leak}) \tag{3.1}$$

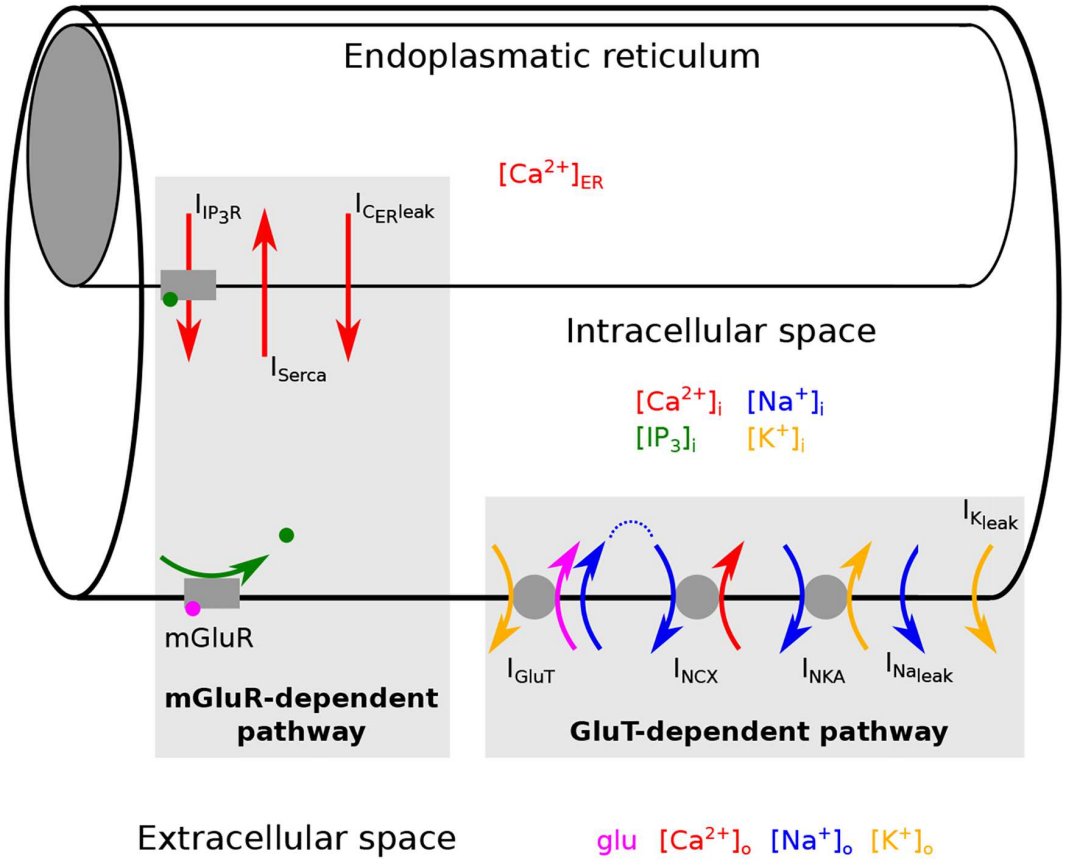

Figure 3.2: Single astrocyte compartmental model scheme. The two designed metabolic pathway are separated and identified by the grey rectangles. Taken from [4].

Where A represents the surface area through which the ionic currents are flowing (in this case the lateral surface area of the intracellular space), therefore the surface where the respective membrane transporter channels are expressed. Then, F represents the Faraday constant and Vol the volume where the ion concentration is evaluated. The previous formulation can be generalized for all possible changes in ion concentrations tracked as state variables in the model, by translating the respective implied ionic currents into flows with the following:

$$\frac{d[ion]}{dt} = \frac{A}{F \cdot Vol} \cdot \sum I_{ion} \tag{3.2}$$

This generalization has also been modeled to be able to define geometrical dimensions of the respective compartments, in fact, using the model, Oschmann

State	Initial Value	Description
$[Ca^{2+}]_{is}$	0.073 μM	Intracellular calcium concentration
$[Ca^{2+}]_{er}$	19.63 μM	Endoplasmatic reticulum calcium concentration
$[Ca^{2+}]_{es}$	1800 μM	Extracellular calcium concentration
$[Na^{+}]_{is}$	15 μM	Intracellular sodium concentration
$[Na^{+}]_{es}$	150 μM	Extracellular sodium concentration
$[K^{+}]_{is}$	100 μM	Intracellular potassium concentration
$[K^{+}]_{es}$	3 μM	Extracellular potassium concentration
V	-85.88 μM	Membrane differential potential
$[IP_3]_{is}$	0.15659 μM	Intracellular Inositol tri-phosphate concentration
h	0.07892 μM	Portion of IP_3 receptor activated channels

Table 3.1: This report the list of initial values for each states of the model. The values are not the ones in Oschmann's article [4], however they are taken from her latest research by private comunications.

investigated on how the calcium signaling was changing, regarding either the behaviors of the two different pathways or the overall dimensions of the main intracellular compartment. The latter, assumed to be containing the endoplasmic reticulum compartment.

Changing dimensions allowed us to analyze calcium signaling, along the different perisynaptic processes, since it is defined that, moving away from the soma, the different astrocytic regions become smaller and also reduce the volume of the endoplasmic reticulum. Oschmann and colleagues simplified the geometry of the astrocyte, using a cylinder compartment, and assumed that the endoplasmic reticulum could be defined as again a cylinder with same length of the intracellular space but different radius. This allowed to define the relationship between the two compartments by saying that $ratio_{er}$ is the ratio between the volume of intracellular space and the volume of the ER. Having the two cylinders the same length, $ratio_{er}$ also allows us to say that $\sqrt{ratio_{er}}$ is the ratio between the lateral surface area of the intracellular space and the one of the ER.

The idea was to define that the lateral surface-to-volume ratio (SVR) and the

volume ratio between the ER and the intracellular space depend on each other throughout the astrocyte process, which would allow defining the expression area of the different transporter channels using only the $ratio_{er}$ and dimensions of the intracellular space. The Oschmann's definition of $ratio_{er}$ is reported in figures [3.3] and follows an exponential decay.

$$ratio_{ER} = 0.15 \cdot e^{-(0.002\mu m \cdot SVR)^{2.32}} \tag{3.3}$$

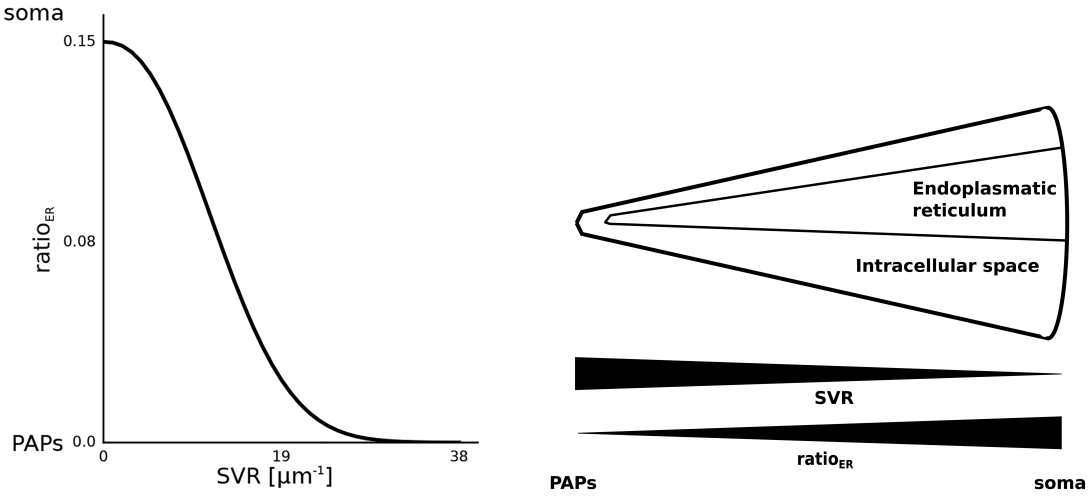

Figure 3.3: On the left the volume ratio between the endoplasmic reticulum and cytosol ($ratio_{er}$) over the surface to volume ratio (SVR). While on the right the dependence of SVR and $ratio_{er}$ on the distance from the soma. Taken from [4].

The calcium signaling is therefore dependent on two main sources deriving from the mGluR-dependent and GluT-dependent pathways, referred in section [2.2.1], by considering the equation [3.1]. The single ion channel transporters vary between having voltage gated or chemically gated activation mechanisms, which may require the tracking of the membrane difference potential, that in case of Oschmann's and colleagues model follows the dynamic:

$$\frac{dV}{dt} = -\frac{1}{C_m}(-2I_{IP_3R} + 2I_{Serca} - 2I_{C_{ER}leak} + I_{NCX} - 2I_{GluT} + I_{NKA} + I_{Na_{leak}} + I_{K_{leak}}) \tag{3.4}$$

Where the C_m represents the membrane capacitance and the other terms represent the respective ionic currents along with the sign and amount of electrical

charges that are carried per ion. Specific modeling of respective ionic currents terms is going to be mathematically described in chapter [4].

The Oschmann and colleagues model focuses on calcium signaling, especially the influence of $ratio_{er}$ over mGluR-driven Ca^{2+} oscillations in terms of frequency and amplitude. To do so, the GluT-dependent pathway was inhibited. This showed, as expected, that by stepping away from the soma the amplitude and frequency of calcium oscillations decreased. With enough low values of $ratio_{er}$, the oscillations disappear, showing that eventually the system leaves the working condition of a stable cycle for a critical value of $ratio_{er} = 0.06$. On the other hand, the model investigated the relationship between sodium accumulation in the intracellular space and the activity of Na^+/Ca^{2+} exchangers. This has shed light on the fact that having calcium transported through the cellular membrane shifted the critical value of $ratio_{er}$ for the onset of Ca^{2+} oscillations to higher values, culminating in really high values of $I_{NCX_{max}}$ in complete suppression of calcium oscillations. Here $I_{NCX_{max}}$ represents the maximal pump current of Na^+/Ca^{2+} exchangers. This was expected, since to make the sodium-calcium exchangers work in reverse mode and prevent an outflux of calcium it is needed a higher sodium intracellular concentration, that is mediated by the GluT transporters channels. In fact, Oschmann et al. showed that by increasing the maximal pump current of glutamate transporters ($I_{GluT_{max}}$) the model allowed calcium oscillation for high values of $I_{NCX_{max}}$. Therefore, a block of the glutamate transporters would lead to a clear attenuation of calcium astrocyte signaling.

The differences between the Oschmann and colleague's model and the one in exam in this thesis, is that Oschmann's does not investigate potassium signaling and does not take into account spatial contributions coming from neighboring parts of the astrocyte. The Oschmann et al. work was the starting point of the preliminary work to this thesis done from Peter Winkler and Lea Fritschi, togheter with the Goordleeva et al. study [5].

3.2 Model by Goordleeva et al.

Intense modeling efforts have been devoted in the evolution of astrocyte research, especially in trying to understand the functional role of astrocytic modulation of

neuronal communication. It is known that elevation of intracellular calcium can trigger the release of various active gliotransmitters, such as glutamate, gamma-aminobutyric acid (GABA), ATP, and D-serine. All neurotransmitters that have an effect on synapsis by representing the modulation action of astrocyte in tripartite synapsis. Goordleeva and colleagues focused over the impact of spatiotemporal patterns of calcium dynamic [5], given that the calcium signal can travel along the processes and trigger the release of neurotransmitters at remote locations.

Goordleeva and colleagues proposed a neuron-astrocyte network with 100 synaptically coupled Hodgkin-Huxley excitatory neurons [28] and two astrocytes connected via gap junctions. Moreover, each astrocyte was modeled using a multicompartmental approach of intercoupled small compartments, all with a cylindrical shape. The different compartments were coupled with diffusion of calcium and IP_3 between neighboring sections of the astrocyte by diffusion gradient. This exchange of material is defined to control, along with metabotropic glutamate channels, the release of calcium stored in the endoplasmatic reticulum. Recalling how it was modeled from Oschmann and colleagues's, the ER is defined with the same cylindrical shape and same length of the intracellular space, the only difference between the two is once again in volume and therefore in radius. This means that the same considerations regarding the geometry relationship between ER and intracellular space made in section [3.1] are applicable in the Goordleeva et al. model.

Goordleeva et al. pursued a multicompartmental model approach to investigate the spatio-temporal patterns, which are created by the propagation of calcium and IP_3 across the different astrocytic processes. Analysis, that were possible to be made by defining a geometrical structure that taken into account an organization of how many processes and how they were structured were present in the model. The actual Goordleeva example is reported in figure [3.4]. Notice how there is no modeling of the GluT-dependent pathway, making the only calcium source coming from the endoplasmatic reticulum of each compartment and diffused across the astrocyte.

Therefore, the calcium dynamics are described in a different way, not having the terms coming form the GluT-dependent pathway but having an additional term coming from diffusion as follow:

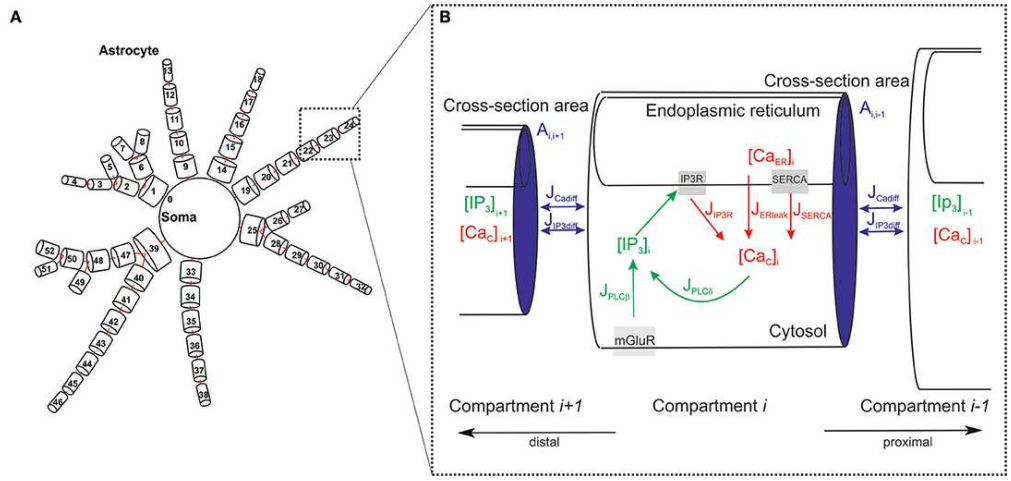

Figure 3.4: Single cell model scheme, with focus on how each process from the soma is subdivided in cylinders interacting with each other through diffusion. As the zoom in figure depict, there is expression of solely mGluR pathway. Taken from [5].

$$\frac{d[Ca]_{is,i}}{dt} = \frac{A_{ER_i}}{F \cdot V_i}(J_{IP_3R} - J_{Serca} + J_{ER_{leak}}) + J_{Ca_{diff}} \tag{3.5}$$

Where every term depends on the index i, of which compartment is being evaluated, with $i = 1, ..., N$, and N being the number of compartments considered in the geometry organization. Then, A_{ER}, represents the lateral surface area of the endoplasmic reticulum, which can be derived from the dimensions of the intracellular space, F represents the faraday constant, and V represents the volume where the ion concentration is evaluated into, in this case the intracellular space. Finally, the flux terms represent all possible influx or outflux of calcium exchange between the endoplasmic reticulum and the cytoplasm, depending on the sign. A particular note on $J_{Ca_{diff}}$, which represents the sum of all fluxes related to diffusion with neighboring astrocytic compartments of compartment i. The single flux terms are discussed in chapter [4] as previously mentioned in section [3.1] along with the mGluR-dependent pathway.

The diffusion term, instead, is defined by Goordleeva and colleagues to be dependent on concentration gradient and is as follows:

$$J_{Ca_{diff}} = d_{Ca(i,i+1)}([Ca]_{is,(i+1)} - [Ca]_{is,i}) + d_{Ca(i,i-1)}([Ca]_{is,(i-1)} - [Ca]_{is,i}) \tag{3.6}$$

Here $d_{Caij} = \frac{D_{Ca}A_{ij}}{V_i \cdot x_{ij}}$ represents the diffusion scaling factor, depending on the geometrical characteristic of the space through which the flow is created. The parameters of d_{Caij} are: D_{Ca}, A_{ij}, x_{ij} representing, respectively, the diffusion constant, the cross-sectional area between compartments i and j, and the distance between the centers of compartments i and j, with $i \neq j$.
It is to notice that the cross section area between neighboring compartments is the one of the smaller between the two adjacent ones.

Analogous modeling is defined by Goordleeva and colleagues for $[IP_3]_{is,i}$ concentration, that along with the production and degradation terms coming from the mGluR-pathways [4], it also takes into account the diffusion term from neighbor compartments:

$$J_{IP_{3_{diff}}} = d_{IP_{3,(i,i+1)}}([IP_3]_{is,(i+1)} - [IP_3]_{is,i}) + d_{IP_{3,(i,i-1)}}([IP_3]_{is,(i-1)} - [IP_3]_{is,i}) \tag{3.7}$$

Regarding the $[IP_3]_{is,i}$ concentration, Goordeeva and colleagues used the same dynamic found from De Pitta et al., [19], and implemented by Oschmann et al. [4]. However, Goordleva et al. considered the additional diffusion term coming from neighbor compartments, trying once again to investigate the spatiotemporal patterns of calcium signaling events. The added diffusion term is defined as follows, and it is modeled, as previously said, in the same way the calcium one was formulated.

$$\frac{d[IP_3]_{is,i}}{dt} = J_{PLC\beta} + J_{PLC\delta} - J_{deg3K} - J_{deg5P} + J_{IP3diff} \tag{3.8}$$

Where the change in intracellular concentration of IP_3 is dependent on two production terms and two consumption term as previously discussed in section [2.2.1]. Mathematical modeling of the single flows is described in chapter [4].

Goordleeva and the colleague's model differs from the one in the exam in this thesis on the focus of the study. No Glutamate transporters channels were considered and therefore no tracking of other ions concentration, apart from calcium, was needed, which means that only calcium signaling was taken into account. The ultimate goal was to investigate how neural activity was triggering calcium events and how those calcium events were then propagating through astrocytes

or astrocyte networks. The secondary research aims attempted to search on how gliotransmitters are then released, and on how the regulatory control actions of astrocyte over tripartite synapses are provided. Goordleeva and colleagues showed that the regulatory activity of astrocytes over synapses resulted, either in long term potentiation of the action potential transmission between pre and post synaptic neurons or in inhibition of it. Moreover, another critical difference is that potassium signaling was not studied and therefore no neurovascular unit was taken into account.

3.3 Model by Witthoft et al.

Witthoft and colleague's study developed from a lineage of models that focused on the neurovascular unit and on the regulatory activity of neurovascular network communication, particularly in terms of astrocytes that mediate cerebral blood flow.

As discussed in chapter [2], one of the central functions of astrocytes is spatial potassium buffering, accomplished by up-taking it from high concentration regions and releasing to low concentration regions. If potassium is released in perivascular areas, it increases and hyperpolarizes nearby smooth muscle cells, which, by expressing the $Kir_{4.1}$ channels, may use it to rebalance the basal values. The transportation of potassium may happen through diffusion and through various channels, in which are found the potassium inward rectifiers channels (Kir), the calcium-sensitive big conductance channels (BK) and the active uptake mechanisms such as sodium-potassium ($Na-K$) pumps and sodium-potassium-chloride cotransporters ($NKCC$). Kir, Na-K pumps and NKCC being expressed in perisynaptic processes and Kir, while BK channels being expressed in perivascular endfeets.

Witthoft and colleagues designed their model by focusing on investigating the potassium dynamics in different domains across the neurovascular unit: in the astrocytic intracellular space, in the extracellular space close to the synapses (synaptic cleft), in the perivascular area and in smooth muscle cells. The model focuses on potassium, but also describes the dynamics of other concentrations of molecules, such as calcium ions, IP_3, sodium ions, and epoxyeicosatrienoic acids

(EETs). The EETs are chosen to be tracked because evidence showed that they impact the gating mechanisms of BK channels; however, there are yet not enough proofs stating that their effect is direct on the activation mechanisms or indirect through moving Ca^{2+} ions with TRPV4 channels.

It is to notice, that differently from other model, the calcium concentration is described considering the following transporters: the IP_3 receptor channels, a calcium pump representing the same functionality of SERCA pumps, but not with the same mathematical description and leak fluxes from the endoplasmic reticulum towards the cytosol. We find below the calcium concentrations dynamics stated as:

$$\frac{d[Ca^{2+}]_{is}}{dt} = \beta(J_{IP_3} - J_{pump} + J_{leak}) + J_{TRP} \tag{3.9}$$

Where the first three terms are representing exchange of calcium between the endoplasmic reticulum and the cytosol, scaled by the β factor.Which according to Witthoft represents the calcium buffering capability of the astrocytic intracellular space. While, the last term represents the calcium influx through the TRPV4, one of the six different channels belonging to the Transient receptor potential ion channel subfamily [6]. In particular, the TRPV4 model, which was introduced in section [2.2.1] and used in Witthoft and colleague's model. The TRPV4 channels are approximated in the model with a simplified description, compared to the much closer to reality one, which is known to have a very high complexity and diverse range of gating properties.

Witthoft and colleague describe all mathematical formulations of tracked ion concentration changes by using inward and outward flows of material, which in the most part may result from ionic channels. The respective ion currents are then translated into material flows by dividing for the astrocyte cell capacitance, scaled by a γ factor. The latter represents the net movement of ion fluxes.

$$J_\star = \frac{I_\star}{C_{ast}\,\gamma} \tag{3.10}$$

The model is single cell and is triggered by a glutamate stimulation coming from the perysinaptic domain that represents local neural activity. The following

figure reports the full scheme as:

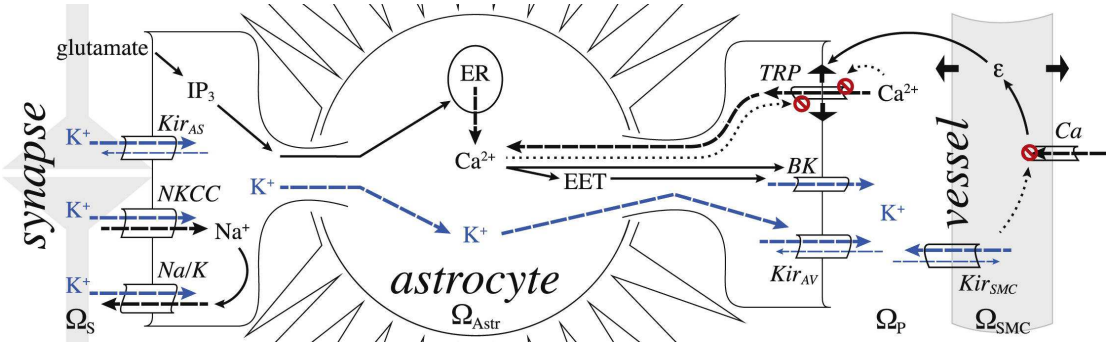

Figure 3.5: Single cell model scheme, with focus on the four different domains. Synaptic domain (Ω_S), Astrocyte domain (Ω_{Astr}), Perivascular domain (Ω_P) and Smooth muscle cell domain (Ω_{SMC}). Taken from [6].

Regarding the perivascular domain, Witthoft and colleagues designed the model to keep track of potassium and calcium accumulation, searching for their role in the chosen mechanistic model of blood vessel's strain. The potassium dynamics in the different domains depends on the local expressed transporters and, therefore, varies. The following are going to describe the different formulations:

$$\frac{d[K^+]_{es}}{dt} = J_{K_s} - (J_{NaK,K} + J_{NKCC} + J_{Kir,AS})\frac{1}{V\ R_{sa}} - R_{dc_{K^+,S}}([K^+]_{es} - [K^+]es, 0) \tag{3.11}$$

$$\frac{d[K^+]_{is}}{dt} = J_{NaK,K} + J_{NKCC} + J_{Kir,As} + J_{BK} + J_{Kir,Pv} - R_{dc_{K^+,is}}([K^+]_{is} - [K^+]_{is,0}) \tag{3.12}$$

$$\frac{d[K^+]_{pv}}{dt} = -\frac{J_{BK} + J_{Kir,Pv}}{V\ R_{pa}} - \frac{J_{Kir,SMC}}{V\ R_{ps}} - R_{dc}([K^+]_{pv} - [K^+]_{pv,0}) \tag{3.13}$$

Where respectively, the three different dynamics in equations ([3.11]-[3.13]) are related to the change in potassium of the perisynaptic space, the cytosol and the perivascular space. Then, the different terms represent the inward or outward fluxes of potassium, respective to which transporters are expressed at the various interfaces of each domain. It is to notice that the Kir channels are designed to be expressed in all domains, but independently, in order to be able to tune their densities the different membranes. Finally, to take into account undesigned terms, the model defines decay rates from each domain, which are dependent on the difference between the ion concentration and the resting state equilibrium.

As introduced before, and possible to be seen on figure [3.5], the different potassium transporters involve the following: smooth pulse approximation of

potassium release from active neurons (J_{K_s}); sodium-potassium-chlorine cotransporters (J_{NKCC}); sodium-potassium atp dependent pumps ($J_{NaK,K}$); KIR4 channels ($J_{Kir,\star}$) and big conductance channels (J_{BK}).

As discussed in section [2.2.1], the potassium signaling in the perivascular space fulfills a critical role in the activity of smooth muscle cells towards cerebral blood flow. Witthoft and colleagues designed the arteriole tone adopting the blood vessel's strain mechanistic model from Gonzalez (1994; [29]), which describes how the level of intracellular calcium in SMC mediate the myogenic contractile behavior. Which may constrict or dilate the neighbor vessels after changes of perivascular potassium concentration, an accumulation of shows to increase the difference in polarity between the two sides of the SMC's membrane, hyperpolarizing it, which ultimately leads to dilation of nearby blood vessels.

Therefore, Witthoft and colleagues' results suggested that after high neural activity, local functional hyperemia was showing, and it was governed by astrocytic Kir channel activity for the fast onset, and by big conductance channels for maintaining the blood vessel dilation. The differences between the previous model and the one in this thesis discern between focusing on potassium signaling, disregarding of the others, unless they were involved in the activation mechanism of any of the potassium transporters. Moreover, it does not search for spatiotemporal patterns without any delay regarding dimensions or geometry of the astrocyte and provides a detailed mathematical description of the smooth muscle cell and blood vessels relationship. Which could have been implemented as well, however, needed more resources at this stage of development. The model in the examination, in fact, assumes a simplified description of the interface of the perivascular space and the SMC and neglects the mechanistic model of the vessels, considering them as future improvements.

4
Methods

In this chapter we are going to discuss the description of every section of the used model, designed to synthetize an astrocyte as a signle cell with a multi compartmental approach. The aforementioned design is a modified version of preliminary work done from Peter Winkler and Lea Fritschi from the Institute of Neural Engineering in Graz University of Technology. The modifications will be designing the interactions between the glial cell and the neurovascular unit, while the implementation will be representing all the mathematical descriptions of the following sections. A brief explanation of the modified code is summarized in appendix [A], while the full parameter list will be displayed in appendix [B].

4.1 General Idea

The general idea behind the design of the model is to start from the state of the art and develop an ensemble of different modeling approaches, in order to provide a not-data driven formulated functioning glial cell interacting with the neurovascular unit at the brain-blood barrier. The model considers the cell as a soma plus its processes, which could be branching out toward either the synapses or the vascular areas. The model follows the lineage of all single astrocyte's present

in literature, and do not consider to have more than one astrocyte connected between each other through gap junctions. Mathematically, it is equivalent to a state-space model.

Every single one of the compartments of the model consists of an intracellular space, an extracellular space and possibly an endoplasmic reticulum, however, the different ones are simplified to be connected only through neighboring intracellular spaces, neglecting every possible exchange of material between different extracellular spaces. Therefore, every spatiotemporal pattern, reported in detail in Section [4.3.4], will be focused on the intracellular space.

The different qualitative domains that the model will be interpreting are: the perisynaptic domain, from which a glutamate stimulation will come to trigger local specific metabolic pathways of the astrocyte. The astrocyte domain, where different signaling states of the model are going to be tracked, and the perivascular domain, where the astrocyte will interact, through its endfeets, with an assumed narrow extracellular space and a simplified version of a smooth muscle cell (compared to other models found in the literature). Smooth muscle cell will not be defined through any mechanistic model such as the Witthoft model [6]. The tracked state variables of the model are going to be calcium, sodium and potassium ion concentrations both in intracellular and extracellular spaces, then IP_3 and EET only in the intracellular spaces. The model consists in a set of coupled ordinary differential equations (ODEs) that evaluate the change of the different state variables between two different time steps.

Moreover, every single compartment is designed to follow the following assumptions:

- Every compound is uniformly distributed in the compartment volume V_i.
- Therefore, the compartment can be completely described by the mass of the compound Q_i or by its concentration $C_i = \frac{Q_i}{V_i}$.
- Fluxes are independent of space and spatial direction of flux.

Each different concentration of compound will depend on various metabolic pathways, which are presented in this chapter [4] in different sections. The general normal compartment scheme is reported in figure [4.1], where, however, particular characteristics of the *endfeet* compartment are not reported.

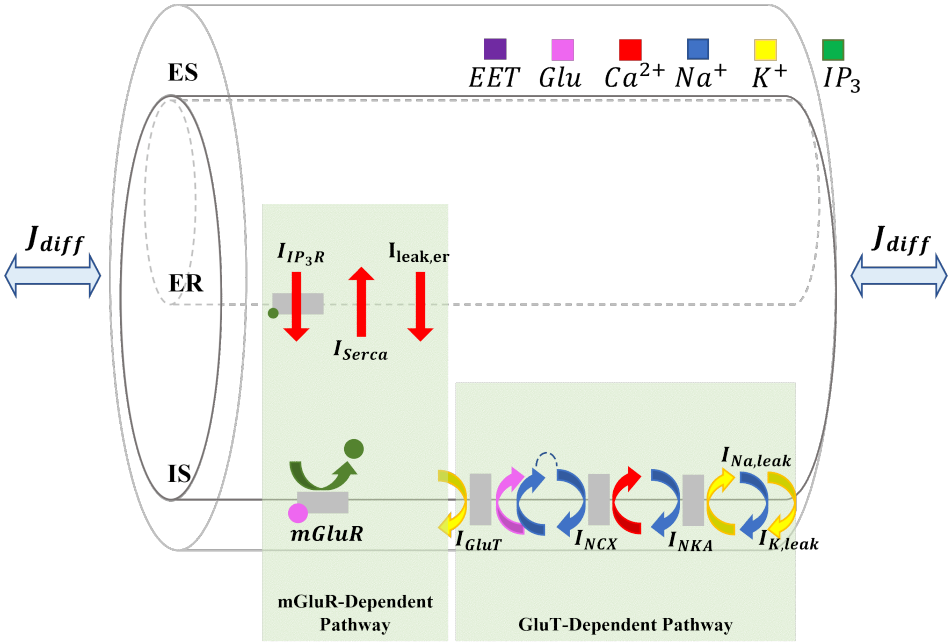

Figure 4.1: Visualization of a not endfeet compartment scheme with zoom on expressed biological pathways. The membrane transporters are color coded with the legend in the top right and are drawn over the membrane that they are expressed into.

4.2 Geometry

The *Astrocyte* class models the whole cell; however, the compartments may differ from each other, in terms of dimensions, position or function. The dimensions and position are analogous, since it has been defined that the farther away the soma, the smaller the process it gets. While functionality instead, may change which of the different metabolic pathways are expressed in the specific compartment.

All compartments of the model are modeled as coaxial cylinders, containing an inner intracellular space and an endoplasmic reticulum (ER) of the same length but different radius, and an outer extracellular space of the same volume of the intracellular one. However, considering that the soma remains the compartment from which every other process branches out, the organization of the processes may differ regarding their functionality. If the branching-out processes are then labeled as perisynaptic, then they are subdivided into sequentially smaller coaxial cylinders compartments, allowing the possibility of splitting at a certain distance. Instead, if labeled as endfeets, they are assumed to be as a single coaxial cylin-

der with length longer than the perisynaptic compartments. The actual endfoot would be only the ending section of the process; however, in the model, they are merged together in one single compartment, which leaves the soma and directly connects to the perivascular domain.

The different compartments of one process or connected to the soma are defined with a set of characteristics, such as: the *radius* (r), the index of which process they belong to (i), the distance from the soma (*level*), the length (x_i), and possibly the $ratio_{er}$. The last one described in sect [3.1] with possibility of being fixed from a look-up table rather than evaluated with the equation used by from Oschmann and colleagues [3.3]. Also the r could be taken from a look-up table once is defined the *level*.

Every compartment is indexed in a dictionary, present in every instance of the *Astrocyte* class, using *name* of the compartment and *number* as key. The very same *number* is also used to evaluate the neighbors of each compartment, critical information used by the evaluation of the diffusion exchanges of material between adjacent compartments. A scheme of the geometrical structure of a compartment is reported in figure [4.2].

Figure 4.2: Visualization of the surface area of each domain in each compartment with other geometrical characteristics. Respectively: Green, the Intracellular space; Blue, the Extracellular space; Orange, the Endoplasmic reticulum.

Other geometrical characteristics are then derived from the provided ones, such as the lateral surface area, the surface area, the volume and the lateral surface

to volume ratio. All of them, needed for defining the translation between the ionic currents and the fluxes going through the single ion channels. The following table represents the look up table for the r, and in case of use, also the one for the $ratio_{er}$. The level of the different compartments acts as link to retrieve the respective value in the look-up table. One notice is that further than level 6, it is assumed that the dimensions do not get smaller and also the $ratio_{er}$ do not get to zero. If the look-up table is not used, then it is possible to use Oschmann and colleague's equation [3.3].

level	radius [μm]	ratio$_{er}$ [/]
0	8	0.15
1	4	0.1
2	3	0.09
3	2	0.08
4	1	0.07
5	0.5	0.06
6	0.25	0.05

Table 4.1: Look-up table between level of distance from the soma and dimensions of the compartment beloging to the process. Level 0 refers to the soma

4.2.1 Possible Geometries

Once defined the structure of each compartment, also the organization of them becomes critical. Especially in a model where adding compartments may affect heavily on the compound concentrations, considering that more volume will be added. During the development, three different geometries were investigated, although, most of the analysis were done and trusted over the simplest geometry. This is due, to the lack of ways to validate most of the results, such as experimental data. The three different geometries are the following, going from simplest to more complex:

- One endfeet attached to soma and soma containing all the other components of astrocyte.

- Two different independent endfeets attached to soma and soma containing all the other components of astrocyte
- Gordlleeva organization up to level two and soma receiving stimulation from further PAPs compartments [5].

As it is going to be discussed in section [4.3], the organization of the spatial geometry has an important role regarding the location of the glutamate stimulus. In the previous first two geometries, the stimulation was provided into the soma, while in the third one, was provided at the furthest perisynaptic processes from the soma. The previously defined examples of geometry are represented in figures [4.3]:

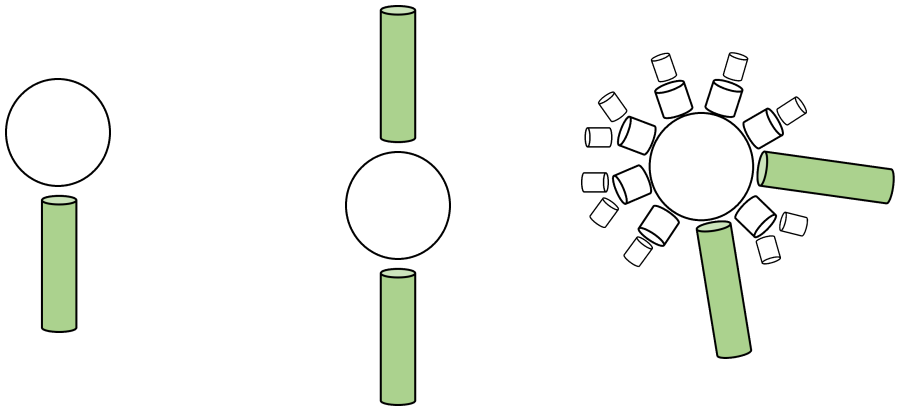

Figure 4.3: Visualization of the three geometries, tested in this model. From left to right, the simplest with one soma and one endfeet (green), then some with two endfeets and at last soma, two endfeets and seven PAPs up to level two of distance from the soma.

4.3 Biological pathways

Astrocytes fulfill many roles in the nervous system, and to do so, various different biophysical pathways were shown to be expressed. In this model the ones that were designed to be useful towards the investigation of potassium buffering were the metabotropic glutamate receptor dependent, the glutamate transporters dependent and as it has been defined in this work, the perivascular pathway. All the previous involve dynamics of different compounds, including ions concentrations and others.

The different coupled Ordinary differential equations will be defined using various terms, involving fluxes and ionic currents of $[\frac{pA}{\mu m^2}]$, in case of being the results of ions transporters, or in other words of electrical charges transporters. Then, the ionic currents will be translated into flows by using a formulation inspired from Oschmann and colleagues [4], which state that dividing them by the Faraday constant and scaling them by the ratio between the respective channel's area of expression and the volume where the concentration of the compound is being evaluated, provides the amount of moles over volumes passing by a surface over time. Therefore, given that the Faraday constant is in $[\frac{A\,s}{mol}]$, then the actual flow becomes of $[\frac{mM}{s}]$ unit of measurement. The general formulation of the translation factor between the ionic currents to ion flows would be formulated as follows:

$$\sum^{N} J_{ion} = \frac{Area}{Volume \cdot F} \cdot \sum^{N} I_{ion} \tag{4.1}$$

Where as previously mentioned, the $Area$ represents the transporters area of expression, while $Volume$ represents the volume where the concentration of the ion is evaluated. Foreseeing the upcoming relationship, let's define the lateral surface (S) to volume (Vol) ratio (SVR), as in $SVR_i = \frac{S_{i,is}}{Vol_{i,is}}$.

The tracked ion concentrations are designed to be different regarding which space they are evaluated into for each compartment ([5];[4]). The following lists respectively calcium for the endoplasmic reticulum,

$$\frac{d[Ca^{2+}]_{i,er}}{dt} = \frac{SVR_i \cdot \sqrt{ratio_{er}}}{ratio_{er} \cdot F} \cdot (-I_{IP_3R} + I_{serca} - I_{Ca_{er}leak}) + J_{Ca_{er}diff} \tag{4.2}$$

Where it is involved diffusion between adjacent compartments and transporters expressed over the lateral surface of the ER, in particular the IP_3R receptor channels, linked to the metabotropic glutamate pathway.

Then, calcium, sodium, potassium, IP_3 and EET for the intracellular space,

$$\frac{d[Ca^{2+}]_{i,is}}{dt} = \frac{SVR_i}{F} \cdot I_{NCX} + \frac{SVR_i \cdot \sqrt{ratio_{er,i}}}{F} \cdot (I_{IP_3R} - I_{Serca} + I_{Ca_{er}leak}) + J_{Ca_{diff}} \tag{4.3}$$

Where the expression of some ionic channels is defined over the astrocytic cellular membrane, and some over the membrane that separates intracellular space and endoplasmic reticulum.

$$\frac{d[Na^{2+}]_{i,is}}{dt} = \frac{SVR_i}{F} \cdot (3I_{glut} - 3I_{NKA} - 3I_{NCX} - I_{Naleak}) + J_{Na_{diff}} \tag{4.4}$$

Where, similarly to calcium and potassium dynamics, some terms are expressed over different surfaces and also are considered the stechiometry of each ionic current by considering how many net ions are exchanged. In this case, are entering 3 sodium ions for each glutamate transporter cycle, and leaving 3 sodium ions for each activation of NKA or NCX channels across the cellular membrane.

$$\frac{d[K^{+}]_{i,is}}{dt} = \frac{SVR_i}{F} \cdot (-I_{glut} + 2I_{NKA} - I_{Kleak}) + J_{K_{diff}} + \frac{A_{i,is}}{Vol_{i,is} \cdot F} \cdot (-I_{kir} - I_{BK}) \tag{4.5}$$

Where the last additive term is different from zero, if and only if, the compartment i represents an endfeet compartment, having the expression of the perivascular metabolic pathway, detailed in section [4.3.3].

$$\frac{d[IP_3]_i}{dt} = prod_{PLC\beta} + prod_{PLC\gamma} - degr_{IP_3-3K} - degr_{IP-5P} \tag{4.6}$$

Where the different production and degradation terms are explained in detail in section [4.3.1].

$$\frac{d[EET]_i}{dt} = \upsilon_{EET} \cdot max([Ca^{2+}]_{i,is} - [Ca^{2+}]_{min}) - k_{EET}[EET]_i \tag{4.7}$$

Where the epoxyeicosatrienoic acids dynamics would strongly depend on calcium concentration, like it is designed in Kenny and colleague's model, which is one developed from the same lineage of the Witthoft's [3.3]. The EET production is governed by υ_{EET} as production rate in $[\frac{1}{sec}]$ and the distance from intracellular calcium and the minimum concentration needed to trigger EET production ($[Ca^{2+}]_{min}$). While, instead the degradation of EET is simply mediated by a linear decay rate over its concentration, with slope and rate defined as k_{EET} in $[\frac{1}{sec}]$.

The different metabolic pathways considers the activity of many different ionic channels, which operate by moving ions through membranes. Their activity may

involve ATP consumption, gradient or others, either way, the result is a flow of electrical charges through the membranes, producing changes in the membrane potential. Many channels depend on voltage for their activation, and therefore, also the membrane voltage is needed as a state variable of the model, with its ordinary differential equation defined in the following:

$$\frac{dV_i}{dt} = -\frac{1}{C_m} \cdot (-2I_{IP_3R} + 2I_{serca} - 2I_{Ca_{er,leak}} + I_{NCX} - 2I_{glut} + I_{NKA} + I_{Naleak} + I_{Kleak} + I_{kir} + I_{bk}) \tag{4.8}$$

Where the C_m represents the membrane capacitance; the IP_3R, Serca pump, Ca_{er}leak are ionic channels terms related to the metabotropic glutamate receptor dependent pathway [4.3.1]; the NCX, GluT, NKA, Naleak and Kleak are ionic channels terms related to the glutamate transporters dependent pathway; the Kir and BK are ionic channels terms related to the perivascular pathway, only expressed in endfeets. Note, that some ion channels provides a net transfer of charges different from one, which requires to be taken into account for each time step. In this case, the net transfer of charges is represented by the stoichiometric scalar digit multiplied individually to each ionic current. The sign, instead, is due to which direction the charges are flowing toward. Considering the minus sign outside the round brackets, another multiplicative minus sign for ionic currents would suggest that charges are entering the intracellular space. Going through each one of the ionic currents, we refer to the chapter [2] for retrieving the physiological interpretation of the stoichiometry.

Starting from the transporters at the ER-IS membrane level, we find the IP_3R, $Ca_{er,leak}$ and Serca channels. Which, respectively, produce: a net transfer of positive charges equal to one calcium ion and two positive charges entering the intracellular space from the ER for the first two and an equal net transfer of charges but in opposite direction and and therefore to making the membrane potential less negative compared to the extracellular space. Then, we find the Serca pumps that act in opposite direction for the Serca.

Following with the GluT-dependent pathway, we describe the NCX exchangers that provide for a counter-transport of three Na^+ and one Ca^{2+} for each cycle, resulting in a net transfer of one positive charge. In the previous formulation it

is defined that the default mode in which these channel operates will move the sodium outside and the calcium inside of the intracellular space, thus the sign inside the round brackets. Moving on with the GluT transporters, their ionic current reports a net transfer of two positive charges inside the cytoplasm for every cycle. This balance of charges is due to the fact that for each glutamate molecule uptake, there are three coupled sodium and one hydrogen entering the intracellular space, with one potassium ion leaving ($3Na^+ + 1Glu^- + 1H^+ - 1K^+ =$ two positive charges). Then there are the NKA channels, which, by consuming one atp molecule, counter-transport three sodium for two potassium ions, providing a net balance of one positive charge leaving the cell. All the following Na_{leak}, K_{leak}, $Kir_{4.1}$, BK channels report to be straightforward to move the charges of the respective sodium and potassium ions, therefore one positive charge.

4.3.1 mGluR-dependent pathway

The metabotropic glutamate receptor dependent pathway, described in section [2.2.1] has a direct impact over the intracellular calcium concentration. The metabolic pathway scheme is reported in figure [4.4]. The metabolic pathway is triggered from an external glutamate stimulus and involve metabotropic glutamate receptors (mGluRs), belonging to the G-protein coupled family.

When the ligand binds to their binding site, the G-protein activates and stimulates the PLCβ and PLCδ to produce IP_3 inside the cytosol. Which mediates the activation of IP_3R receptor channels over the endoplasmic reticulum membrane, causing the release of calcium into the intracellular space. At the same time, higher concentrations of IP_3R increase the degradation of it by activating the $IP_3 3K$ and the $IP - 5P$. The four terms, involved in the production and degradation of IP_3 are mathematically formulated as follows [19]:

$$prod_{PLC\beta} = \upsilon_\beta \cdot \frac{g^{0.7}}{g^{0.7} + (K_R + K_p \cdot \frac{[Ca^{2+}]_{i,is}}{[Ca^{2+}]_{i,is} + K_\pi})^{0.7}} \tag{4.9}$$

Where υ_β represents the maximal rate of IP_3 production by PLCβ; g the glutamate stimulation; K_R the glutamate affinity to the receptor, which in other words is the extent or fraction to which a ligand binds to receptors at any given ligand

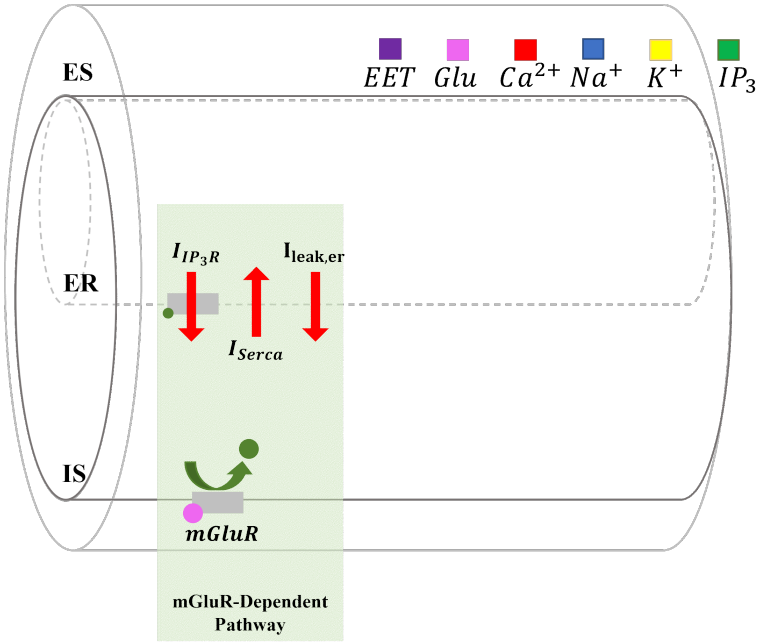

Figure 4.4: Visualization of a zoom of the mGluR-dependent pathway with color coding of which ion and towards which are direction are moved by the transporters. Note that the notation design the activation variable of any transporters as small color coded circles attached to the channels.

concentration or the firmness with which the same ligand binds to the receptor; K_p scaling factor of the inhibition in IP_3 production when calcium concentration gets too high; and at last K_π that represents the affinity between calcium and PLC. It is to notice that the $prod_{PLC\beta}$ term is dependent on both glutamate and calcium, where by fixing one or the other at one value and ranging the other we notice that, if glutamate tends to provide really strong stimulations and calcium is fixed, then the production term saturate at υ_β, while if instead calcium tends to reach high intracellular concentration and the stimulation does not change, then the half saturation coefficient of the production term becomes equal to $(K_R + K_p)^{0.7}$.

$$prod_{PLC\delta} = \frac{\upsilon_\delta}{1 + \frac{[IP_3]_{i,is}}{k_\delta}} \cdot \frac{[Ca^{2+}]^2_{i,is}}{[Ca^{2+}]^2_{i,is} + K^2_{PLC\delta}} \tag{4.10}$$

Where the production term is mediated from both $[IP_{3_{i,is}}$ and $[Ca^{2+}]_{i,is}$ with respectively a negative regulation and a hill function of order 2. The maximal rate of IP_3 production by PLCδ is then represented by υ_δ, scaled by the two other

terms dependent on the concentrations of inositol and calcium. The inhibition of PLCδ on inositol concentration is evaluated according to the half inhibition constant k_δ, while the relationship on calcium concentration is evaluated according to the half saturation constant $K_{PLC\delta}$. Physiologically, $K_{PLC\delta}$ is interpretable as the calcium affinity towards PLCδ.

$$degr_{IP_3-3K} = \upsilon_{3K} \frac{[Ca^{2+}]^4_{i,is}}{[Ca^{2+}]^4_{i,is} + K_D^4} \cdot \frac{[IP_3]_{i,is}}{[IP_3]_{i,is} + K_3} \tag{4.11}$$

Where the inositol triphosphate 3-kinase degradation term is mediated by an hill function of order 4 on calcium concentration and a Michaelis-Menten relationship on inositol triphosphate concentration. The maximal degradation rate of IP_3 is represented by υ_{3K}, while the half saturation constant of the two other terms are respectively, the calcium affinity with $IP_3 - 3K$, noted as K_D for the hill function dependent on calcium, and the IP_3 affinity with $IP_3 - 3K$, noted as K_3 for the Michaelis-Menten relationship.

$$degr_{IP-5P} = \upsilon_{5p} \cdot \frac{[IP_3]_{i,is}}{[IP_3]_{i,is} + K_5} \approx r_{5p} \cdot [IP_3]_{i,is} \tag{4.12}$$

Where the degradation term, due to dephosphorylation of IP_3 could be considered as a Michaelis-Menten relationship on IP_3, however, the half saturation constant is $K_5 > 10\mu M$. Which value is way above the physiological levels of IP_3, and unlikely to be saturated, therefore, it follows that the rate of IP_3 degradation by $IP - 5P$ could be linearly approximated, with $r_{5p} = \frac{\upsilon_{5p}}{K_5}$, representing the maximal rate of degradation [19].

Once the dynamics of intracellular $[IP_3]$ are defined, then it is possible to understand how the diffusion term, coming from the rest of the astrocyte, or the term coming from the mGluRs receptors are regulating the calcium CICR from the endoplasmic reticulum. In previous section we have defined that the exchange of calcium between intracellular space and ER is mediated by the IP_3R receptors, the *Serca* pump and, possibly, the leak of calcium ions between the two.

The IP_3 receptor channel's calcium ions rate is modeled as a maximum permeability, times the channel's open probability, which is gated through binding of IP_3 and Ca^{2+}. The gating mechanisms assumes the existence of three binding

sites on each sub unit of IP_3R: one for IP_3 and two for Ca^{2+}. The latter, including an activation site and a separate site for deactivation. The three different binding sites are not independent, therefore, the probabilities of each site of being in bound or unbound state are multiplied. The driving force of the channel, multiplied by the open probability of it, is evaluated over the difference in calcium concentration between the endoplasmic reticulum and the cytosol.

$$I_{IP_3R} = \frac{F \cdot Vol_{i,is}}{S_{i,er}} \cdot r_c \cdot \left(\frac{[IP_3]_{i,is}}{[IP_3]_{i,is} + d_1}\right)^3 \cdot \left(\frac{[Ca^{2+}]_{i,is}}{[Ca^{2+}]_{i,is} + d_5}\right)^3 \cdot h^3 \cdot ([Ca^{2+}]_{i,er} - [Ca^{2+}]_{i,is}) \tag{4.13}$$

Where, formally, the term that is used in the model is the respective ion current of calcium ions, flowing through the channels at each cycle. The parameter r_c represents the maximum rate of transported Ca^{2+} ions, which is then multiplied by the probability of the channel to be in open state and characterized by two activation hill functions of order 3 and a third variable h raised to the third. The two hill functions are respectively evaluated over the saturation of intracellular $[IP_3]$ and intracellular $[Ca^{2+}]$, also they are respectively representing the binding of IP_3 and Ca^{2+} on the binding site of the IP_3R channels. Their mathematical definitions consider to design the dissociation constants as half saturation constants, noted as d_1 and d_5.

As aforementioned, the gating mechanism is not fully defined by the two hill functions alone; there is also the h variable, which represents the fraction of activated IP_3R channel. The activated state is possible when one Ca^{2+} ion and one IP_3 molecule bind to the first two activation binding sites, while instead, the channels inactivate when a second Ca^{2+} ion binds to the third binding site. It is to notice that the maximum rate of transported ions is a frequency unit, multiplied with the adimensional probability of the channel being in open state and with the driving force of difference in calcium concentration in molar units. Which overall, represents a flow of ions, that is therefore, translated in ion currents by being scaled with the Faraday constant and the volume, where the ion's concentration is evaluated into $Vol_{i,is} = Vol_i - Vol_{er} = V_i \cdot (1 - ratio_{er})$, and then divided by the area of expression of the receptor channel $S_{i,er} = S_i \cdot \sqrt{ratio_{er}}$.

The activation and behavior of IP_3R receptor channels is taken from Li and Renzel formalization [30], which reduces the full model of IP_3R gating mecha-

nisms into a two variable model of $[Ca^{2+}]_{is}$ dynamics and h, fraction of activated channel, noted as follows:

$$\frac{dh}{dt} = a_2 \cdot \left(d_2 \cdot \frac{[IP_3]_{i,is} + d_1}{[IP_3]_{i,is} + d_3} \cdot (1 - h) - h \cdot [Ca^{2+}]_{i,is} \right) \tag{4.14}$$

Where, following the previous statements, a_2 represents the binding rate of calcium ions to the inactivation binding site; d_2 and d_3, respectively, represent the inactivation dissociation constants of Ca^{2+} and IP_3. It is to notice, that physiologically d_1, d_2, d_3 and d_5 are analogous, but associated to different sub-units of the protein channel. In the following figures [4.5], are going to be reported the evolution of the fraction of activated IP_3R channels as steady spaces, dependent on calcium and IP_3.

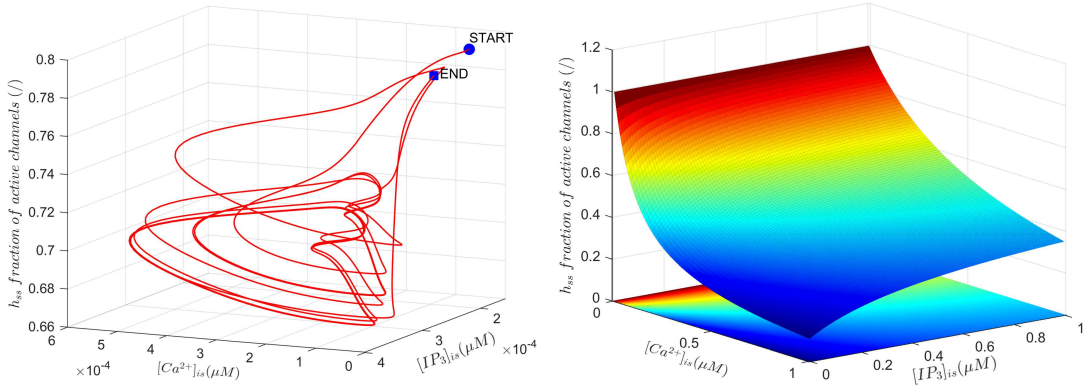

Figure 4.5: Visualization of the dynamic characteristic of the fraction of activated IP_3R channels. On the left phase portrait of h evolution over changes in $[Ca^{2+}]_{is}$ and $[IP_3]_{is}$. On the right, the surface plot of the h_{ss} nullcline function, dependent on two variables in possible working range.

Recalling the equation [4.2], along with the IP_3R receptor channels, there are other two different ion currents present at the exchange between endoplasmic reticulum and intracellular space level: the Serca pump and all the other negligible terms, approximated with a leak. The Serca pump activity is increasing with intracellular calcium concentration, and can be thought as a channel that has a maximum rate of calcium uptake, with opening probability dependent on $[Ca^{2+}]_{i,is}$.

$$I_{Serca} = \frac{F \cdot Vol_{i,is}}{S_{i,er}} \cdot v_{er} \cdot \frac{[Ca^{2+}]^2_{i,is}}{[Ca^{2+}]^2_{i,is} + K^2_{er}} \tag{4.15}$$

Where the calcium ion's flux is evaluated as maximum rate of calcium uptake, represented by υ_{er}. υ_{er} is then scaled by an activation hill function of order 2, dependent on calcium intracellular's concentration. The half saturation constant of the hill function is represented by K_{er}, which physiologically is interpretable as the Ca^{2+} affinity with the SERCA pump, that in other words means the calcium concentration at which the pump works at half of its maximal capability. In order to relate the flows with the actual ion current passing through the membrane, the flows of ions, similarly to equation [4.13], is translated by multiplying it with the volume of the intracellular space and by dividing it with the channel's area of expression, therefore, the lateral surface of the ER.

The leak term, instead, is represented by a leak of Ca^{2+} ions from the ER into the cytosol. This term was modeled to take into account all the other possible exchanges that are individually negligible. The leak was assumed to be proportional to the Ca^{2+} gradient across the ER membrane.

$$I_{Ca_{ER}leak} = \frac{F \cdot Vol_{i,is}}{S_{i,er}} \cdot r_L \cdot ([Ca^{2+}]_{i,er} - [Ca^{2+}]_{i,is}) \tag{4.16}$$

Where r_L represents the leak rate, or maximal possible leakage from ER. In order to relate the flux of calcium ions to an ionic current, it was applied the same translation of equation [4.13]. In case the intracellular calcium concentration would become larger than the ER's, which is physiologically unlikely, this formulation would allow a reverse mode of the leakage itself.

4.3.2 GluT-dependent pathway

The Glutamate Transporters dependent pathway represents the second source of calcium designed in the model. Most of the calcium ions flowing into the intracellular space are related to the last exchanges of this metabolic pathway and are transported by the Na^+/Ca^{2+} exchangers (NCX). Which, as described in section [2.2.1], are transporters that mediate the exchange of three Na^+ ions for one Ca^{2+}. Their range of activity can be either in forward mode or reverse mode, with the reverse mode being the one capable of moving outside of the intracellular space the sodium ions and inside the calcium ions. The switch from the basal

forward mode into the reverse mode is induced by an increased intracellular Na^+ concentration. The overall metabolic pathway, however, is reported in figure [4.6].

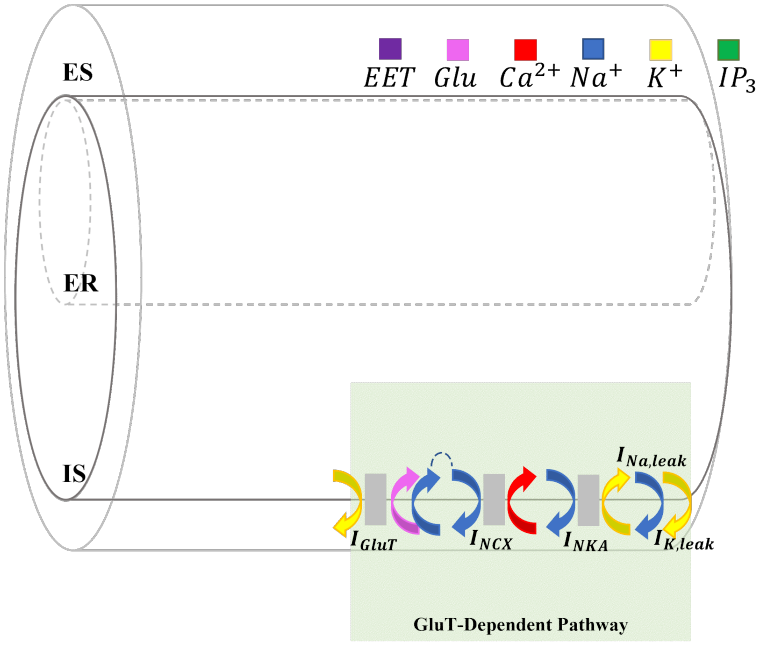

Figure 4.6: Visualization of a zoom of the GluT-dependent pathway with every exchange of material color coded. Note the coupling of sodium inflow and outflow of the co-localized GluT and NCX.

The gating mechanism of NCX is dependent on five different variables: the intra and extracellular sodium concentration ($[Na^+]_{i,is}$,$[Na^+]_{i,es}$), the intra and extracellular calcium concentration ($[Ca^{2+}]_{i,is}$;$[Ca^{2+}]_{i,es}$) and the membrane potential. The outer ion concentrations predominantly define the probability of the channel being in open state, while, the inner ion concentrations define the mode in which the channel is working. Particularly the sodium concentrations, as described in equation [4.17], can have larger difference in concentration between the intra and extracellular ones, defining the sign of the ionic current.

$$I_{NCX} = I_{NCX_{max}} \cdot \frac{[Na^+]^3_{i,es}}{K^3_{NCX_{Na}} + [Na^+]^3_{i,es}} \cdot \frac{[Ca^{2+}]_{i,es}}{K_{NCX_{Ca}} + [Ca^{2+}]_{i,es}} \cdot \frac{\frac{[Na^+]^3_{i,is}}{[Na^+]^3_{i,es}} \cdot exp\left(\eta \cdot \frac{V \cdot F}{R \cdot T}\right) - \frac{[Ca^{2+}]_{i,is}}{[Ca^{2+}]_{i,es}} \cdot exp\left((\eta - 1) \cdot \frac{V \cdot F}{R \cdot T}\right)}{1 + k_{sat} \cdot exp\left((\eta - 1) \cdot \frac{V \cdot F}{R \cdot T}\right)} \tag{4.17}$$

Where the strength of the ionic current is saturated at a maximal pump current

$I_{NCX_{max}}$. Which is multiplied by the probability of being open, dependent on two different hill functions, respectively, of order 3 dependent on extracellular sodium saturation and of order 1 dependent on extracellular calcium saturation. The half saturation constants are given by $K_{NCX_{Na}}$ and $K_{NCX_{Ca}}$. The last term instead, defines somewhat the sign of the ionic current, and therefore the mode in which the channel is operating. In particular, the numerator is what drives the switch between the forward and the reverse mode, with forward mode as basal conditions stated at a smaller intracellular sodium concentration, compared to the extracellular one. The opposite comparison needs to be done for the calcium ions.

The equilibrium potential for I_{NCX} current is generally slightly negative to 0 mV, therefore, near the resting potential the NCX works in normal mode and generates an inward current, while transiently switch to reverse mode when both the membrane potential and the sodium intracellular concentration enter the reverse working point range. The model of this channel was first proposed, by fitting experimental data, by Mullins [31], then simplified by DiFrancesco and Noble [32], which last design was not satisfying more recent experiments, and therefore adjusted by Luo and Rudy [33]. From evidence, the curve were fitted and the new parameters of the simplification were then defined as η being the position of the energy barrier controlling the NCX voltage dependence and k_{sat} being the saturation factor able to ensure saturation at large negative potentials, therefore reducing the channel activity. Note that the two exponential terms, present at the numerator have a direction opposite to each other, one being always descending and the other ascending.

We have understood that the Glutamate transporters pathway ends up with calcium ions entering the intracellular space when intracellular sodium concentration rises. This transient is caused predominantly by GluT transporters, that as discussed in section [2.2.1] are locally expressed near NCX exchangers. Glutamate transporters, or EAAT channels are known to co-transport three Na^+, one H^+ and counter-transport one K^+ for each glutamate molecule that they are able to uptake from the extracellular space. The concentrations of H^+ and glutamate are not tracked this thesis, however the glutamate stimulation is still managed as an input to specific locations of the astrocyte. Therefore, in case of external gluta-

mate stimulation, these transporters provide a large influx of sodium ions leading the NCX exchangers to switch into reverse mode. The glutamate transporters opening is mediated by the different co-transported and counter transported ions, due to their binding to the protein structure. The following is the mathematical design of their functioning:

$$I_{GluT} = I_{GluT_{max}} \cdot \frac{[K^+]_{i,is}}{[K^+]_{i,is} + K_{GluT_K}} \cdot \frac{[Na^+]^3_{i,es}}{[Na^+]^3_{i,es} + K^3_{GluT_{Na}}} \cdot \frac{g}{g + K_{GluT_g}} \tag{4.18}$$

Where the ionic current that the GluT are able to build up is defined as the maximal transport current $I_{GluT_{max}}$ times the probability of the transporter being activated. Which probability is defined as the conditional probability of the three independent events of intracellular potassium ion, extracellular sodium ions and external glutamate transported and bound to the trans-membrane protein. These events are mathematically defined as hill functions respectively of order 1, 3 and 1 with half saturation constants represented by the terms K_{GluT_K}, $K_{GluT_{Na}}$ and K_{GluT_g} [4]. The external glutamate stimulus concentration is defined the same way as before, thus as g.

The activity of GluT transporters and NCX, as discussed, influences the dynamics of sodium and potassium ion concentration. The event could lead to unbalances compared to resting conditions, which requires a solution, that for astrocyte is represented by the capability of expressing Na^+/K^+-ATPase pumps (NKA) and voltage-dependent channels. The first ones being trans-membrane proteins, capable of transporting sodium and potassium ions against their concentration gradient by energy consumption. While the second ones being channels able to, respectively, let sodium or potassium ions pass through the cellular membrane regarding the membrane potential.

Focusing first on the NKA, these are channels that actively co-transport, in different directions, sodium and potassium ions when ATP binds to the channel and dephosphorylates into ADP. This phenomenon produces the energy needed for the transportation.

The directions are against gradient, which means that potassium ions are going to be transported from the extracellular space into the intracellular space and

viceversa for the sodium ions. Their mathematical formulation is similar to some other that are seen previously in the model.

$$I_{NKA} = I_{NKA_{max}} \cdot \frac{[Na^+]_{i,is}^{1.5}}{[Na^+]_{i,is}^{1.5} + K_{NKA_{Na}}^{1.5}} \cdot \frac{[K^+]_{i,es}}{[K^+]_{i,es} + K_{NKA_K}} \tag{4.19}$$

Where $I_{NKA_{max}}$ represents the maximal pumping activity of the NKA, which is then scaled by the probability of the channels to be activated, defined to not be dependent on energy due to the assumption of energy overabundance. The activation was therefore designed, to be dependent on ions concentration defining a limit of channel activity by saturation, of either the intracellular sodium or extracellular potassium, as independent events. When the intracellular sodium gets really high, particularly during neural activity and there is activation of GluT, then the NKA channels have higher probability of being activated at maximum of their possible pumping activity. Analogous for extracellular potassium, if there is too much potassium in the extracellular space, which can also cause severe issues, then the NKA channels have possibility of being activated. The probability of being activated depends on the ions concentration, defined respectively to be an hill function of order 1.5 and another one order 1, with half saturation constants represented by $K_{NKA_{Na}}$ and K_{NKA_K}.

While instead, the leak currents corresponds to voltage gated channels of Na^+ and K^+ ions. They can work in forward or reverse mode regarding the membrane potential and their reverse potential, given from the Nernst potential. The design of the respective currents is the analogous.

$$I_{Na_{leak}} = g_{Na_{leak}} \cdot (V_i - E_{Na}) \tag{4.20}$$

$$I_{K_{leak}} = g_{K_{leak}} \cdot (V_i - E_K) \tag{4.21}$$

Where, the currents are given from the respective conductance are represented by $g_{Na_{leak}}$ and $g_{K_{leak}}$ in $\frac{pS}{\mu m^2}$, which unit of measurement defines a conductance over surface. Physiologically this could be interpreted not like a single channel conductance, but more like the density of expression of the specific channels. The direction of the leak currents instead, is defined by the difference between the membrane potential and the reversal potential, evaluated as the Nernst poten-

tial $E_{ion} = \frac{R \cdot T}{F} \cdot log\left(\frac{[ion]_{i,es}}{[ion]_{i,is}}\right)$. Where, R represents the gas constants; T the temperature and F the Faraday's constant. The Nernst potential represents the membrane potential at which there is no net flow of the particular ion from one side of the membrane to the other.

4.3.3 Perivascular Pathway

Astrocytes full-fill their role of potassium spatial buffers by up-taking it from high concentration regions and releasing it into low concentration regions. High potassium concentration events take usual place when high neural activity is happening, which requires a bigger supply of nutrients and oxygen, therefore, astrocytes provide support to the CNS in this matter by integrating into the neurovascular unit and plastering blood vessels with the endfoot.

The endfeets reach the perivascular areas and plaster the smooth muscle cells (SMC), which then control the vasculature strain. It has been discussed that SMCs are able to either dilate or constrict the adjacent blood vessels, regarding of their membrane polarization which is dependent on the net exchange of electrical charges through the cellular membrane.

In this model no direct contact was designed between the endfeets and the SMCs, thus the only exchange of material needs to pass through the perivascular space. Moreover, no mechanistic model of the blood vessel strain was yet implemented at this stage of development, detailed formulation of the simplified model are found in section [4.5].

The astrocyte capability of regulating the local SMCs is then related to the interactions with the perivascular space, by mediating the ions concentrations. Assuming that the endfeet is a single cylinder compartment, it needs to have all the other biological pathways of standard *Compartment* class, and some other features that characterize it. The area of contact with the perivascular space was designed to be the surface area of the further end from the soma, a side of the endfeet that was designed to express different membrane channels from the rest of it.

These different channels, as reported previously, are specific transporters towards the perivascular space, such as inward rectifier channels ($Kir_{4.1}$) and big

conductance channels (BK). Both potassium transporters having different gating mechanisms and designed to be part of the so called perivascular metabolic pathway by being expressed only over the surface area of the further end from the soma, therefore, their ionic current contribution would be different from zero only in those compartments labeled as endfeets [4.8]. The overall perivascular pathway scheme is reported in figure [4.7].

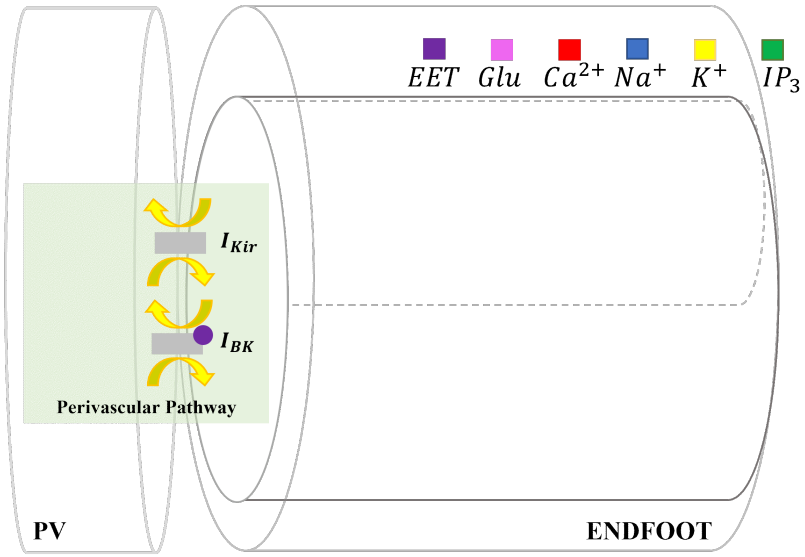

Figure 4.7: Visualization of a zoom of the perivascular pathway, expressed exclusively in endfeet compartments.

Starting from the Kir channels, a buildup of intracellular K^+ results in a potassium efflux into the perivascular space, which would be counterintuitive given the name of the channel, however it is to remember from previous discussion that even if the $Kir_{4.1}$ channels activation is voltage dependent, their reversal potential and conductance are dependent on both intracellular and perivascular potassium concentration.

The ionic current term, found in equation [4.8], is then designed as follows, where at each cycle one potassium ion pass through the membrane.

$$I_{Kir} = g_{Kir,i} \cdot (V_i - V_{Kir,i}) \tag{4.22}$$

Where $g_{Kir,i}$ represents the channel conductance dependent on the perivascular potassium concentration with a monotone dependence [34], the higher the concen-

tration, the higher the conductance. While the term $V_{Kir,i}$ represents the reversal potential, evaluated as a Nernst potential of a channel located at the point of contact between the endfeet and the perivascular space.

$$g_{Kir,i} = g_{Kir,V} \cdot \sqrt{[K^+]_{pv,i}} \qquad V_{Kir,i} = E_{K,endf} \cdot log\frac{[K^+]_{pv,i}}{[K^+]_{is,i}} \tag{4.23}$$

Where in the first term it is defined the monotonic dependence as the square root of the perivascular potassium concentration, scaled by a conductance parameter, found experimentally from Farr and David [26]. Similarly to previous conductance parameters, also $g_{Kir,V}$ is defined over area, not denoting a single channel conductance, but physiologically interpretable as the local density of the channel expression. While, instead the reversal potential $V_{Kir,i}$ is evaluated as the Nernst potential with $E_{K,endf}$ being the potassium Nernst constant over the membrane between the intracellular space and the perivascular space. For both terms it is still maintained the i compartment indexing, considering that the endfeets are instances of *Compartment* class, just like the perisynaptic processes.

Focusing on the Big conductance channels, these are potassium transporters that are voltage and Ca^{2+} gated with influence from EET over the activation mechanism. It is unclear whether EETs act directly on the BK channels or indirectly by activating the TRPV4 channels, introduced in section [2.2.1]. The activation of the TRPV4 channels would result in Ca^{2+} influx and membrane depolarization, which both activate BK channels, and this is why, given that the TRPV4 channels are not designed into the model, the EET dependence over the BK gating mechanism is maintained. The opening of BK channels results in a release of potassium ions into the perivascular space, and as the name suggest, and therefore in a ionic current, larger than the $Kir_{4.1}$. The difference in amplitude is mainly provided by the single channel conductance, a few magnitude orders above the $Kir_{4.1}$'s one.

The ionic current can be described as the following ohmic relationship.

$$I_{BK} = g_{BK} n_i (V_i - V_{BK,i}) \tag{4.24}$$

Where the ionic current is evaluated as the channel conductance over surface

area (g_{BK}), scaled by the probability of the channel being open (n_{BK}) and by the driving membrane potential force, where V_{BK} represents the Nernst reversal potential.

The BK channel equations are taken from Gonzalez-Fernandez and Ermentrout [29], which study found a suitable model over fitting experimental data. The same work showed that the probability of the channel being open could be interpreted as the fraction of BK channels in open states (n), described in a similar fashion as the Morris and Lecar or Hudgkin and Huxley models ([35]) with the first order kinetics of opening:

$$\frac{dn_i}{dt} = \phi_{BK}(n_{\infty,i} - n_i) \tag{4.25}$$

Where ϕ_{BK} represents a time constant associated with the opening of the BK channels, based on statistical considerations governed by hyperbolic functions. While instead, n_{BK_∞} represents the fraction of open channels after an infinite amount of time, which in case of stable systems and not changing environment conditions is associated with the equilibrium. The very same n_{BK_∞} would also represent on average how many channels would be open fixing the voltage and the concentration of EETs.

$$n_{\infty,i} = 0.5 \cdot \left(1 + tanh\left(\frac{V_i + EET_{shift} \cdot [EET]_{i,is} - \upsilon_{3,BK}}{\upsilon_{4,BK}}\right)\right) \tag{4.26}$$

Where the value of open BK channels at equilibrium is in fact given from an hyperbolic tangent function, dependent on both membrane potential and concentration of EETs. The hyperbolic function is shifted upwards by 1 and stretched by the 0.5 scaling factor, which makes it similar to an activation function with the co-domain ranging between [0,1]. The argument of the activation function may theoretically vary in an infinite scale, however the negative and stable resting membrane potential of astrocytes influences their homeostatic capabilities through the electrodriving force, produced by the ion flows of the numerous membrane transporters. Which, does not make the membrane potential vastly diverge from the hyperpolarized resting potential close to -80 mV. Instead, the influence in the activation mechanism of EETs is designed to be scaled by the parameter

EET_{shift}, which represents the EET-dependent voltage shift as in the relationship given by Gonzalez-Fernandez and Ermentrout [29]. Then, $\upsilon_{4,BK}$ represents the spread of the distribution of open BK channels, the larger, the more spread is the population of channels and therefore less open channels. While, $\upsilon_{3,BK}$ incorporates a calcium-dependent shift of the distribution of BK channel open states with respect to the membrane potential associated with the probability of having half of the channels open. It depends on the intracellular calcium.

$$\upsilon_{3,BK} = -\frac{\upsilon_{5,BK}}{2} \cdot tanh\left(\frac{[Ca^{2+}]_{i,is} - Ca_3}{Ca_4}\right) + \upsilon_{6,BK} \tag{4.27}$$

Where the shift of the distribution of open channels dependence on the intracellular calcium, is itself dependent on Ca_3 and Ca_4, which have a similar effect to $\upsilon_{3,BK}$ and $upsilon_{4,BK}$ in equation [4.26]. Instead, $\upsilon_{5,BK}$ and $\upsilon_{6,BK}$ affects the distribution of the $n_{\infty,i}$ shift as intracellular $[Ca^{2+}]$ varies. $\upsilon_{5,BK}$ represents the range of the shift of $n_{\infty,i}$, while $\upsilon_{6,BK}$ shifts it up.

Recalling the time course of the fraction of BK channels in open states, the n state variable changes are based on statistical considerations over the time constant ϕ_{BK}, designed as:

$$\phi_{BK} = \psi_{BK} \cdot cosh\left(\frac{V_i - \upsilon_{3,BK}}{2\upsilon_{4,BK}}\right) \tag{4.28}$$

Where ψ_{BK} is a constant parameter scaling the output of the *cosh* function, that is dependent on the membrane potential, with $\upsilon_{3,BK}$ and $\upsilon_{4,BK}$ affecting the shape of the hyperbolic function.

Another possible way of modeling BK channels, that has been investigated in scientific literature is the one found in Montefusco and colleagues study [36]. The study in particular pursues the evidences from other studies, where BK channels finds themselves to be co-located with voltage gated calcium channels, and considers them to be related to the gating mechanisms of the BK channels. In this latter study, the BK channels are treated as stochastic channels, where it is investigated how the number of involved subunits of the protein channel affects the change of state from close to open of the channel itself.

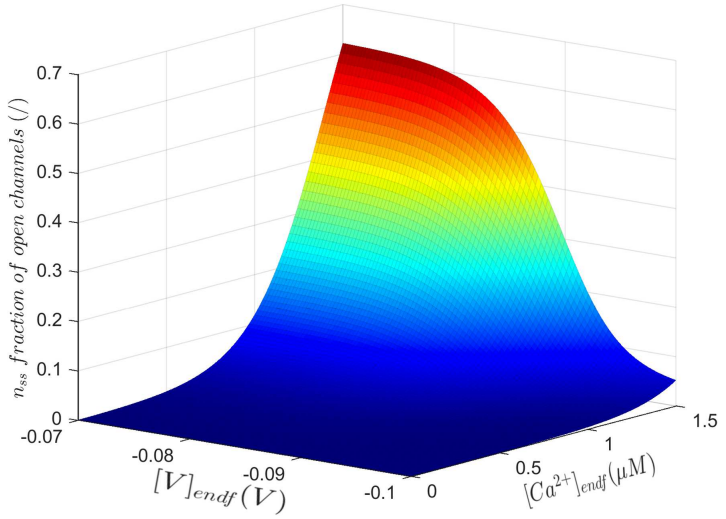

Figure 4.8: Visualization of n's nullcline surface plot at changing of $[Ca^{2+}]_{endf}$ and V_{endf}, with fixed $[EET]_{endf}$ at maximum found concentration. This shows how the fraction of activated BK channels is more sensible to changes in calcium, compared to changes in voltage.

4.3.4 Diffusion

The geometry of the model allows for the possibility of having more compartments, interconnected between each other by adjacency. The model assumes that adjacent compartments are able to exchange all material present in the cytosol. However, evidence showed that the processes branching out of the soma might be relatively long and expressing organels such as the endoplasmic reticulum or the Golgi apparatus, which as discussed in section [2.2], provides the astrocyte with the ability of locally expressing proteins. Therefore, in the model it was assumed that the ER was representable with a cylinder form of equal length to the intracellular space's, thus being directly connected to the ERs of the adjacent compartments.

The exchange of material is then happening, independently, between intracellular spaces and endoplasmic reticulums of adjacent compartments. The independence of the two events is due to the presence of the ER membrane separating the two spaces, however the exchange of material was assumed to be driven by the same force, that is by diffusion due to concentration gradient. Moreover, diffusion was not only designed inside the astrocyte, but it was also assumed to be happening in the extracellular spaces surrounding adjacent compartments, differing

only by the diffusion constant.

Adjacent compartments are defined by using characteristics of the class *Compartment*, such as the $process_{num}$, the *number* and the *level*. The adjacency was found considering that the building of the class receives in input a preconfiguration of the geometry and sequentially instantiating of each process one compartment at a time. Therefore, unless it is the end of the process, is quite trivial to understand that sequential compartments in *number* are also adjacent in the geometry.

To this stage of development, the adjacency does not take into account possible connections between neighboring branches, or possible local influences between processes that at some point splits in two or more. However, it already considers that extracellular spaces of adjacent compartments are able to exchange material between each other, again by passive diffusion. The following figure, represents the different fluxes exchanged between adjacent compartments, and their contact area.

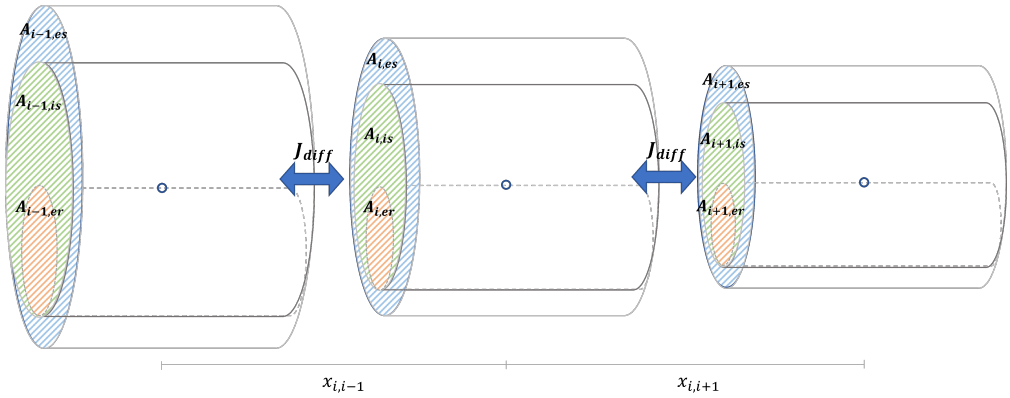

Figure 4.9: Visualization of general scheme of diffusion between adjacent compartments. J_{diff} is then built out of individual fluxes between different spaces and domains.

Following there will be the mathematical description of the respective fluxes between adjacent ERs, adjacent extracellular spaces and at last adjacent intracellular spaces. However, all of the possible are driven by the same gradient of concentration, and the differences will be about the diffusion constant and depending on which compartment geometry they are evaluated into. Together with the formulation of each different set of fluxes, a figure is going to represent the scheme of which terms are defining each set ([4.10];[4.11];[4.12]).

It is to notice that the possible diffusion term incoming in a compartment is at maximum the one able to pass through the cross-section area between respective spaces, which means the one of the smaller compartment between two adjacent ones. The diffusion term will be designed in the same manner for each flux and will be as follows:

$$d_{Ca_{ij}} = \frac{D_{Ca}\ A_{ij}}{Vol_i \cdot x_{ij}} \qquad d_{IP_{3_{ij}}} = \frac{D_{IP_3}\ A_{ij}}{Vol_i \cdot x_{ij}} \qquad d_{Na_{ij}} = \frac{D_{Na}\ A_{ij}}{Vol_i \cdot x_{ij}} \qquad d_{K_{ij}} = \frac{D_K\ A_{ij}}{Vol_i \cdot x_{ij}}$$

Where the diffusion terms, noted with smaller d, are going to be dependent: on the diffusion constants D, which is also different for each compound and for each possible space (IS, ES, ER); on the cross-section area A_{ij}; on the volume that is receiving the material by diffusion and finally on the distance between the centers of the two adjacent compartments x_{ij}.

Every geometry term is indexed with i and j, where i is the compartment that is receiving the flux and j the one giving the flux. However, it is to notice that the driving force of the diffusion is the concentration gradient, which is the actual definer of the sign of the flux, and therefore the qualitative direction of it. The i and j are a mathematical notation to design consistently each term, and corresponds to the *number* characteristic of each *Compartment* class instance. Both i and j will belong to the $\mathbb{C}$ set of compartment *numbers* of all possible adjacent compartments, for each instance of *Compartment* class, in other words $\mathbb{C}$ will represent the set of neighbors for each compartment.

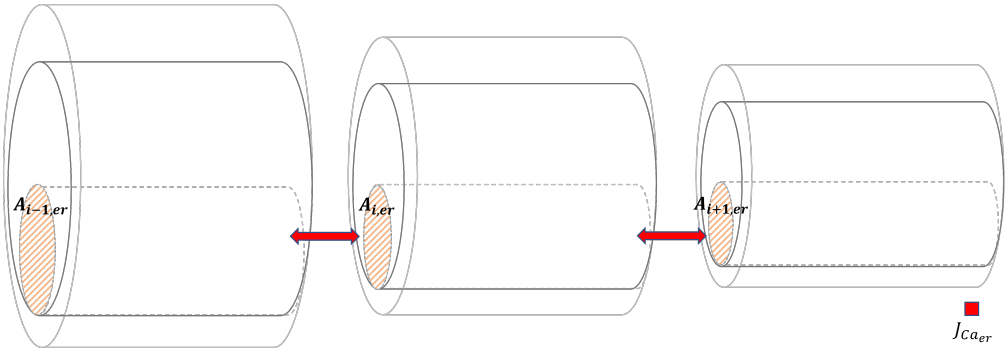

Figure 4.10: Visualization of diffusion fluxes between adjacent endoplasmic reticulum of neighbor compartments. The legend of which compounds are exchanged is portrait on bottom right of the picture.

Starting with ERs as in figure [4.10], the only assumed ion able to diffuse

between adjacent compartments is calcium.

Recalling the *geometry* section [4.2], the endoplasmic reticulum gets progressively smaller the further the process gets from the soma, which means that we expect these fluxes to be progressively smaller between adjacent compartments close to the end of the process.

The calcium diffusion between adjacent ERs is accounted by the following flux:

$$J_{Ca_{diff,er},i} = \sum_{j \in \mathbb{C};\ j \neq i} d_{Ca_{ij},er} \cdot ([Ca^{2+}]_{er,j} - [Ca^{2+}]_{er,i}) \tag{4.29}$$

Where the overall flux incoming into the compartment i will be the sum of all the possible fluxes entering or leaving the compartment itself, with all possible j being part of the set of neighbors of compartment i. The cross-section area is straight forward as the cylinder surface area of the smaller compartment's ER, while the distance between the centers of the different ERs is just equal to the length of one compartment.

Following with extracellular spaces, the possible exchanges of material tracked in the model are calcium ions, sodium ions and potassium ions. The extracellular spaces, recalling the geometry section, are considered as circular crowns, therefore the cross-section area will need to be derived.

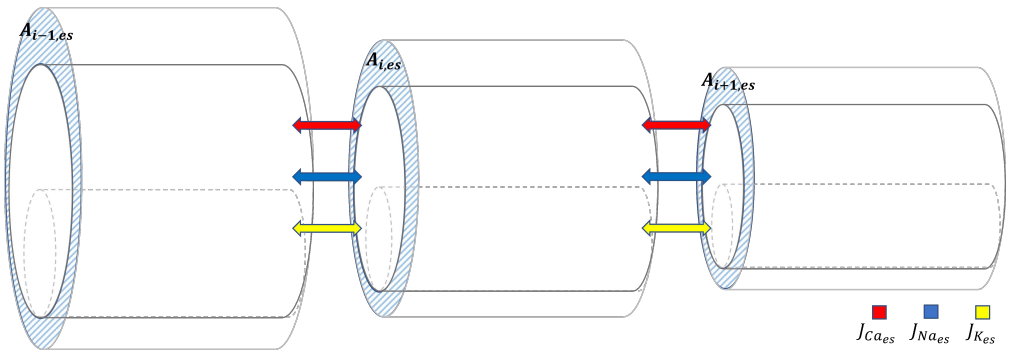

Figure 4.11: Visualization of diffusion fluxes between adjacent extracellular spaces of neighbor compartments. The legend of which compounds are exchanged is portrait on bottom right of the picture.

The extracellular diffusion fluxes incoming in compartment i are accounted as

follows:

$$
\begin{aligned}
J_{Ca_{diff,es},i} &= \sum_{j\in\mathbb{C};\ j\neq i} d_{Ca_{ij},es}\cdot\left([Ca^{2+}]_{es,j}-[Ca^{2+}]_{es,i}\right)+J_{Ca_{diff,pv},i}\\
J_{Na_{diff,es},i} &= \sum_{j\in\mathbb{C};\ j\neq i} d_{Na_{ij},es}\cdot\left([Na^{+}]_{es,j}-[Na^{+}]_{es,i}\right)J_{Na_{diff,pv},i}\\
J_{K_{diff,es},i} &= \sum_{j\in\mathbb{C};\ j\neq i} d_{K_{ij},es}\cdot\left([K^{+}]_{es,j}-[K^{+}]_{es,i}\right)J_{K_{diff,pv},i}
\end{aligned}
\tag{4.30}
$$

Where the mathematical formulation is analogous to the previous one of endoplasmic reticulums, involving instead, calcium, sodium, potassium ions. The diffusion term needs a couple of consideration regarding the cross-section area, which is represented in figure [4.11]. The cross section area of diffusion is the surface area of the circular crown of the smaller compartment between two neighbors and the fluxes, involving the perivascular space, will be different from zero only for the endfeets compartments, which are having the extracellular space in direct contact with the perivascular space at the end of the process.

At last with intracellular spaces, the diffusion fluxes that are taken in consideration involve every free compound in the cytosol, apart from the EETs. This assumption was taken to not over complicate the dynamics of specific metabolic pathways. The cross section areas, as represented in figure [4.12], are going to take into account that no diffusion between different intracellular spaces will happen between the surface area, occupied by the ERs.

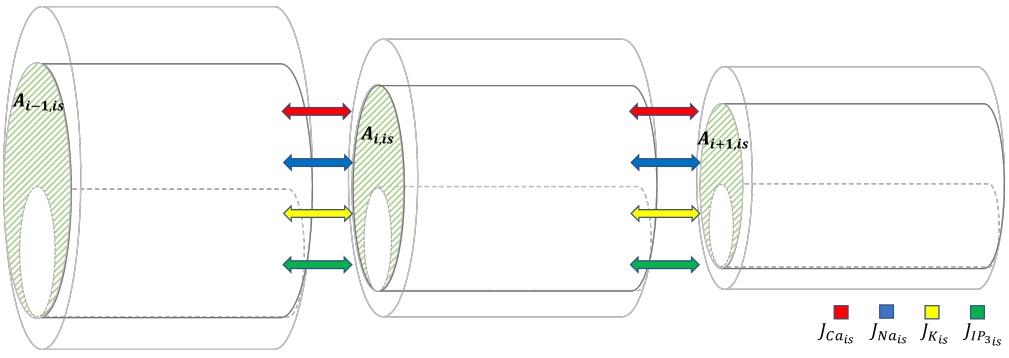

Figure 4.12: Visualization of diffusion fluxes between adjacent intracellular spaces of neighbor compartments. The legend of which compounds are exchanged is portrait on bottom right of the picture.

$$
\begin{aligned}
J_{Ca_{diff,is,i}} &= \sum_{j \in \mathbb{C};\ j \neq i} d_{Ca_{ij},is} \cdot \left([Ca^{2+}]_{is,j} - [Ca^{2+}]_{is,i}\right) \\
J_{Na_{diff,is,i}} &= \sum_{j \in \mathbb{C};\ j \neq i} d_{Na_{ij},is} \cdot \left([Na^{+}]_{is,j} - [Na^{+}]_{is,i}\right) \\
J_{K_{diff,is,i}} &= \sum_{j \in \mathbb{C};\ j \neq i} d_{K_{ij},is} \cdot \left([K^{+}]_{is,j} - [K^{+}]_{is,i}\right) \\
J_{IP3diff,is,i} &= \sum_{j \in \mathbb{C};\ j \neq i} d_{IP3_{ij},is} \cdot \left([IP_3]_{is,j} - [IP_3]_{is,i}\right)
\end{aligned}
\tag{4.31}
$$

Where the mathematical formulation is analogous to the previous ones, involving all the same material of extracellular spaces, with additional diffusion of IP_3 between adjacent compartments.

Greater interest is to be noted on the perivascular space, where the diffusion would influence the exchanges of material between the extracellular space, around the endfeet, and the perivascular space itself. The diffusion flux between the two was assumed to be existent, considering that physiologically there is no restriction between the two and are qualitatively part of the same interstitial fluid.

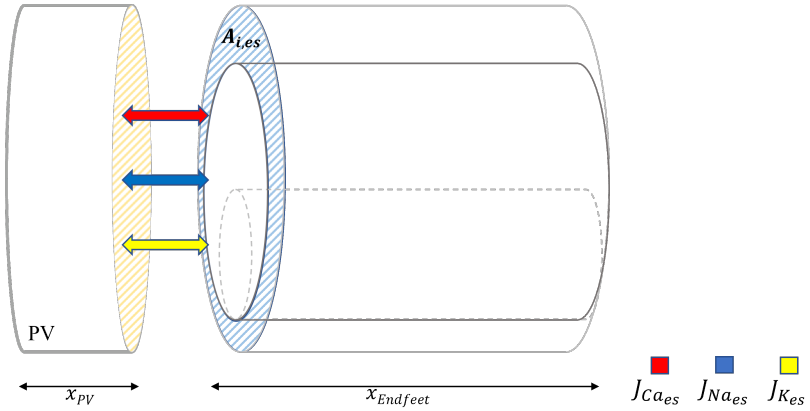

Figure 4.13: Visualization of diffusion fluxes between endfeet and adjacent perivascular space. The legend of which compounds are exchanged is portrait on bottom right of the picture.

$$
\begin{aligned}
J_{Ca_{diff,pv},i} &= d_{Ca_i,pv} \cdot \left([Ca^{2+}]_{pv,i} - [Ca^{2+}]_{es,i}\right) \\
J_{Na_{diff,pv},i} &= d_{Na_i,pv} \cdot \left([Na^{+}]_{pv,i} - [Na^{+}]_{es,i}\right) \\
J_{K_{diff,pv},i} &= d_{K_i,pv} \cdot \left([K^{+}]_{pv,i} - [K^{+}]_{es,i}\right)
\end{aligned}
\tag{4.32}
$$

Where there is no more indexing of different possible fluxes since it was assumed that each endfeet is adjacent to only one perivascular space, and its perivascular

space is exchanging material with its extracellular space. Therefore, the concentration gradient for the different calcium, sodium and potassium ions will be evaluated between the PV and the ES of the specific endfeet i. It is still used the i indexing, since this term is used to evaluate the overall diffusion of the ES of compartment i.

Furthermore, the geometry between the extracellular space and the perivascular space is very different to how it is defined for previous diffusion fluxes. As it is reported in figure [4.13], the perivascular space is considered to be at the end of the endfeet in contact to the extracellular space through the surface area of it. Another difference is also related to the distance between the center of the two spaces, where two possible definitions were considered.

The first one was considered to be equal to half of the length of the compartment, assuming that the perivascular space is significantly smaller than the endfeet and only wide enough to match the extracellular space surface area. While the second one, was considering the perivascular space to be a cylinder with diameter, as wide as the one of the ES and length, as long as needed to have a perivascular volume significantly lower than the endfeet one. Precisely, one thousands times less [27].

$$x_{es,pv} = \frac{l_{endf}}{2} \qquad\qquad x_{es,pv} = l_{endf} \cdot \left(\frac{R_{pv}+2}{4}\right) \tag{4.33}$$

Where R_{pv} represents the ratio between the perivascular space volume and the intracellular one, taken from Kenny and colleague's model.

4.4 Perivascular Space Domain

The focus of this thesis is to understand how the astrocytes act as a potassium spatial buffer in the CNS, however it has been already discussed that these cells do not merely stop at up-taking or releasing it. They are also capable of transporting it where it is more appropriate to release, for example to low concentration regions or at perivascular spaces. In the second case, the purpose is to provide for the potassium signaling and regulating the cerebral blood flow by hyperpolarization of nearby smooth muscle cells.

The astrocytes are, therefore, capable of such feat due to the presence of the endfeets, which may plaster various local perivascular areas and numerous smooth muscle cells, however, the design of this model allows every endfeet to interact with one and only one smooth muscle cell. This was done to simplify the complexity at a primary stage of development, as the one in this thesis.

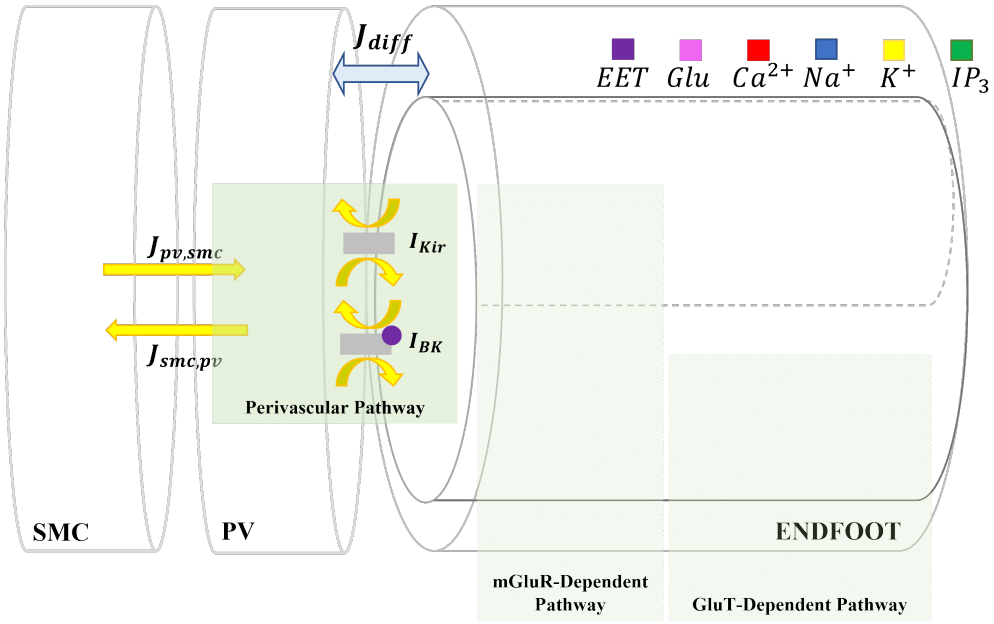

Figure 4.14: Visualization of all possible material's exchanges, happening between the perivascular space domain and the adjacent domains, such as the endfeet compartments or the SMCs

The potassium dynamics in the perivascular space domain are affected by its exchanges between the endfeet compartment and the smooth muscle cell, which include the so called perivascular metabolic pathway [4.3.3] and the interactions with the SMC domain. The first ones, comprehending the exchanges of material with the extracellular space belonging to the endfeet compartment, while the second ones, modeled with a linear first order relationship with constant rate of material transport on potassium concentrations.

$$\frac{[K^+]_{i,pv}}{dt} = \frac{A_{i,is}}{Vol_{i,is} \cdot R_{pv} \cdot F} \cdot (I_{kir} + I_{BK}) + k_{pv,smc} \cdot [K^+]_{i,smc} - k_{smc,pv} \cdot [K^+]_{i,pv} + J_{K,diff} \tag{4.34}$$

Where R_{pv} represents the ratio between the perivascular space volume and the intracellular one, taken from Kenny and colleague's model. All the other terms

are found in detailed description in previous sections, apart from the exchanges of materials with the SMC domain. Which, has been designed as a bilateral flux of ions with in both direction a linear dependence on the respective potassium concentration of the compartment from which the flow of ions is starting. The constant transfer rates of the bilateral exchange of potassium are respectively $k_{smc,pv}$ and $k_{pv,smc}$. The indexing of the constant transfer rates is k_{ij}, where i represents the receiving compartments and j the sending compartment.

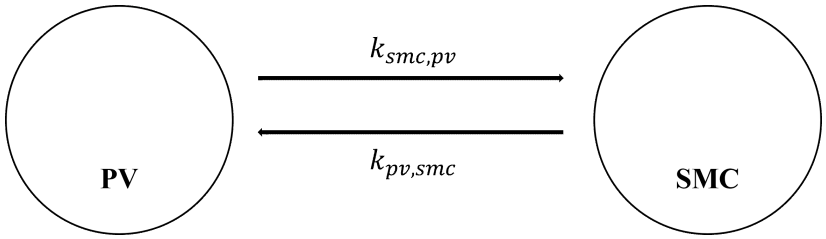

Figure 4.15: Visualization of the compartmental modeling approach between the perivascular space domain and the smooth muscle cell domains.

Recalling the diffusion section [4.3.4], it has been discussed that there is exchange of material between the extracellular space of the adjacent endfeet and the perivascular space itself. This exchange of material is driven by diffusion and involves calcium and sodium ions, along with the tracked potassium. Which means that in the model it has been also designed that the perivascular space sodium and calcium ions concentrations represent two different state variables, with the following ODEs:

$$\frac{[Na^+]_{i,pv}}{dt} = -J_{Na_{diff,pv},i}$$
$$\frac{[Ca^{2+}]_{i,pv}}{dt} = -J_{Ca_{diff,pv},i}$$

Where both ions concentrations are only affected by diffusion terms. The minus sign is been chosen because in equations [4.32] the direction of the gradients is towards the ES from the PV. Which means, that in case the flow of respective ions evaluates to be negative, therefore directed from the perivascular space, then it would become a positive term for the increment of the differential concentration equation.

4.5 Smooth Muscle Cell Domain

Starting from the state of the art in the Smooth muscle cell domain, another possible way of designing their functioning would be the one found in Witthoft and colleague's model [6]. However, in this thesis no mechanistic model of the blood vessel's strain was investigated, therefore, no control action over it coming from SMC was needed.

Instead, as anticipated in previous section, the smooth muscle cells were designed to exchange potassium with the perivascular space through a bilateral linear rate of material transport.

$$\frac{[K^+]_{i,smc}}{dt} = -k_{smc,pv} \cdot [K^+]_{i,smc} + k_{pv,smc} \cdot [K^+]_{i,pv}$$

The idea is that there is exchange of material between the perivascular space and the adjacent smooth muscle cells, however, no usage of SMC potassium is implemented in the model, therefore, following the compartmental modeling approach a linear rate of material transport seemed to show interesting behaviors.

5
Results

In this section, the reasoning behind the analysis of the model behaviors will be presented. All simulations were launched within a defined time window of 300 seconds, in which every instance of the *Astrocyte* class would evolve its state variables. During this time, astrocyte instances were stimulated with two different glutamate stimuli of different intensity but of equal duration.

The location of the glutamate stimulus was dependent on which geometry was decided [4.2], with the possibilities reported in figure [5.1] and labeled with the thunderbolt icon.

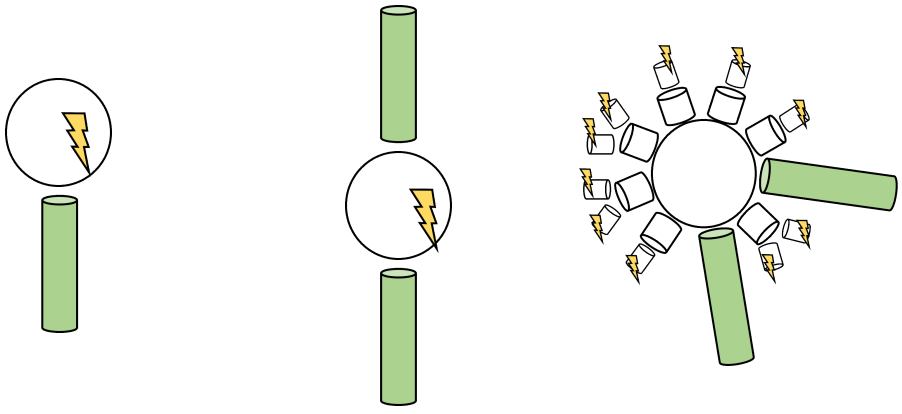

Figure 5.1: Visualization of the three different geometries, implemented in the computational model, related to position of stimulation, noted with a thunderbolt icon.

The strength of the two different stimulus window is respectively of 1 mM and 6 mM, which makes us expect a stronger calcium signaling during the second glutamate stimulus, in respect to the first one. Therefore, a stronger transmission of calcium events across the different compartments of the astrocyte, including the endfeets. Recalling chapter [4], we expect that an increment of calcium events and intracellular calcium concentration in the endfeets would trigger the activation of potassium transporters, such as the $Kir_{4.1}$ and the BK. The representation of glutamate stimulation is reported in Figure [5.2].

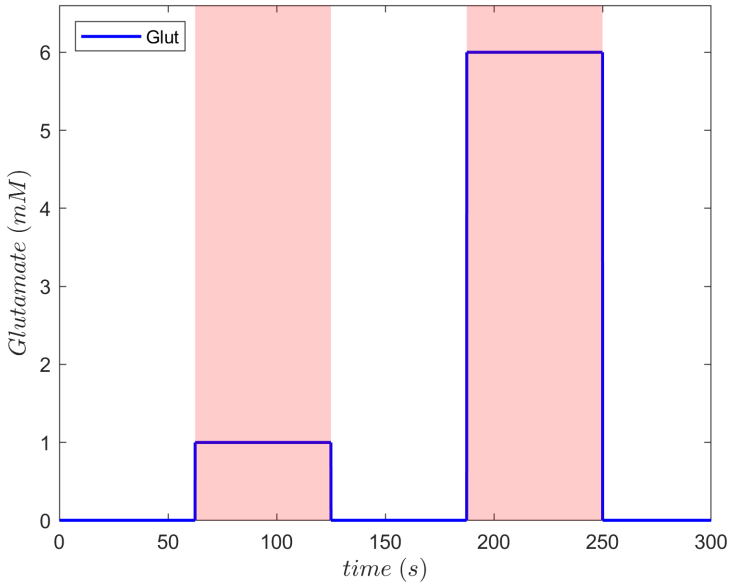

Figure 5.2: Visualization of the external Glutamate stimulation signal

5.1 Astrocyte Evolution

Every instance of class *Astrocyte* is provided with a *solve* method that launches the evolution of every state variable starting from its initial conditions, assumed to be those at rest. The mathematical integration of the solution is done with the implicit Runge-Kutta method of the Radau IIA family of order 5, implemented in the *scipy* Python library. It seemed to not be possible to use the explicit Runge-Kutta methods, due to issues in the solution converging to a result. The possible explanation could emerge from the fact that many of the state variables

dynamics are dependent on others states in various ways, such as the diffusion terms.

Moreover, during simulations, it was possible to notice that the integrator's *scipy* implementation worked using an adaptive time step, which changed regarding how fast the different states were varying, or in other terms, how large were the right-side terms of the different ODEs. The adaptive time steps made difficult to plan time separation analysis due to lack of a fixed time grid to follow or to lack of the temporary integration grid that the solver implements.

The model is designed to have 11 state variables for each perisynaptic compartment and soma, with 16 additional ones for each endfeet compartment, which makes the complexity of the model hardly leave any room for model reduction analysis. At each time step of the mathematical integration, every state variable updates, depending on the right side of the ODE and on the time step itself, which is changing through the simulation. The result is an array of values that contains the full evolution of the *Astrocyte* instance.

In particular, the results are represented in picture [**??**] as whole cell visualization, while the zooms of specific state variables may be represented separately. ([5.4];[5.5];[5.6]).

Particular interest is focused on calcium dynamics, which directly affects potassium release in the endfeet compartments into the perivascular space. Consequentially, it is portrayed in figures ([5.4];[5.5];[5.6]) the evolution of the intracellular calcium concentrations of specific *significant compartments* for each one of the three possible geometries. It can be seen that intracellular calcium starts to oscillate during glutamate stimulus windows due to how it functions the metabotropic glutamate pathway. Recalling the section [4.3.1], during a glutamate stimulus window there is an increase in IP_3 production, which triggers calcium release from the ER into the intracellular space. Once the intracellular calcium rises toward high concentration levels, the activity of the SERCA pumps and leak channels starts up taking calcium ions into the ER once again leading to intracellular calcium concentration oscillations.

Furthermore, it should be noted that changing the geometry of the model has a strong impact on the triggering of calcium oscillations, where for the *second* or *third* geometries, no oscillations are found during the weak stimulation win-

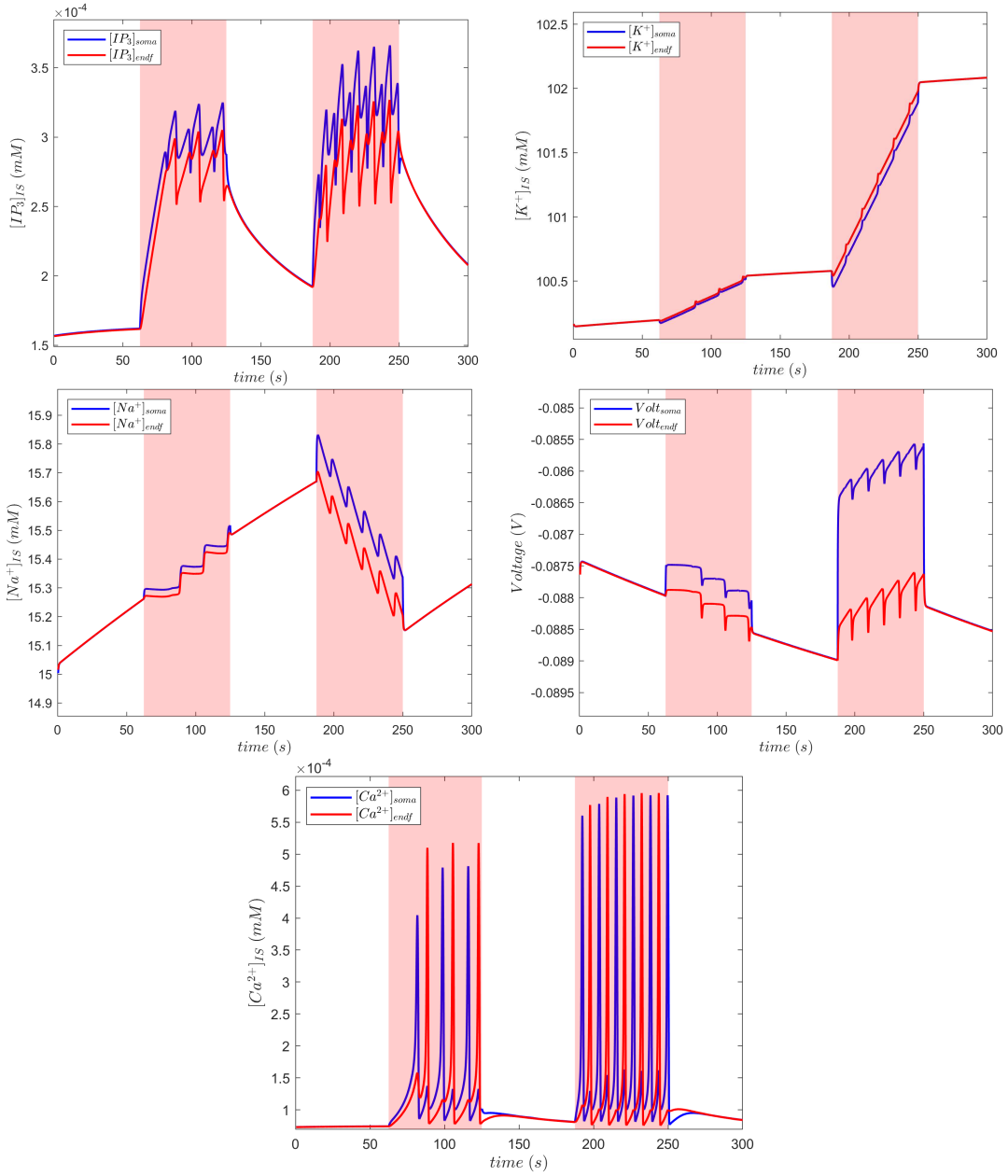

Figure 5.3: Visualization of the model simulation of specific state variables in first geometry settings. From the top, going left to right, are reported $[IP_3]$, $[K^+]$, $[Na^+]$, V and $[Ca^{2+}]$ state variables.

dow ([5.5];[5.6]). This may be caused, for the second geometry, by the fact that increasing the number of compartments would increase the volume where the calcium ions are dispersed, while for the third geometry, by the fact that having the stimulation in a compartment with higher *level* would produce smaller ex-

changes with the ER, and therefore less probability of entering in oscillation. At this point, it could have been possible to design a bifurcation analysis to search for a bifurcation parameter affecting the system entering in oscillation behavior; however, it is not a trivial task due to the amount of parameter that may affect the intracellular concentration of calcium. Narrowing the possible amount of choices, it was discussed to investigate either the radius of the perisynaptic compartments, the number of compartments, or $ratio_{er}$.

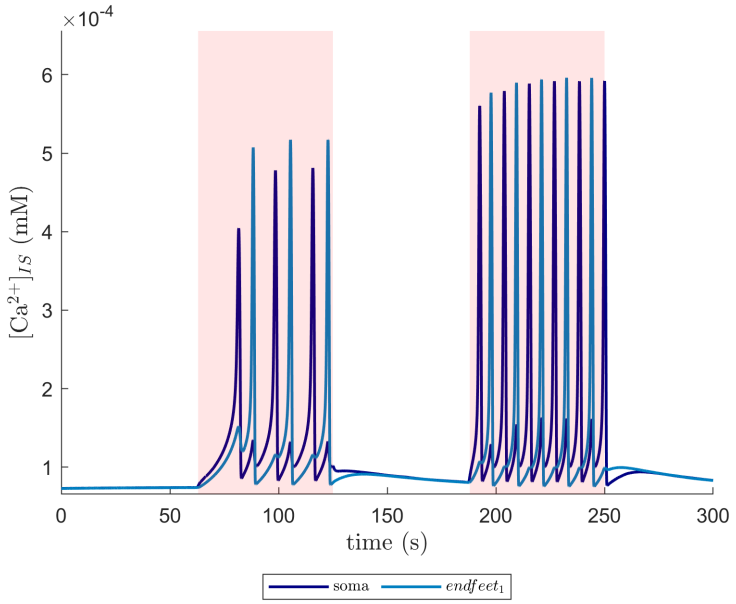

Figure 5.4: Representation of the intracellular calcium concentration evolution between different compartments of first geometry. There is presence of spatio-temporal patterns between adjacent compartments.

The calcium signaling appears to present a delay between adjacent compartments, which is verifying the assumptions made by the multicompartmental modeling approach and verifying that actually the astrocytes are able to propagate the information brought by their first messenger variable. However, the propagation seems to depend on the dimensions of the stimulated compartment, making it weaker. This claim is mainly supported by the second and third geometries, which shows that the stimulated compartments are the first ones to present oscillations, however, during the weak stimulation they do not manifest oscillations. For example, we notice how the $paps_{17}$, being at level two in third geometry settings, is among the first ones to present oscillations when triggered.

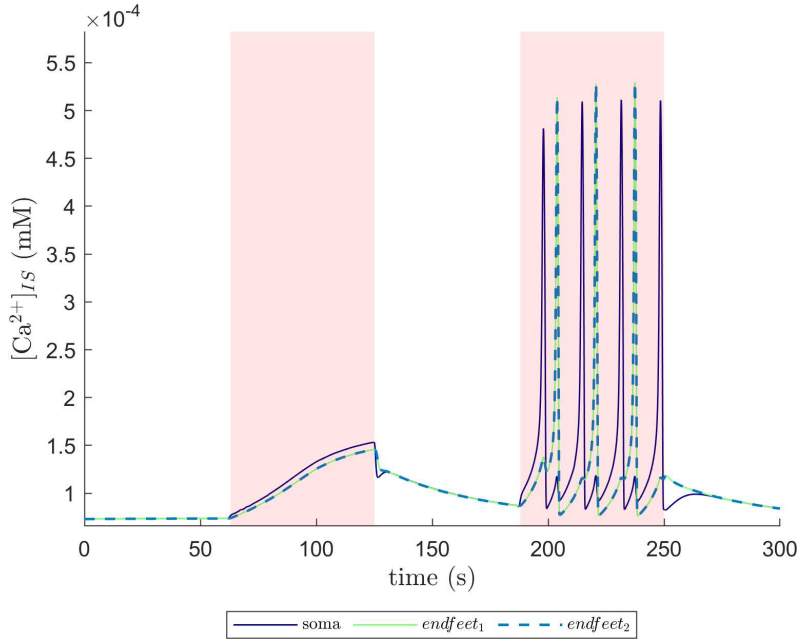

Figure 5.5: Representation of the intracellular calcium concentration between soma and endfeets of second geometry. The endfeets, given the deterministic nature of the model, are superimposed.

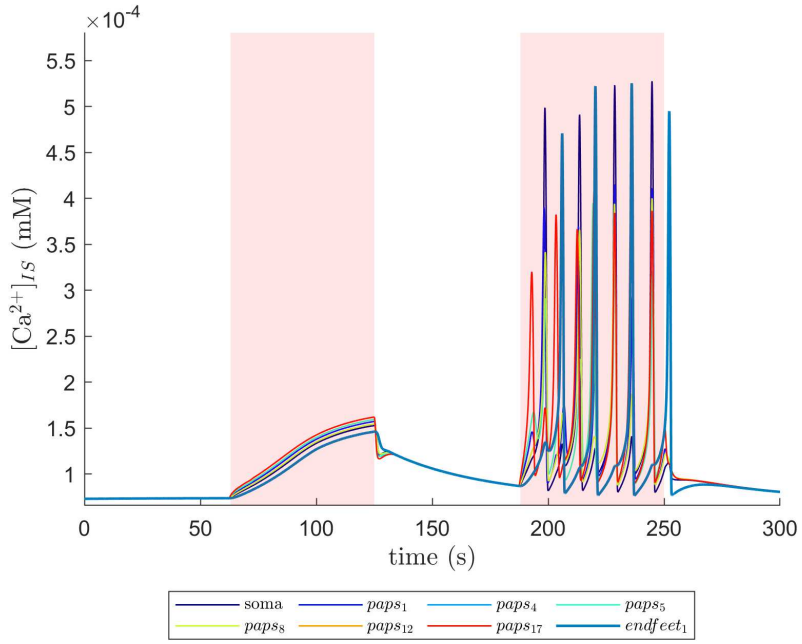

Figure 5.6: Representation of intracellular calcium concentration in third geometry, focusing only on some significant compartments. The evolution of the endfoot's one is shown by a thicker line. The calcium signaling appears to have smaller oscillations.

The calcium signaling is also capable of propagating from *soma* to *endfeets*, bringing the request to provide a response to high neural activity. The response would hopefully be an increase in local cerebral blood flow, thus an hyperpolarization of smooth muscle cells and an outflow of potassium ions towards the perivascular space. Furthermore, considering how the model is designed, every *endfeet* compartment is connected to the soma without a spatial distinction, which makes every *endfeet* compartment equal to each other. Thus in figure ([5.5]), the intracellular calcium concentration of $endfeet_1$ is superimposed to the one of $endfeet_2$, and that is happening for every simulation setting. To tip the scale only the number of *endfeets* really matters to how the *soma* is propagating the calcium signaling.

5.1.1 Mixed mode oscillations in Intracellular Calcium

Looking at the proposed result in the previous section, we can notice how the calcium intracellular concentration reports a peculiar dynamic. The one that has been called in literature "mixed mode oscillations", it is the generation of oscillation patterns that belong to two different time scales and limit cycles. Focusing only on the simplest geometry, this behavior can be seen in figure [5.4], where the oscillations of the intracellular calcium concentration of the soma alternate two different amplitudes. The difference in the two is related to the behavior of the IP_3R channels, that propose the same behavior in their activation variable h. In order to analyze the phenomenon we can investigate the evolution of the fraction of activated IP_3R channels, at changing of calcium and IP_3, as in figure [5.7].

The difference in time scales, during the evolution of the system in the two limit cycles, can be shown by looking at the duration of which the system remains in one or the other. Unfortunately, the feeling is not that trivial to catch looking at a picture; however, it was clearly visible with a real-time visual inspection that the smaller limit cycle, therefore, the smaller oscillation, had a slower timescale.

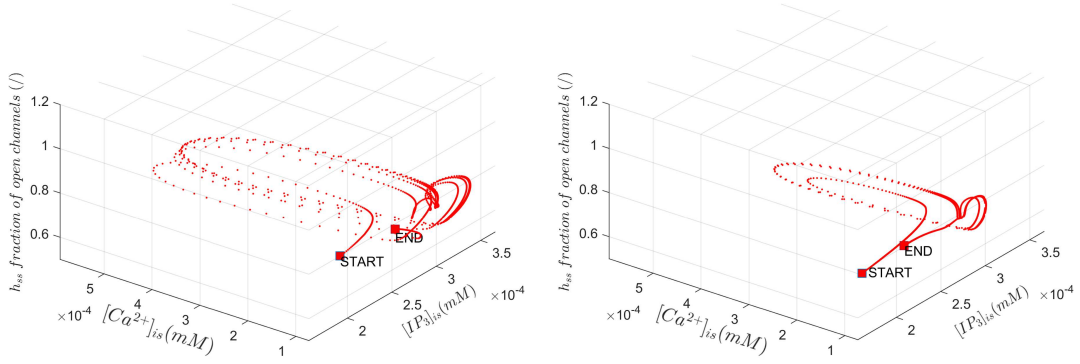

Figure 5.7: Visualization of the fraction of IP_3R open channels at changing of intracellular calcium or IP_3 concentrations. On the left the evolution during the first stimulation window, on the right the second stimulation window.

5.2 Potassium release in perivascular space

In this section it will be reported the response to the perisynaptic glutamate stimulation, which focuses on the perivascular potassium concentration. According to the results of the previous section, calcium signaling is propagated towards the perivascular space at the end of *endfoot*, triggering the release of potassium from $Kir_{4.1}$ channels and from BK channels. To better understand the role of one or the other, the ionic current produced by the $Kir_{4.1}$ and BK channels with the first geometry settings was represented in the figures (5.8]; 5.9]). The choice of geometry was to start from the simplest configuration, before moving on with the more complex second or third ones.

The $Kir_{4.1}$ channels appears to be up-taking potassium ions from the perivascular space in resting conditions, while releasing during glutamate stimulations. Particularly in correspondence of the calcium oscillations, that owing to the inflow of calcium ions positive charges into the intracellular space depolarize the astrocyte and switch the $Kir_{4.1}$ channels mode. However, the produced ionic current, and therefore the ion flux, reports to be tiny compared to other exchanges. Indeed, compared to the BK ionic current, there are various orders of magnitude of different, however, the BK channels are able to only activate in correspondence of the calcium oscillations and for little span of time.

The perivascular potassium concentration is therefore, the result of the flows produced by the endfeet transporters and by the exchange with the smooth muscle

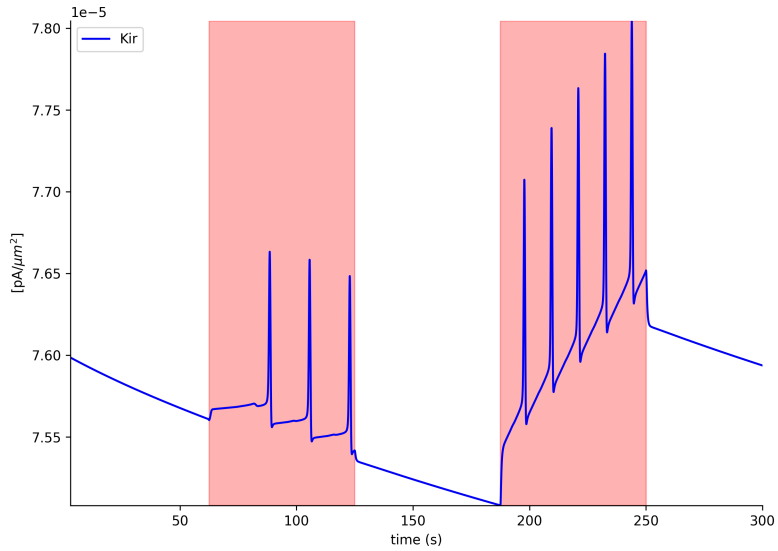

Figure 5.8: Representation of the Kir channel current in first geometry configuration. It appear to be positive, therefore releasing positive charges towards the outside of the endfoot.

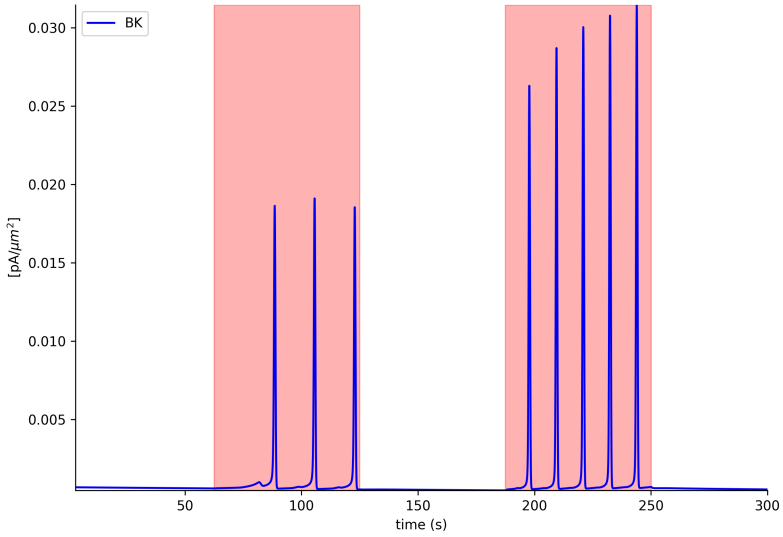

Figure 5.9: Representation of the BK channel current in first geometry configuration. The amplitude of the produced ion current is much higher compared to the $Kir_{4.1}$ channels, however, they are opening only during stimulation window, in correspondence of calcium oscillations.

cell, which releases potassium as well into the perivascular space, hyperpolarizing. The dynamics are charted in figure ([5.10]).

It can be seen that in the third geometry settings, the perivascular potassium

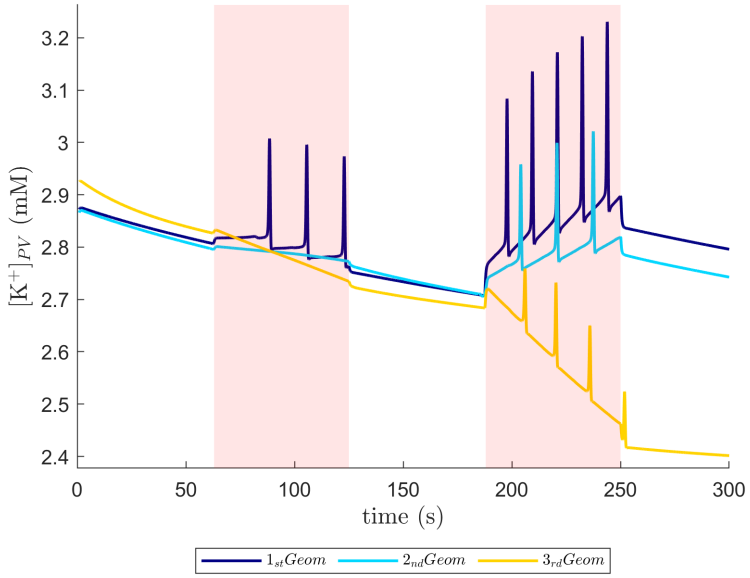

Figure 5.10: Comparison of the perivascular potassium concentration between the three geometry configurations.

concentration continues to decrease, which is given by an excess of exchanges between the adjacent extracellular space of compartment *endfoot* and the PV, along with an excess of potassium entering the nearby SMC. Moreover, in case of third geometry the membrane potential appears to be more negative compared to the first or the second, making the activation of $Kir_{4.1}$ and BK channels more difficult.

To be sure that the third geometry is highly affected by the presence of the SMC, it was simulated the same set of geometry settings with inhibition of the SMC. The results have shown that the strong decrement in the third geometry disappear, suggesting that the SMC design would need to be re-thought and reconsidered. For example, potassium transporters could be modeled on the SMC membrane aswell. The former simulation is provided in figure [5.11].

5.2.1 Impact of Smooth Muscle cell simplification

In this subsection it will be discussed how the simplified design of SMC cell's interactions with the perivascular space may be impacting on the overall results. It is undeniable that this stage of development is not fully correct and still needs time to be polished. The main reason why it is not going to fit the physiological

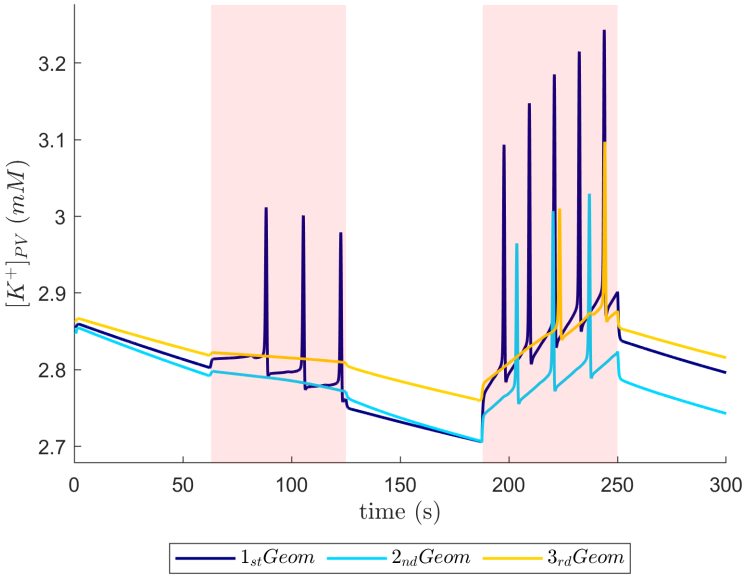

Figure 5.11: Comparison of the perivascular potassium concentration between the three geometry configurations with inhibition of the SMC domain.

behavior is about the fact that a linear transport of material dependent on the merely potassium concentration will not fully fit the problem. We know that in the case of an astrocyte bringing information to the perivascular space to request an increment in CBF, adjacent SMC cells would provide to that by hyperpolarizing, which means releasing potassium ions and dilating the plastered blood vessels.

Instead, when the astrocyte is stimulated, it takes potassium from the regions of high neural activity and, propagating calcium, it is capable of releasing it into the perivascular space. Which would trigger the adjacent Smooth muscle cells to do the same, until the perivascular potassium concentration raises to high and the $Kir_{4.1}$ channels switch mode to uptake it inside the intracellular spaces once again. Moreover, the mere increase of perivascular potassium concentration, due to the release from the astrocytes, would contribute to increasing the amount of positive charges outside of the SMC cells, therefore, hyperpolarizing them.

The choice of the $k_{smc,pv}$ and $k_{pv,smc}$ was completely empirical, due to the lack of data to fit against. Therefore, to not add additional complexity, the values chosen for the simplest geometry, were kept for the other configurations.

The empirical decision was made through visual inspection of both the evolu-

tions of perivascular potassium concentration and smooth muscle cell potassium concentration, as depicted in figures ([5.10];[5.12]).

$k_{smc,pv}$ $[s^{-1}]$	$k_{pv,smc}$ $[s^{-1}]$
1.25	0.027

Table 5.1: Representation of chosen values for PV-SMC linear compartmental modeling parameters.

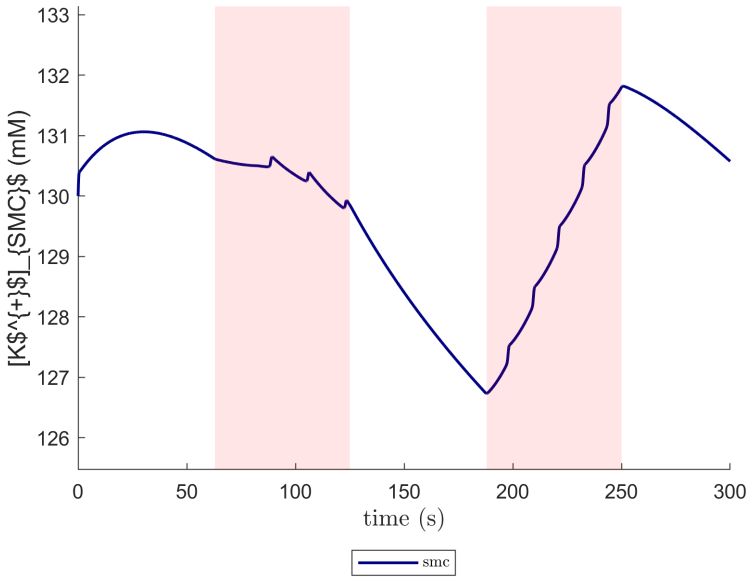

Figure 5.12: Representation of SMC's potassium concentration during first geometry setting's simulation.

It can be seen that the SMC's potassium concentration is not what we would desire, therefore, a linear relationship might not be suitable for the case. A chance could be given to a Michaelis-Menten relationship using saturation of the ion concentration, which would require some data to fit or the literature to be based on. We recall that we would expect the SMC potassium to decrease during stimulation windows, possibly with an increase in case the extracellular potassium gets to high, switching the SMC's $Kir_{4.1}$ channels mode. However, during the rest period we would expect to see potassium return to rest, which does not happen, particularly between the two stimulation windows. The explanation to that would be that, using a bilateral linear transport of material, the outflow from the SMCs would easily overtake the inflow from the perivascular space, therefore, making the SMC's concentration decrease.

5.3 Impact of parameters on potassium

Looking at the behaviors of the model, one interesting aspect of what was searched during this thesis, was how specific parts of it were influencing the potassium dynamics in the perivascular space. In particular, how specific parameters, with a defined physiological interpretation, could have been perturbed to directly affect the potassium release and uptake, using for each one the same glutamate stimulation settings.

To do so, a set of chosen parameters was perturbed 5 times ranging from being individually scaled of the following factors $\{0.25; 0.5; 1; 2; 4\}$. This means that for each chosen parameter, at least 5 simulations were launched to provide results. The chosen set of parameters was including the following:

$\upsilon_{5,BK}$ representing the change in the distribution of the fraction of open BK channels at varying calcium [4.27], decreasing it would make the opening of Bk channels less calcium sensitive, while increasing it would shift the distribution to increase $n_{\infty,BK}$ at lower intracellular concentrations.

g_{BK} representing the conductance over the surface area of the BK channels [4.24], which could physiologically be interpreted as the density of expression of these channels over the base surface area between the endfeet and the perivascular space.

$g_{kir,V}$ that represents the conductance over surface area of the $Kir_{4.1}$ channels [4.22], which could physiologically interpreted as the density of expression of these channels over the base surface area between the endfeet and the perivascular space.

$k_{smc,pv}$ that represents the constant transfer rate of potassium from the smooth muscle cells towards the perivascular space [4.34]. It scales the intracellular SMC potassium concentration to define its potassium out-flux, that ultimately leads to hyperpolarization of the cell itself.

The metrics that were used to quantify the changes of the different perturbations involved the potassium oscillatory behavior in the perivascular space,

particularly its peaks and nadir when oscillating. This required to implement a peak detection algorithm that made use of a Laplacian kernel smoother to select only the slow potassium dynamic component.

$$K(x,\lambda) = \begin{cases} \lambda \cdot exp(-\lambda \cdot x) & \text{for x} > 0 \\ \lambda \cdot exp(\lambda \cdot x) & \text{for x} <= 0 \end{cases}$$

Where the Kernel (K) represents a piecewise function with two different inputs: the x position in respect of the numerical series we are smoothing and λ, that defines the bulking of the kernel function.

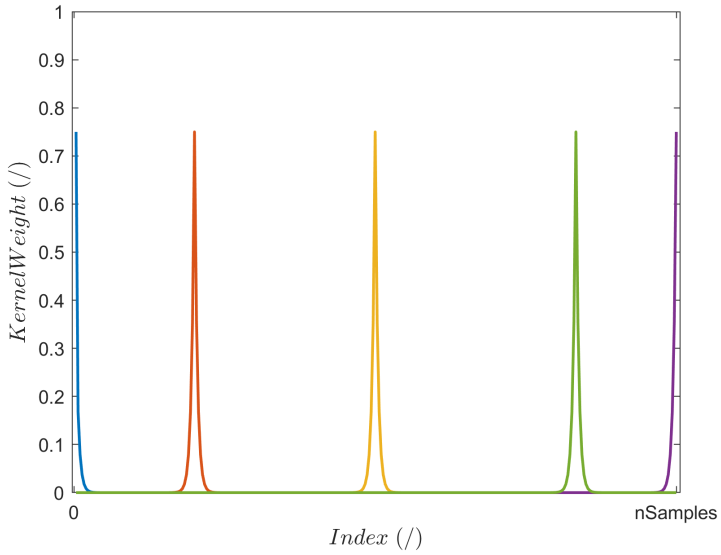

Figure 5.13: Representation of the Kernel shape at each instant of the virtual grid. The kernel was used for a local smoothing, therefore, regarding of the index of the time virtual grid, the weights were put to the adjacent samples respective to the position of the laplacian kernel.

However, the aim was to understand the oscillatory behavior, which would be related to the fast component of the potassium dynamics, therefore, a subtraction from the original evolution of the state variable of the evaluated slow component was computed. Following, the fast component was used to identify some metrics, such as the average of the peaks and nadirs during three different windows of time independently.

- Weak glutamate stimulus
- Strong glutamate stimulus
- No stimulus refractory period

The selection of the various peaks and nadirs was carried out with a simple peak detection pipeline, using a threshold based on the 70% of the maximum value reached. Every point higher than the threshold was treated as a candidate peak, and compared to the other candidates in a local region of the signal to produce the least amount of false positive. The pipeline adjusted for the nadirs, by negating the fast component, searching once again for peaks that in reality would represent nadirs. This made possible the search of a undefined number of peaks and nadirs during examination windows.

The numerous amounts of peaks and nadirs were then averaged for each time window along with the average value, and then averaged once again across the different perturbations of each parameter. The final results could be graphed with a look-alike error bar chart, that represented for each parameter the three time windows. Related to each time window, there would be the respective average value between the average of the peaks and the average of the nadirs, across all the different perturbations. The results are reported in the following figure.

However, a greater interest was specifically on the stimulation windows; therefore, two other proper error bar graphs were produced for each parameter, showing the average ± standard deviation of, respectively, the average values, the peaks and the nadirs. Thus, a distinction was made between the strong glutamate window and the weak glutamate window.

As we can evince from the previous figures, two parameters that increased the amplitude of the potassium oscillations were found to be the $\upsilon_{5,BK}$, and the $k_{smc,pv}$. The first one could be expected to behave in that manner, because of how the model is designed, this specific parameter directly influences the calcium gated activation mechanisms of BK channels. It has been discussed that its role is to shift the range of distribution of the fraction of open channels at equilibrium as calcium varies and, with increasing $\upsilon_{5,BK}$, lower intracellular calcium concentrations become capable of opening more channels on average. Which leads to an higher efflux of potassium towards the perivascular space. Therefore, changing $\upsilon_{5,BK}$ makes the BK channels more or less sensitive to changes in calcium concentrations. Furthermore, perturbing the parameter $k_{smc,pv}$ shows that increasing it confirms the expectation of having a higher basal efflux of potassium from smooth muscle cells into the perivascular space.

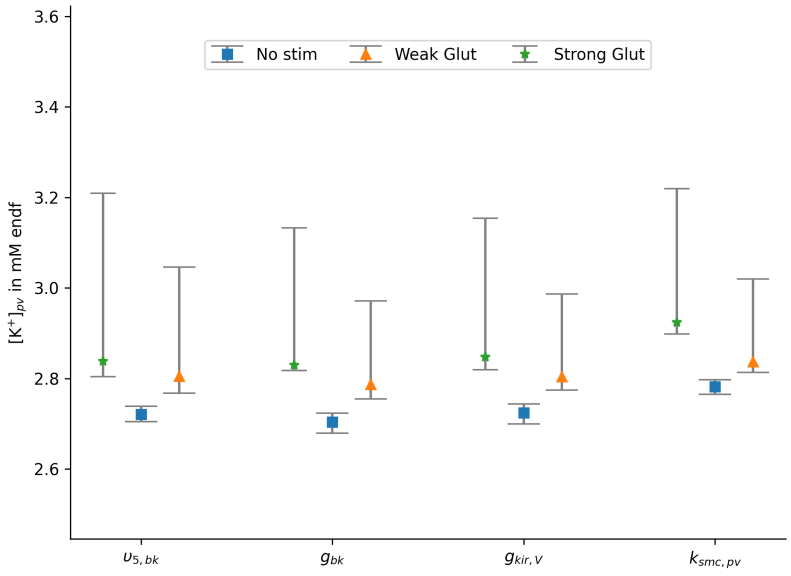

Figure 5.14: Visualization of impact of perturbing specific parameters over potassium release oscillations in perivascular space. The error bar are color coded between different periods of simulation, and are set as follows: the center of the error bar would correspond of the average between the averages of perivascular potassium concentration, while the tails of would correspond, respectively, to the average of all peaks and nadirs of potassium concentration.

The other two parameters that were tested, $g_{kir,V}$ and g_{BK}, instead showed a smaller impact in the change of potassium oscillations. For the second parameter, the reason could be that, even when the conductance increases over the surface area, the probability of opening a large number of channels remains low and would not be affected by the parameter. Which ultimately would lead to a smaller increase in release of potassium, while for the conductance of the $kir_{4.1}$ channels, the increase of the parameter would not be enough, since the flux of ions appear to be way smaller than the involved others.

Recalling the impact of perturbing $\upsilon_{5,bk}$, it is clearly possible to see the effect of it on the fraction of open BK channels after infinite stimulation time and at changes of $[Ca^{2+}]_{endf}$ and V_{endf}. It can be noticed in figures [5.17], how changing $\upsilon_{5,bk}$ increases the probability of having a higher fraction of open channels in the working range of calcium concentrations. However, the fact that the overall fraction of open channels appears to be more sensitive to calcium concentrations

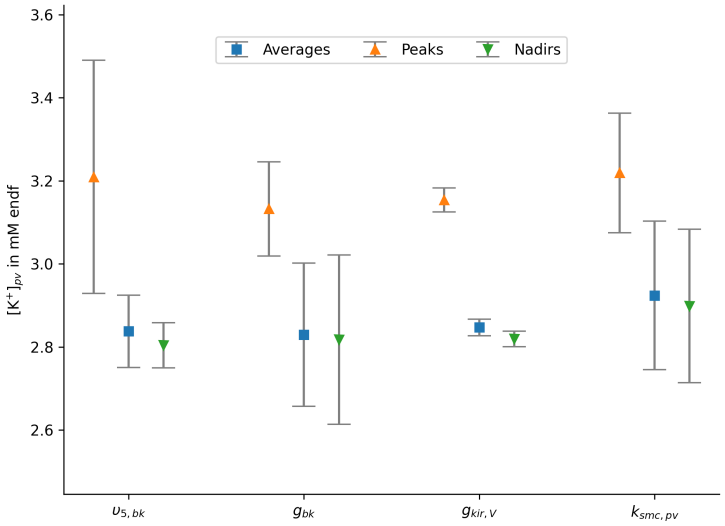

Figure 5.15: Visualization of impact of perturbing specific parameters over potassium release in PV during the second stimulation window. In this case the error bar are color coded regarding the average of concentration, the peaks or nadirs. The error bars are the standard average ± standard deviation across different perturbation.

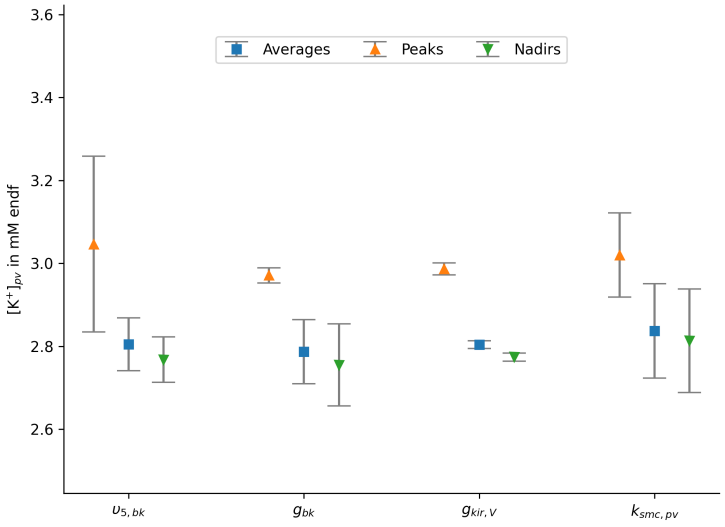

Figure 5.16: Visualization of impact of perturbing specific parameters over potassium release in PV during the first stimulation window. In this case the error bar are color coded regarding the average of concentration, the peaks or nadirs. The error bars are the standard average ± standard deviation across different perturbation.

compared to voltage concentrations is still preserved.

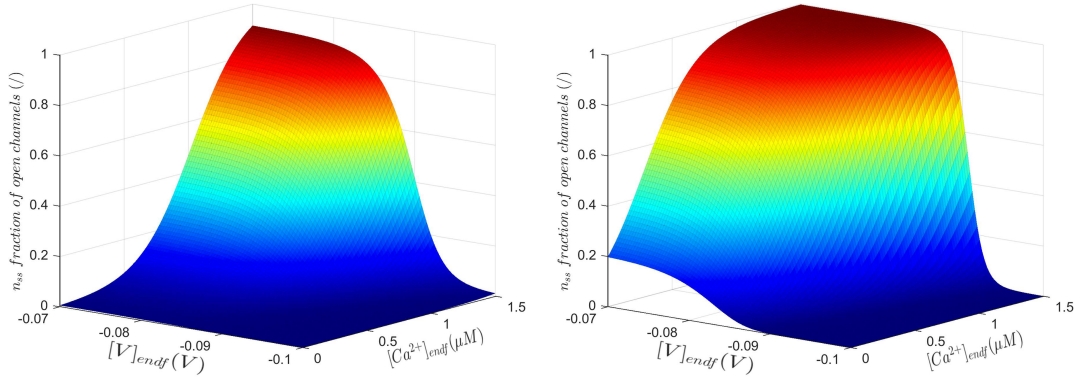

Figure 5.17: Visualization of impact of perturbing $v_{5,BK}$ over the fraction of open BK channels at changing calcium concentration and membrane potential. On the left the surface plot of n nullcline with $v_{5,BK}$ times 2; On the right the surface plot of n nullcline with $v_{5,BK}$ times 4;

6

Conclusion

Astrocytes are the supportive cells of the CNS, and they operate on regulating many processes at all levels of organization of the nervous tissue. To the very best of the scientific community knowledge, which needs to develop further and further, the astrocytes are now thought as the primary homeostatic, and defensive cells of the CNS, which, without their presence, simply couldn't exist. In fact, the multiple functions of astroglia, somewhat reflect the evolutionary selection of the majority of characteristics that differentiate the capabilities of a human brain, compared to lower life entities one's. Focusing on potassium buffering towards regulating CBF by integrating into the NVU, this computational model set the field for future implementations of a mechanistic model for the blood vessel's strain at changing of surrounding smooth muscle cells polarization.

The results that have been presented in the previous section shows that there is in fact correlation between the propagation of calcium signaling and release of potassium in the PV. Where this release is mostly controlled by the activity of the BK channels, driven by the calcium oscillations. In fact, perturbing the BK's sensibility to calcium changes ($\upsilon_{5,BK}$), has shown an increment in average channels opening and an increment in potassium release. Moreover, the results have shown how the approximation of the SMC domain is still not suitable to

model the potassium exchanges with the PV. Therefore, a redesign of the SMC's potassium transporters would be needed to further investigate regulation of CBF.

During glutamate stimulation, an hyperpolarization of local smooth muscle cells was found to be possible, leading the idea that the activity of astrocyte potassium buffering and neural activity stimulation could be linked with changes in cerebral blood flow. Which, ultimately could be put in use with monitoring tests, such as functional MRIs and blood-oxygen-level dependent (BOLD) contrast metric.

Future steps about the computational model, apart from continuing the developing of the NVU, could include a full spatial organization with interactions between nearby processes and not only between adjacent compartments, belonging to the same process. Moreover, investigating the possibility of adding stochastic behaviors in activation mechanisms of different channels, or on glutamate stimulation.

I would like to conclude by saying that, once the model would be validated, either by acquiring data respecting its behavior or by investigating a medical case of study. The aim would be to use the very same computational model and inspect, if by changing its properties, pathological condition effect or causes could be reproducible and analysable. Always keeping in mind the goal of proceeding with making the model and the analysis intuitive, understandable and more importantly reproducible.

A

Pseudo-code

The computational model is a modified version of preliminary work done from Peter Winkler and Lea Fritschi from the Institute of Neural Engineering. It uses an object-oriented approach, where the main class is *astrocyte* contains all the others. The overall description of the relationship between different classes follows a composition of classes, rather than inheritance. The modified version differs from the preliminary work, implementing the *endfeet* compartment, the PV domain and the SMC domain, while adapting previous sections of code to merge together with the additional features. The *endfeet* compartment inherits from *compartment* class and extend the set of coupled ordinary differential equations making the state space model to track a larger set of state variables and, in case of presence of any endfeet in *geometry* class, adapt the *solve* astrocyte method. In order to instantiate an *astrocyte* object, it is required to provide a *geometry* object and a set of model parameters, if different from default ones. The core of the astrocyte definition relies on a dictionary containing all instantiated compartments, where the identification could be done using the compartment number as *key*.

Once the astrocyte is built, it can be immediately launched the *solve* method, which integrate the evolution of all state space variables. In order to handle

all coupled ODEs, every metabolic pathway is described as an independent class with *compute_currents* methods that compute the terms on the right side of each ODE.

The following summarizing pseudo-code describes the pipeline to build an *astrocyte* object and launch the simulation, given the position and amplitude of the external glutamate stimulation. Inside the *solve* method, there are nested other two class methods, defined as *dxdt* and *update*, which have been updated to handle the additional features. The first one defines the right side of all the coupled ODEs by going through all possible compartments in aforementioned dictionary. The second one, updates the instantaneous value of each state variable for each compartment regarding the output of *dxdt* and the adaptive time step. The full code implementation can be found at the following link: [Github repository]

Algorithm A.1 Building and solving an astrocyte class's instance

Require: $Geometry; nComp := \#Compartments$
  $Parameters \leftarrow Loading\ parameters\ from\ .ini\ file$
  $astrocyte \leftarrow InstantiateanAstrocyteclassobject$
  for $Comp\ in\ Compartments$
    $instantiate\ Comp$
    $instantiate\ Comp\ domains\ (IS, ER, ES)$
    $instantiate\ Comp\ connections$
    $astrocyte.d \leftarrow Definition\ of\ compartment\ dictionary$
    if $Comp \in Endfeet$
      $Comp \leftarrow Get\ perivascular\ pathway$
      $Comp \leftarrow Get\ perivascular\ domain$
      $Comp \leftarrow Get\ smc\ domain$
    end if
  end for
  $Launch\ solve\_ivp\ method$
  $Initial\ values \leftarrow Resting\ condition$
  while $Solve$
    $Do\ dxdt \leftarrow Compute\ Right\ side\ of\ coupled\ ODEs$
    $Do\ update \leftarrow Update\ state\ variables$
    $Solution \leftarrow Append\ states\ values$
  end while
  return $Solution$

B

Parameter List

x_{pap}	Length of perisynaptic compartment	10 $[\mu m]$
x_{endf}	Length of endfoot compartment	30 $[\mu m]$
r_{endf}	Radius of endfoot compartment	3 $[\mu m]$
$ratio_{er,endf}$	Ratio between Vol_{IS} and Vol_{ER} of an Endfoot compartment	0.15 $[/]$

Table B.1: Compartment geometrical parameters

t_1	Time of first glutamate stimulation	62.5 $[s]$
t_2	Time of second glutamate stimulation	187.5 $[s]$
t_{dur}	Duration of glutamate stimulation	62.5 $[s]$
$glut_1$	First glutamate external concentration	1 $[mM]$
$glut_2$	Second glutamate external concentration	6 $[mM]$
$glut_0$	Basal glutamate external concentration	0.002 $[mM]$

Table B.2: Glutamate stimulation parameters

υ_β	Maximal rate of IP3 production by PLCβ	0.0001 $[mM\ s^{-1}]$	[19]
K_R	Glutamate affinity with mGluR	0.0013 $[mM]$	[19]
K_P	Scaling factor of IP_3 inhibition from $[Ca^{2+}]$	0.0015 $[mM]$	[19]
K_π	Affinity between calcium and PLCβ	0.0006 $[mM]$	[19]
υ_δ	Maximal rate of IP3 production by PLCδ	$2{\cdot}10^{-5}$ $[mM\ s^{-1}]$	[19]
k_δ	PLCδ half inhibition constant	0.0015 $[mM]$	[19]
$K_{PLC\delta}$	Affinity between calcium and PLCδ	0.0001 $[mM]$	[19]
υ_{3K}	Maximal rate of IP3 degradation by 3-K	0.002 $[mM\ s^{-1}]$	[19]
K_D	Affinity between calcium and 3-K	0.0007 $[mM]$	[19]
K_3	Affinity between IP_3 and 3-K	0.001 $[mM]$	[19]
r_{5P}	Maximal rate of IP_3 degradation by IP-5P	0.04 $[s^{-1}]$	[19]

Table B.3: IP_3 production parameters

d_1	Affinity between IP_3 and IP_3R	$1.3{\cdot}10^{-4}$ $[mM]$	[30]
d_2	Calcium dissociation constant	$1.049{\cdot}10^{-3}$ $[mM]$	[30]
d_3	IP_3 dissociation constant	$9.434{\cdot}10^{-4}$ $[mM]$	[30]
d_5	Affinity between calcium and IP_3R	$8.234{\cdot}10^{-5}$ $[mM]$	[30]
r_c	Maximal rate of transported Ca^{2+}	3.0 $[s^{-1}]$	[4]
a_2	Binding rate for Ca^{2+} inhibition	200 $[s^{-1}]$	*
v_{er}	Maximal rate of Ca^{2+} Serca up-take	$4.5{\cdot}10^{-3}$ $[mMs^{-1}]$	[4]
K_{er}	Affinity between calcium and Serca	$1{\cdot}10^{-4}$ $[mM]$	[4]
r_L	Maximal rate of transported Ca^{2+}	0.055 $[s^{-1}]$	[30]

Table B.4: mGluR pathway parameters

$I_{NCX_{max}}$	Maximal NCX pump current	0.001 $[pA\ \mu m^{-2}]$	[4]
$K_{NCX_{Na}}$	Affinity between Na^+ and NCX	87.5 $[mM]$	[4]
$K_{NCX_{Ca}}$	Affinity between Ca^{2+} and NCX	1.38 $[mM]$	[4]
η	position of energy barrier	0.35 $[mM]$	[4]
k_{sat}	saturation factor	0.1 [/]	[4]
$I_{GluT_{max}}$	Maximal GluT pump current	0.75 $[pA\ \mu m^{-2}]$	[4]
K_{GluT_K}	Affinity between K^+ and NCX	5 $[mM]$	[4]
$K_{GluT_{Na}}$	Affinity between Na^+ and NCX	15 $[mM]$	[4]
K_{GluT_g}	Affinity between glutamate and NCX	0.034 $[mM]$	[4]
$I_{NKA_{max}}$	Maximal NKA pump current	1.52 $[pA\ \mu m^{-2}]$	[4]
$K_{NKA_{Na}}$	Affinity between Na^+ and NKA	10 $[mM]$	[4]
K_{NKA_K}	Affinity between K^+ and NKA	1.5 $[mM]$	[4]
$g_{Na_{leak}}$	Sodium leak current conductance	13 $[pS\ \mu m^{-2}]$	[4]
$g_{K_{leak}}$	Sodium leak current conductance	162.46 $[pS\ \mu m^{-2}]$	[4]

Table B.5: GluT pathway parameters

υ_{EET}	Maximal rate of EET production	72 $[s^{-1}]$	[26]
k_{EET}	EET decay rate	7.2 $[s^{-1}]$	[26]
$[Ca^{2+}]_{min}$	minimum $[Ca^{2+}]$ for EET production	$0.1{\cdot}10^{-3}$ $[mM]$	[26]

Table B.6: EET production parameters

$g_{Kir,V}$	$Kir_{4.1}$ conductance over surface area	0.001 $[pA\ mV^{-1}\ \mu m^{-2}]$	[34]
$E_{K,endf}$	Potassium Nernst constant	$[V]$	[34]
g_{BK}	BK conductance over surface area	$1.16{\cdot}10^{3}$ $[S\ m^{-2}]$	[16]
ψ_{BK}	BK channel time opening	2.664 $[s^{-1}]$	[26]
EET_{shift}	EET-dependent voltage shift	2 $[V\ mM^{-1}]$	[26]
$\upsilon_{4,BK}$	Measures the spread of n_∞ distribution	$8{\cdot}10^{-3}$ $[V]$	[26]
$\upsilon_{5,BK}$	Regulates the n_∞'s dependence on calcium	$15{\cdot}10^{-3}$ $[V]$	[26]
$\upsilon_{6,BK}$	Shifts up the range of n_∞	$-55{\cdot}10^{-3}$ $[V]$	[26]
Ca_3	Shifts n_∞ regarding calcium	$0.4{\cdot}10^{-3}$ $[mM]$	[26]
Ca_4	Shifts n_∞ regarding calcium	$0.35{\cdot}10^{-3}$ $[mM]$	[26]

Table B.7: Perivascular pathway parameters

$D_{Ca,er}$	Ca^{2+} diffusion constant between ER	$0.13{\cdot}10^{-10}$ $[m^2\ s^{-1}]$	[5]
$D_{Ca,is}$	Ca^{2+} diffusion constant between IS	$0.13{\cdot}10^{-10}$ $[m^2\ s^{-1}]$	[4]
$D_{Na,is}$	Na^{+} diffusion constant between IS	$1.33{\cdot}10^{-9}$ $[m^2\ s^{-1}]$	[5]
$D_{K,is}$	K^{+} diffusion constant between IS	$1.96{\cdot}10^{-9}$ $[m^2\ s^{-1}]$	[5]
$D_{IP3,is}$	IP_3 diffusion constant between IS	$3{\cdot}10^{-10}$ $[m^2\ s^{-1}]$	[4]
$D_{Ca,es}$	Ca^{2+} diffusion constant between ES	$0.13{\cdot}10^{-10}$ $[m^2\ s^{-1}]$	[4]
$D_{Na,es}$	Na^{+} diffusion constant between ES	$1.33{\cdot}10^{-9}$ $[m^2\ s^{-1}]$	[5]
$D_{K,es}$	K^{+} diffusion constant between ES	$1.96{\cdot}10^{-9}$ $[m^2\ s^{-1}]$	[5]
$D_{Ca,pv}$	Ca^{2+} diffusion constant between ES|PV	$0.13{\cdot}10^{-10}$ $[m^2\ s^{-1}]$	[4]
$D_{Na,pv}$	Na^{+} diffusion constant between ES|PV	$1.33{\cdot}10^{-9}$ $[m^2\ s^{-1}]$	[5]
$D_{K,pv}$	K^{+} diffusion constant between ES|PV	$1.96{\cdot}10^{-9}$ $[m^2\ s^{-1}]$	[5]

Table B.8: Diffusion parameters

$k_{pv,smc}$	Constant transport rate from SMC to PV	1.25 $[s^{-1}]$	
$k_{smc,pv}$	Constant transport rate from PV to SMC	0.027 $[s^{-1}]$	
R_{pv}	Ratio between Vol_{pv} and Vol_{is} of an End-foot compartment	$1{\cdot}10^{-3}$ $[/]$	[27]

Table B.9: Perivascular space domain parameters

$[Ca^{2+}]_{0,ER}$	Rest $[Ca^{2+}]$ in ER	$19.63{\cdot}10^{-3}$ $[mM]$	[4]
$[Ca^{2+}]_{0,IS}$	Rest $[Ca^{2+}]$ in IS	$0.073{\cdot}10^{-3}$ $[mM]$	[4]
$[Na^{+}]_{0,IS}$	Rest $[NA^{+}]$ in IS	15 $[mM]$	[4]
$[K^{+}]_{0,IS}$	Rest $[K^{+}]$ in IS	100 $[mM]$	[4]
$[IP_3]_{0,IS}$	Rest $[IP_3]$ in IS	$0.15659{\cdot}10^{-3}$ $[mM]$	[4]
$[EET]_{0,IS}$	Rest $[EET]$ in IS	$0.1{\cdot}10^{-6}$ $[mM]$	[27]
$[Ca^{2+}]_{0,ES}$	Rest $[Ca^{2+}]$ in ES	1.8 $[mM]$	[4]
$[Na^{+}]_{0,ES}$	Rest $[NA^{+}]$ in ES	150 $[mM]$	[4]
$[K^{+}]_{0,ES}$	Rest $[K^{+}]$ in ES	3 $[mM]$	[4]
$[Ca^{2+}]_{0,PV}$	Rest $[Ca^{2+}]$ in PV	1.8 $[mM]$	[4]
$[Na^{+}]_{0,PV}$	Rest $[NA^{+}]$ in PV	150 $[mM]$	[4]
$[K^{+}]_{0,PV}$	Rest $[K^{+}]$ in PV	1 $[mM]$	[27]
$[K^{+}]_{0,SMC}$	Rest $[K^{+}]$ in SMC	130 $[mM]$	[27]
V_0	Rest Voltage in astrocyte	$-85.88{\cdot}10^{-3}$ $[V]$	[4]
C_m	Astrocyte's membrane capacitance	0.01 $[F\ m^{-2}]$	[4]

Table B.10: Initial conditions

References

[1] A. Verkhratsky and M. Nedergaard, "Physiology of astroglia," *Physiol Rev*, vol. 98, no. 1, pp. 239–389, Jan. 2018.

[2] C. Escartin, E. Galea, A. Lakatos, J. P. O'Callaghan *et al.*, "Reactive astrocyte nomenclature, definitions, and future directions," *Nature Neuroscience*, vol. 24, no. 3, pp. 312–325, Mar 2021. [Online]. Available: https://doi.org/10.1038/s41593-020-00783-4

[3] T. Manninen, R. Havela, and M.-L. Linne, "Computational models for calcium-mediated astrocyte functions," *Frontiers in Computational Neuroscience*, vol. 12, 2018. [Online]. Available: https://doi.org/10.3389/fncom.2018.00014

[4] F. Oschmann, K. Mergenthaler, E. Jungnickel, and K. Obermayer, "Spatial separation of two different pathways accounting for the generation of calcium signals in astrocytes," *PLOS Computational Biology*, vol. 13, 2017. [Online]. Available: https://doi.org/10.1371/journal.pcbi.1005377

[5] S. Y. Gordleeva, A. V. Ermolaeva, I. A. Kastalskiy, and V. B. Kazantsev, "Astrocyte as spatiotemporal integrating detector of neuronal activity," *Frontiers in Physiology*, vol. 10, 2019. [Online]. Available: https://doi.org/10.3389/fphys.2019.00294

[6] A. Witthoft, J. A. Filosa, and G. E. Karniadakis, "Potassium buffering in the neurovascular unit: Models and sensitivity analysis," *Biophysical Journal*, vol. 105, 2013. [Online]. Available: https://doi.org/10.1016/j.bpj.2013.09.012

[7] K. MacCord, "Ectoderm," *Embryo Project Encyclopedia*, dec 2013. [Online]. Available: http://embryo.asu.edu/handle/10776/6642

[8] V. Parpura and A. Verkhratsky, "Astrocytes revisited: concise historic outlook on glutamate homeostasis and signaling." *Croat Med J.*, vol. 53, no. 6, Dec 2012. [Online]. Available: https://doi.org/10.3325/cmj.2012.53.518

[9] Y. Bernardinelli, D. Muller, and I. Nikonenko, "Astrocyte-synapse structural plasticity," *Neural Plast*, 2014. [Online]. Available: https://doi.org/10.1155/2014/232105

[10] A. Kriegstein and A. Alvarez-Buylla, "The glial nature of embryonic and adult neural stem cells," *Annual review of Neuroscience*, vol. 32, no. 1, pp. 149–184, 2009, pMID:19555289. [Online]. Available: https://doi.org/10.1146/annurev.neuro.051508.135600

[11] D. Kirdajova and M. Anderova, "Ng2 cells and their neurogenic potential," *Current Opinion in Pharmacology*, vol. 50, pp. 53–60, 2020, neurosciences: Neurogenesis. [Online]. Available: https://www.sciencedirect.com/science/article/pii/S1471489219301158

[12] K. Nakashima, S. Wiese, M. Yanagisawa *et al.*, "Developmental requirement of gp130 signaling in neuronal survival and astrocyte differentiation," *Journal of Neuroscience*, vol. 19, no. 13, pp. 5429–5434, 1999. [Online]. Available: https://www.jneurosci.org/content/19/13/5429

[13] A. P. Antunes *et al.*, "Higher brain extracellular potassium is associated with brain metabolic distress and poor outcome after aneurysmal subarachnoid hemorrhage." *Critical care*, vol. 18, no. 3, 2014. [Online]. Available: https://doi.org/10.1186/cc13916

[14] P. Kofuji and E. Newman, "Potassium buffering in the central nervous system."

[15] Y. Kucheryavykh, L. Kucheryavykh *et al.*, "Downregulation of kir4.1 inward rectifying potassium channel subunits by rnai impairs potassium transfer and glutamate uptake by cultured cortical astrocytes," *Glia*, vol. 55, pp. 274–281, 2007. [Online]. Available: https://doi.org/10.1002/glia.20455

[16] J. Filosa, A. Bonev *et al.*, "Local potassium signaling couples neuronal activity to vasodilation in the brain." *Nat Neurosci*, vol. 9, pp. 1397–1403, 2006. [Online]. Available: https://doi.org/10.1038/nn1779

[17] S. E. Nwaobi, V. A. Cuddapah *et al.*, "The role of glial-specific kir4.1 in normal and pathological states of the cns." *Acta neuropathologica*, vol. 132, pp. 1–21, 2016. [Online]. Available: https://doi.org/10.1007/s00401-016-1553-1

[18] C. Contet *et al.*, "Bk channels in the central nervous system," *International review of neurobiology*, vol. 128, pp. 281–342, 2016. [Online]. Available: https://doi.org/10.1016/bs.irn.2016.04.001

[19] M. De Pittà and V. Volman, "Glutamate regulation of calcium and ip3 oscillating and pulsating dynamics in astrocytes," *J Biol Phys*, vol. 35, 2009. [Online]. Available: https://doi.org/10.1113/10.1007/s10867-009-9155-y

[20] H. J. XIA and G. YANG, "Inositol 1,4,5-trisphosphate 3-kinases: functions and regulations," *Cell Research*, vol. 15, pp. 83–91, 2005. [Online]. Available: https://doi.org/10.1038/sj.cr.7290270

[21] A. Tzingounis and J. Wadiche, "Glutamate transporters: confining runaway excitation by shaping synaptic transmission." *Nat Rev Neurosci*, vol. 8, pp. 935–947, 2007. [Online]. Available: https://doi.org/10.1038/nrn2274

[22] ——, "The glial sodium-calcium exchanger: A new target for nitric oxide-mediated cellular toxicity." *Current protein Peptide Science*, vol. 14, pp. 43–50, 2013. [Online]. Available: 10.2174/1389203711314010007

[23] S. YU, S. Huang, Y. Ding *et al.*, "Transient receptor potential ion-channel subfamily v member 4: a potential target for cancer treatment," *Cell Death Dis*, vol. 10, 2019. [Online]. Available: https://doi.org/10.1038/s41419-019-1708-9

[24] H. Kubotera *et al.*, "Astrocytic endfeet re-cover blood vessels after removal by laser ablation," *Scientific Reports*, February 2019. [Online]. Available: https://doi.org/10.1038/s41598-018-37419-4

[25] K. M. Dunn and M. T. Nelson, "Potassium channels and neurovascular coupling," *Circulation journal : official journal of the Japanese Circulation Society*, vol. 74, pp. 608–616, 2010. [Online]. Available: https://doi.org/10,1253/circj.cj-10-0174

[26] H. Farr and T. David, "Models of neurovascular coupling via potassium and eet signalling," *Journal of theoretical biology*, vol. 286, 2011. [Online]. Available: https://doi.org/10.1016/j.jtbi.2011.07.006

[27] A. Kenny, M. J. Plank, and T. David, "The role of astrocytic calcium and trpv4 channels in neurovascular coupling," *J Comput Neurosci*, vol. 44, 2018. [Online]. Available: https://doi.org/10.1007/s10827-017-0671-7

[28] A. Hodgkin and A. Huxley, "A quantitative description of membrane current and its application to conduction and excitation in nerve," *J Physiol*, vol. 117, 1952. [Online]. Available: https://doi.org/10.1113/jphysiol.1952.sp004764

[29] J. Gonzalez-Fernandez and B. Ermentrout, "On the origin and dynamics of the vasomotion of small arteries," *Math Biosci*, vol. 119, 1994. [Online]. Available: https://doi.org/10.1016/0025-5564(94)90074-4

[30] Y.-X. Li and J. Rinzel, "Equations for insp3 receptor-mediated [ca2+]i oscillations derived from a detailed kinetic model: A hodgkin-huxley like formalism," *Journal of Theoretical Biology*, vol. 166, 1994. [Online]. Available: https://doi.org/10.1006/jtbi.1994.1041

[31] L. J. Mullins, "A mechanism for na/ca transport." *J Gen Physiol*, vol. 70, 1977. [Online]. Available: https://doi.org/10.1085/jgp.70.6.681

[32] D. DiFrancesco and D. Noble, "A model of cardiac electrical activity incorporating ionic pumps and concentration changes." *Philos Trans R Soc Lond Biol*, vol. 307, 1985. [Online]. Available: https://doi.org/10.1098/rstb.1985.0001

[33] C. H. Luo and R. Y., "A dynamic model of the cardiac ventricular action potential. i. simulations of ionic currents and concentration

changes." *Circulation Research*, vol. 74, 1994. [Online]. Available: https://doi.org/10.1006/jtbi.1994.1041

[34] S. Murakami and Y. Kurachi, "Mechanisms of astrocytic k+ clearance and swelling under high extracellular k+ concentrations," *J Physiol Sci*, vol. 66, 2016. [Online]. Available: https://doi.org/10.1007/s12576-015-0404-5

[35] C. Morris and H. Lecar, "Voltage oscillations in the barnacle giant muscle fiber," *Biophys. J.*, vol. 35, 1981. [Online]. Available: https://doi.org/10.1016/S0006-3495(81)84782-0

[36] F. Montefusco, A. Tagliavini, M. Ferrante, and M. G. Pedersen, "Concise whole-cell modeling of bkca-cav activity controlled by local coupling and stoichiometry," *Biophysical Journal*, vol. 112, 2017. [Online]. Available: https://doi.org/10.1016/j.bpj.2017.04.035

Acknowledgments

Scrivo questa sezione per ringraziare tutte le persone che mi sono state vicine nel mio percorso di studi. Ho apprezzato ogni momento, e sono contento che la maggior parte di loro stia trovando la loro passione, così come spero di averla trovata io.
Ringrazio la mia famiglia, che, seppur in silenzio, si è sempre fatta sentire vicina e di supporto. In particolare, mio padre che avrebbe sempre voluto studiare più di quello che ha fatto, ma ha dovuto fare scelte differenti per permettere a me e a mio fratello di avere libertà di scegliere. Mia mamma, che non mi ha mai fatto mancare niente. Mio fratello, che seppur possa sembrare lontano nelle parole, nei fatti è tutto al contrario. E ai miei nonni, i quali sarebbero stati felici di vedere anche il loro ultimo nipote concludere il primo passo del suo percorso.
Ringrazio la mia ragazza, Emma, che mi sopporta e mi ascolta a prescindere dal contesto. Sono fiero di lei.
Ringrazio i miei amici di sempre, la mia seconda famiglia. So che con loro, a prescindere da quale sia la mia richiesta, la risposta sarà sempre si. Vorrei mettere tutti i nomi, ma so che loro saprebbero di chi parlo. Farei di tutto per vederli realizzare i loro sogni.
Ringrazio le persone magnifiche che ho conosciuto a Graz, le stesso persone con cui ho condiviso le frustrazioni della tesi e che in un modo o nell'altro mi hanno aiutato ad arrivare al traguardo.
Ringrazio i miei compagni di studi, Matteo, Alessandro e Alessio, coi quali ho condiviso il mio percorso, e riuscito a togliermi diverse soddisfazioni personali. Sono contento stiate trovando la vostra strada e sono curioso di sapere cosa riuscirete a fare in futuro.
Ringrazio il professor Pedersen, il quale è stato di prezioso e paziente supporto nelle fasi finali dello sviluppo dell'elaborato.
I would like to thank all the people in the Institute of neural engineering, where I

stayed doing my master thesis. You all welcomed me as one of you and gave me precious hints and suggestions every time I needed them. A special mention to my supervisor, professor Lenk, for giving me the opportunity of working in her lab and developing this project.
Per concludere, ringrazio me stesso per essere riuscito a portare a conclusione questo lavoro con il minimo supporto e in completa autonomia.